UCGE Reports
Number 20277

Department of Geomatics Engineering

Ultra Wideband Augmented GPS
(URL: http://www.geomatics.ucalgary.ca/research/publications)

by

David Sung-Tat Chiu

December 2008

SCHULICH
School of Engineering   UNIVERSITY OF CALGARY

UNIVERSITY OF CALGARY

Ultra Wideband Augmented GPS

by

David Sung-Tat Chiu

A THESIS

SUBMITTED TO THE FACULTY OF GRADUATE STUDIES

IN PARTIAL FULFILMENT OF THE REQUIREMENT FOR THE

DEGREE OF MASTER OF SCIENCE

DEPARTMENT OF GEOMATICS ENGINEERING

CALGARY, ALBERTA

DECEMBER, 2008

ABSTRACT

UWB has several characteristics that enable accurate positioning in situations where GPS has difficulties. UWB and GPS measurements are combined using tightly-coupled integration.

Prior to integration, it is shown that UWB-only positioning results in significantly improved accuracy and precision compared to code DGPS-only positioning in poor signal environments.

Integrating multiple UWB ranges to code DGPS demonstrates that UWB can replace GPS when it suffers from a complete satellite outage indoors. Sub-metre level accuracy during this time is sufficient for indoor pedestrian navigation applications. Then, multiple UWB ranges augmented RTK float solutions are tested in several signal conditions. The worst case, with 2 satellites and 3 UWB ranges, results in centimetre-level horizontal accuracies and sub-metre precision.

Through testing UWB-GPS integration in numerous scenarios, this thesis proves that UWB is a feasible solution to augment, enhance and/or replace GPS in the benign and hostile signal environments.

TABLE OF CONTENTS

LIST OF FIGURES

LIST OF TABLES

LIST OF ABBREVIATIONS

AGPS	Assisted GPS
C/A code	Coarse-Acquisition Code
C/N_0	Carrier-to-Noise density
CDMA	Code Division Multiple Access
CRLB	Cramer-Rao Lower Bound
DARPA	Defense Advanced Research Projects Agency
DGPS	Differential GPS
DLL	Delay Lock Loop
DOP	Dilution of Precision
DSSS	Direct Sequence Spread Spectrum
ECEF	Earth-Centred-Earth-Fixed
EIRP	Equivalent Isotropically Radited Power
FAA	Federal Aviation Administration
FCC	Federal Communications Commission
GDOP	Geometric Dilution of Precision
GLONASS	Global Navigation Satellite System (Russia)
GNSS	Global Navigation Satellite System
GPS	Global Positioning System
HDOP	Horizontal Dilution of Precision
HSGPS	High Sensitivity GPS
ICT	Information and Communications Technologies building
IGS	International GNSS Service
INS	Inertial Navigation System
LAMBDA	Least-Squares AMBiguity Decorrelation Adjustment
LOS	Line-of-Sight
MC-UWB	Multicarrier Ultra Wideband
MSS	Multispectral Solutions
NLOS	Non-Line-of-Sight
NTIA	National Telecommunications and Information Administration
OFDM	Orthogonal Frequency Division Multiplexing
OTF	On-the-fly
P code	Precise Code
PAM	Pulse Amplitude Modulation

PDOP	Position Dilution of Precision
PLL	Phase Lock Loop
PPM	Pulse Position Modulation
PPS	Precise Positioning Service
PRN	Pseudorandom Noise
PVT	Position, Velocity and Time
P(Y) code	Encrypted P-code
RF	Radio Frequency
RMS	Root Mean Square
RTK	Real-Time Kinematic
SA	Selective Availability
SNR	Signal-to-Noise ratio
SPS	Standard Positioning Service
TD	Time Domain
TDOA	Time Difference of Arrival
TDOP	Time Dilution of Precision
TGO	Trimble Geomatics Office
TOA	Time of Arrival
UAV	Unmanned Aerial Vehicle
UD	Unit Upper Triangular and Diagonal
UERE	User-Equivalent Range Error
UGV	Unmanned Ground Vehicle
US DoD	US Department of Defense
UWB	Ultra Wideband
UTC	Coordinated Universal Time
VDOP	Vertical Dilution of Precision
WGS84	World Geodetic System 1984
WLAN	Wireless Local Area Network
WPAN	Wireless Personal Area Network

CHAPTER 1: ULTRA WIDEBAND AUGMENTED GPS

The Global Positioning System (GPS) relies on accurate time, satellite position and delay of the signal. To ensure position accuracy, all three of these components must be known or estimated correctly. However, while current time and satellite position can be estimated quite well, knowing correct signal delay can be difficult especially if it suffers from error effects. Some of these error sources, such as ionospheric and tropospheric delay, can be estimated with innovative techniques, whereas multipath correction is more problematic. Furthermore, under poor signal conditions, not only can multipath be prominent, but signal masking, fading and attenuation may all lead to the degradation of the position solution. Eventually, any or all of these errors may result in receiver loss-of-lock and an estimated solution is no longer possible.

Since GPS signal strengths are so weak, a GPS receiver typically requires a line-of-sight (LOS) path to the satellites in order to be able to detect its signals. However, receiver-to-satellite visibility is not always achievable in environments where the position solutions are required. Common blockages from buildings, trees, and hills, may prevent a GPS receiver from acquiring satellite signals with standard algorithms, thus causing the system to be unusable. Furthermore, users expect good availability, accuracy, reliability and integrity. Location and navigation ubiquitously would be ideal; however, until now, any of the aforementioned user expectations are somewhat limited in sub-optimal operating environments. Even if the receiver is able to track the satellites and estimate pseudoranges, errors such as multipath, attenuation and fading, may degrade the position solution. Unfortunately, these errors are also amplified under these signal conditions. Therefore, it is necessary to find an alternative method to acquire and maintain good positioning accuracy in both clear and hostile signal environments.

Ultra wideband (UWB) radio frequency (RF) signals have several characteristics that enable them to be superior to GPS signals in poor to limited signal environments. UWB ranging provides the capability to augment GPS through high accuracy ranges. Furthermore, UWB's ability for fine time resolution and its seemingly robust performance in high multipath environments, enable a code GPS navigation system, such

as for pedestrian positioning or an outdoor real-time kinematic (RTK) positioning system, to boost its operational environment indoors, as well as outdoors. Frequency selective fading from materials is also mitigated since UWB's power is spread over such a large bandwidth. To create a large bandwidth, short pulses of energy are needed, which can also give a high data rate performance in multi-user network applications.

1.1 RESEARCH OBJECTIVES

The major objective of the research presented in this thesis is to evaluate the effectiveness of UWB range measurements as both an augmentation to, and replacement for, GPS observations in both navigation and surveying applications.

To fully understand how UWB can benefit GPS, several assessments are made. Firstly, it is important to analyze the operational range and accuracy of the UWB ranging system. Results of tests conducted indoors, as well as outdoors, are presented in the thesis. Two commercially available UWB ranging systems from two different manufacturers are evaluated in this thesis. Once UWB range accuracy and reliability is quantified and understood, it can then be integrated with GPS. Since UWB radios report a range (and no carrier phase is present), it is natural to compare UWB-only positioning to code-based differential GPS (DGPS). The purpose of doing this is to show that UWB-only positioning is more accurate, precise and reliable than code DGPS. If it is shown that UWB-only positioning is better than code DGPS then augmenting GPS with UWB will provide positioning improvements. The next logical step, once UWB range accuracy has been verified, is to integrate UWB range measurements with code DGPS observations and to actually demonstrate a quantifiable improvement over the code DGPS-only solution in both benign and hostile GPS signal environments. Code DGPS only provides metre level accuracy and this is often sufficient for numerous applications, such as with indoor pedestrian navigation. However, metre level accuracy can be inadequate for a number of other applications, which require sub-metre accuracy; hence for GPS, carrier-phase measurements are needed. It will be shown that augmenting UWB to the carrier phase GPS float solution will also result in notable improvements in position accuracy and reliability, especially in poor signal conditions.

The goal of this research is to demonstrate that UWB technology can assist and improve overall GPS accuracy and reliability in varying signal environments. To summarize the assessments:

♦ UWB range accuracy and signal effects are assessed in multipath conditions

♦ UWB positioning is compared to code DGPS positioning in benign and hostile environments

♦ UWB augmented code DGPS positioning in clear sky, hostile and indoor conditions is demonstrated and compared to DGPS alone.

♦ UWB augmented carrier phase GPS in clear and hostile signal environments

1.2 SIGNIFICANCE

The results and analysis shown in this work are both novel and significant. While UWB technology dates back to the 1960's, use of UWB signals for positioning purposes is innovative. Employing UWB ranges to augment GPS observations is even more novel and this topic is rarely found in published literature by any group, company or university in the world. At the time of writing, one group from the University of Malaga in Spain has combined UWB and GPS measurements in a loosely-coupled way and research work is also being done by a group at the University of Nottingham in England. The work shown in this thesis is one of the first (if not the first) published to combine UWB and GPS measurements in a tightly-coupled method. It represents a first step in understanding a topic that will inevitably grow as UWB technology matures and as UWB/GPS integration becomes more common.

1.3 THESIS OUTLINE

The thesis is organized into eight chapters, as follows:

♦ Chapter 2 introduces GPS. It begins with a history of the technology, followed by a brief description of GPS basics, including problems with this technology that are relevant to this thesis.

♦ In Chapter 3, UWB will be discussed. Topics such as UWB history, characteristics, advantages and disadvantages of using this technology, interference issues and UWB applications are described. The chapter will conclude with the topic of GPS/UWB integration. A literature review on this subject, along with methods to do the integration is considered.

♦ Estimation methods and equipment used in the research are described in Chapter 4. A short review of least-squares estimation and Kalman filtering is shown followed by a detailed development of Bierman-Thornton square root filtering. This filter is used in the thesis and its characteristics, equations and advantages are discussed. The chapter ends with a presentation of all the equipment used for the tests.

♦ Chapter 5 takes a look into the characteristics and range accuracy of two different UWB systems: Time Domain (TD) UWB PulSON 210 UWB development kit and Multispectral Solutions (MSS) UWB ranging radios. Both systems are used in the research work. Results and analysis of several tests are presented to evaluate the accuracy of these radios and methods.

♦ The first part of Chapter 6 is a comparison between positioning using UWB ranges alone versus code DGPS positioning in benign and hostile environments. It is shown that UWB positioning is more accurate than code DGPS positioning. Therefore, augmenting GPS with UWB is beneficial. The second part of this chapter deals with the augmentation of code DGPS with UWB range measurements. The requirement to have reliable positioning everywhere is becoming increasingly important, and can be used for pedestrian positioning and other indoor positioning applications. Single and multiple UWB ranges are used to augment code GPS in good to poor signal conditions. Multiple UWB ranges are employed indoors to augment and/or replace the GPS system once GPS signals are too weak to detect or are corrupted by multipath. Details of these tests' motivations, procedures, results and analysis are fully described. This section concludes with a discussion on the results and indoor pedestrian navigation as it relates to UWB-code DGPS integration. Studying ways to position indoors is the next step in attaining seamless outdoor-to-indoor

pedestrian positioning and navigation. UWB-code DGPS combined can only provide metre-level accuracy, which is sufficient for pedestrian navigation purposes, but not enough for sub-metre level applications. For this reason, carrier phase GPS will need to be used.

♦ In Chapter 7, augmentation of carrier phase GPS with UWB ranges is discussed. Single and multiple UWB ranges combined with GPS RTK in benign and poor GPS signal conditions are studied. The investigation's methods and results are analyzed in terms of positioning accuracy and reliability.

♦ Lastly, Chapter 8 will summarize important test results. Future work and limitations conclude this discussion.

1.4 SCOPE

This thesis studies the augmentation of code DGPS and GPS RTK solution with single and multiple UWB ranges. Only the float solution of GPS RTK is used in this research. Resolution of ambiguities, in order to arrive at a fixed solution, is beyond the scope of this thesis and hence, the effects of UWB ranges added to a GPS RTK fixed solution is not investigated.

1.5 PUBLICATIONS

Part of the work described in the thesis has been presented in the Institute of Navigation (ION) National Technical Meeting (NTM) 2008 and ION Global Navigation Satellite Systems (GNSS) 2008 conferences:

Chiu, D.S., K. O'Keefe (2008) "Bierman-Thornton UD Filtering for Double-Differenced Carrier Phase Estimation Accounting for Full Mathematical Correlation," in *Proceedings of ION NTM 2008*, 28-30 January, San Diego CA, U.S. Institute of Navigation, Fairfax VA

Chiu, D.S., G. MacGougan, K. O'Keefe (2008) "UWB Assisted GPS RTK in Hostile Environments," in *Proceedings of ION NTM 2008*, 28-30 January, San Diego CA, U.S. Institute of Navigation, Fairfax VA

Chiu, D.S., K. O'Keefe (2008) "UWB Seamless Outdoor-to-Indoor Pedestrian Navigation using GPS and UWB," in *Proceedings of ION GNSS 2008*, 17-19 September, Savannah GA, U.S. Institute of Navigation, Fairfax VA

CHAPTER 2: NAVSTAR GPS

In this chapter, the basic concepts of GPS that are related to this thesis are discussed. Topics include error sources, DGPS, indoor positioning, and more.

2.1 GPS FUNDAMENTALS

The origins of GPS date back to the 1960's when the US Department of Defense (DoD) began studying ways to position and navigate using RF signals. Several systems, such as Transit, Timation and System 621B, were developed, which led to the eventual conglomeration of the systems in the 1970's to form NAVSTAR Global Positioning System (Pace et al 1995).

This system uses time-of-arrival (TOA) to determine user range and position. Essentially, TOA is the measure of the time it takes a signal to be transmitted from the satellite to the receiver. However, as will be explained in Section 2.3, certain error sources affect the accurate determination of the signal propagation time.

The entire GPS system can be split into three segments: the space segment, control segment and user segment. All of these segments must be operating correctly in order for the entire GPS system to function. The space segment encompasses all satellites that users can make measurements from, while the control segment is responsible for maintaining GPS satellite operability. The user segment is generally the GPS receiver. Anything that contains a GPS receiver and receives satellite signals is part of the user segment.

GPS signals are broadcast over two frequencies in the L-band. The L1 signal is transmitted at 154 times the fundamental frequency or 1575.42 MHz, while the secondary signal, L2, is sent at 120 times the fundamental frequency or 1227.60 MHz. L1 is modulated by two different pseudorandom noise (PRN) codes (Course-Acquisition (C/A) code and Precise (P) code) and a common navigation message, while L2 is modulated by only one PRN code (P code) and the navigation message.

The C/A code is available for civilian-use (Standard Positioning Service (SPS)), while the P code is available for military-use only (Precise Positioning Service (PPS)).

The discussion of GPS fundamentals has been kept short. For further details on GPS concepts, please refer to Kaplan & Hegarty (2006).

2.2 OBSERVABLES

The goal of a GPS receiver is to generate four different measurement outputs: pseudorange, carrier-phase, Doppler and the carrier-to-noise density (C/N_0). Pseudorange, Doppler and carrier-to-noise density are raw measurements, while the carrier-phase is derived from Doppler measurements.

2.2.1 Pseudorange measurement

Pseudorange is the measure of propagation time from the satellite to the receiver. Because pseudorange is a measure of time, any clock errors in the satellite and/or receiver will directly affect the pseudorange. Large range errors may result even from small clock errors since it is multiplied by the speed of light.

Since satellite clock errors are small and corrections are sent via the navigation message, the dominant clock error is from the receiver.

2.2.2 Doppler measurement

The Doppler measurement is calculated by the difference between the measured frequency and the transmitted frequency using the satellite clock drift rate found in the navigation message.

2.2.3 Carrier-phase measurement

The carrier-phase measurement is derived from the Doppler measurement. Integrating Doppler measurements results in carrier-phase measurements and a carrier-phase ambiguity term. Carrier-phase results in very accurate ranging, but only gives relative positions if the ambiguity term is not estimated.

2.2.4 Carrier-to-Noise density (C/N_0)

The carrier-to-noise density reports the quality of the signal. A high carrier-to-noise density means a strong signal. Since the value is receiver-dependent, a general rule of thumb is that any value over 40 dB-Hz is considered a strong signal, while values below 32 may cause the receiver to lose lock (Raquet 2006).

2.3 STAND-ALONE GPS ERROR SOURCES

There are a number of errors that affect the propagation time of the signal as seen in Equation 2.1. As a result of these error sources, the propagation time and resultant calculated distance is actually longer than it really is compared to the signal propagating through a vacuum.

$$p = \rho + d\rho + d_{ion} + d_{trop} + cdt - cdT + n(p) \tag{2.1}$$

where

$\rho = \sqrt{(x - x_p)^2 + (y - y_p)^2 + (z - z_p)^2}$ (geometric range of satellite to receiver)

$d\rho$ = satellite orbital errors

d_{ion} = ionosphere error

d_{trop} = troposphere error

cdt = satellite clock error

cdT = receiver clock error

$n(p)$ = noise

A similar error calculation and illustration can be done for carrier-phase. Instead of multiplying propagation time by the speed of light to retrieve a distance – as is the case for pseudoranges – carrier-phase multiples the carrier wavelength by the number of cycles to attain the range.

2.3.1 Orbital Errors

Satellite orbit error corrections are calculated by the control segment and are broadcast through the navigation message. The magnitude of these errors is a function of how well the Kepler parameters used to calculate these errors are estimated. For real-time use, errors are about 2.6 m (Lachapelle et al 2006). However, a service provided by the International GNSS Service (IGS) is able to provide more accurate corrections shown in Table 2.1, below.

Table 2.1: Orbital Error correction service types (from Lachapelle et al 2006)

Service Type	Accuracy	Wait-time
Broadcast	2.6 m	Real-time
Ultra-Rapid (IGS)	0.25 m	Real-time
Rapid (IGS)	0.05 m	17 hours
Final Precise (IGS)	< 0.05 m	13-20 days

2.3.2 Clock

Two clock errors affect the accuracy of the pseudorange measurement: satellite clock and receiver clock. Please refer to Figure 2.1, below.
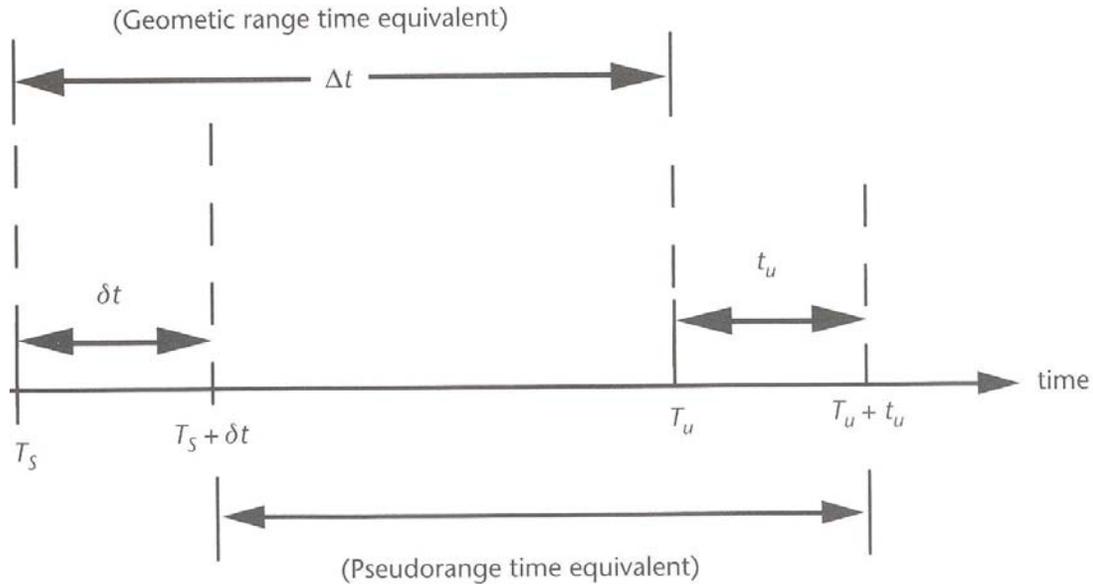
Figure 2.1: Two clock errors are shown to affect the pseudorange measurement in this figure with δt being the satellite clock error and t_u representing the receiver clock error (from Kaplan & Hegarty 2006)

2.3.2.1 Receiver Clock

In the determination of a point in 3-dimensional space, trilateration requires a minimum of three ranges. However, in the case of GPS, a minimum of four ranges is needed to determine a user's position based on satellite ranges. Cesium and/or rubidium clocks are used on all satellites. While these oscillators are very accurate, they are also extremely expensive. To avoid such costs to the user, a fourth satellite range is used to estimate the receiver's clock error when the user uses a less expensive clock.

2.3.2.2 Satellite Clock

Atomic clocks are found onboard each satellite vehicle and these clocks are extremely stable and accurate. However, the master control station maintains accuracy of these clocks and is in charge of transmitting satellite clock corrections to users via the navigation message. Errors range in magnitude from 0.8 m to 4 m (Kaplan & Hegarty 2006).

Prior to May 2000, an additional error, known as Selective Availability (SA) was also present in the satellite clock. This intentional satellite clock dithering was added by the DoD, but has since been discontinued.

2.3.3 Ionosphere

The ionosphere is a dispersive medium that exists from about 50 km to over 1000 km above the Earth. Free electrons characterize the region and the number of electrons is quantified as electron density. Electron density is a function of geographic location, altitude, time of day, time of year, and more. Because the ionosphere is dispersive, ionospheric errors can be measured by using two frequencies. Typical differential error magnitudes are 1-3 ppm (RMS) with extremes reaching up to 30 ppm in lower latitudes (Lachapelle et al 2006).

2.3.4 Troposphere

The troposphere is a neutral part of the atmosphere, which extends from the ground to about 45 km. A wet delay and a dry/hydrostatic delay is a result of the troposphere. The wet delay accounts for about 10% of the error, while the hydrostatic delay accounts for 90%. However, both of these delays can be modeled. The troposphere affects the signal in several ways: range delay (index of refraction > 1), ray bending, absorption and scintillation. The total delay is about 2.4 m at zenith and 9.3 m at 15 degrees elevation (Lachapelle et al 2006).

2.3.5 Multipath

The direct path from a satellite to the receiver always results in the shortest distance and propagation time. When the signal reflects or diffracts off of surrounding objects, the receiver measures these delayed replicas of the signal. This is known as multipath. When the multipath signal is received longer than twice the spreading code symbol period for the modulation, the receiver is able to distinguish between the direct signal and the multipath signal. However, when the multipath arrives quite soon after the direct signal (tens of nanoseconds, for example), then the multipath signal can distort the correlation function between the incoming signal and the receiver's replica code. Phase

can also be distorted. When distortion happens, pseudorange and carrier-phase measurements may introduce positioning errors.

Shadowing is the attenuation of the direct signal by some obstruction between the LOS of the satellite to receiver. This can happen outdoors in an area with foliage or indoors. Shadowing becomes a greater concern when the power received from a multipath signal is much, much greater than the shadowed direct path. If shadowing is severe, then total blockage of the direct signal may occur and the receiver may only detect multipath signals, possibly leading to large positioning errors.

2.3.6 Receiver Noise

Receiver noise is created by the receiver's tracking loops. For pseudorange measurements, the delay lock loop (DLL) suffers from thermal noise jitter and interference effects. The magnitude of DLL induced errors are usually 10 cm or less (1σ) but this is quite minimal compared to multipath generated errors. For carrier-phase measurements, the phase lock loop (PLL) causes receiver noise and resolution errors, which have errors of 1.2 mm (1σ) and 1.6 mm (1σ) when tracking the C/A code and P(Y) code, respectively (Kaplan & Hegarty 2006).

2.4 DIFFERENTIAL GPS

Stand-alone GPS typically has an accuracy of several to tens of metres. If more accuracy is desired, a local reference station can be used to correct for some of the errors encountered by a nearby rover receiver. There are several categories of DGPS, such as code-based or carrier-based and absolute or relative differential positioning; which to use depends on the desired application.

Local-Area DGPS is one of the simpler forms of DGPS, where a stand-alone GPS unit is placed on a well known, surveyed point. Because the absolute position of the point is known, any difference between the estimated position and the surveyed position is from GPS pseudorange error sources. These errors include satellite and receiver clock errors, orbit errors, ionospheric errors, tropospheric errors, multipath and noise. Please see

Table 2.2, below. The differences can be used by a nearby rover to correct or reduce several these errors. Since these errors are time and spatially correlated, the distance between the DGPS base station and rover should not exceed several hundred kilometres. A drawback of DGPS is that noise from the reference station receiver and rover receiver is added together (Kaplan & Hegarty 2006).

Table 2.2: Comparing pseudorange errors with GPS-only and local-area DGPS (after Kaplan & Hegarty 2006)

Segment	Error Source	GPS-only error (1σ m)	GPS & local-area DGPS (1σ m)
User	Ionosphere	7.0	0.2-4 cm/km x baseline in km
	Troposphere	0.2	1-4 cm/km x baseline in km
	Receiver noise	0.1	0.1
	Multipath	0.2	0.3
Space/Control	Broadcast clock	1.1	0.0
	L1 P(Y)-L1 C/A group delay	0.3	0.0
	Broadcast ephemeris	0.8	0.1-0.6 mm/km x baseline in km
Total System User Equivalent Range Error (UERE)		7.1	0.3 m + 1-6 cm/km x baseline in km

2.5 REAL-TIME KINEMATIC GPS

When sub-metre-level accuracy from DGPS is not sufficient, a feasible alternative is to use RTK positioning. This type of positioning is able to provide up to centimetre-level accuracy in optimal signal conditions only with the use of carrier-phase measurements with carrier-phase ambiguities resolved. This is known as a GPS RTK fixed solution. If the carrier-phase ambiguities are unknown, then the resultant solution is a GPS RTK float solution, where sub-decimetre-level accuracy is attained.

Like DGPS, GPS RTK uses a base station set up on a known surveyed point, where this base station can send corrections to a nearby rover receiver. These corrections are then used by the rover receiver to reduce some of the common errors experienced by both base station and rover receiver. Since these errors are time and spatially correlated, baseline distances should not exceed 10 kilometres.

2.6 CURRENT PROBLEMS WITH GPS

RTK positioning using GPS provides centimetre-level accuracies only under nominal signal conditions. This technique is now common in industry but is limited in application primarily due to signal masking, attenuation and multipath in hostile environments. Urban canyons, forests and congested construction sites are prime examples of these environments, where surveying is frequently done in poor signal conditions. Currently, RTK, alone, may not be sufficient in estimating a position solution or aiding reacquisition of lost GPS signals when the receiver lacks a clear view of its satellites.

Carrier-phase multipath may cause up to 0.25 λ of error (and up to 1 metre for code), while attenuation and fading, such as under foliage or in urban canyons, may cause a signal to become undetectable. A substantial processing gain (over the nominal received signal-to-noise ratio (SNR) for L1 C/A code is required to detect the signal under these conditions. Without High Sensitivity GPS (HSGPS) or Assisted GPS (AGPS), this may not be possible. Further, in order to obtain a reliable position solution, a sufficient number of measurements are required. In the case of the GPS receiver, this means that a certain number of LOS measurements must be present. When the number of measurements decreases, the solution's reliability also decreases until a point where a solution cannot be evaluated. So, an alternative method to overcome these problems is needed.

2.7 INDOOR POSITIONING

While GPS is able to provide highly accurate solutions outdoors, indoor positioning is a totally different case. Indoor measurements are plagued with problems such as severe multipath, attenuation and fading.

Under the best case clear signal conditions, the nominal received SNR for L1 C/A code is -19 dB. Since the typical detection threshold for a satellite's signal is +14 dB, a processing gain of 33 dB is required in order to detect the signal. However, signal attenuation and fading indoors can require an additional 40+ dB of gain (on top of the 33 dB gain requirement for the nominal case) by the receiver to detect the signal. This is normally not possible with a standard GPS receiver. Furthermore, indoor Dilution of Precision (DOP) and User Equivalent Range Error (UERE) can increase to 10-100 and tens of metres, respectively (Kaplan & Hegarty 2006). All these factors are the reason why reliable indoor positioning by GPS has not been reported in previous literature.

Indoor multipath is much more complex and difficult to predict than outdoor multipath. Aside from changing satellite geometry, indoor multipath is also affected by satellite elevation, material of the building, location of the building, and the location of the receiver within the building itself. Additionally, it is also difficult for a receiver to differentiate between tracking a weak, but correct signal, and a potential strong and incorrect multipath signal; with the latter possibly giving way to large ranging errors.

2.8 ACCURACY METRICS

2.8.1 Dilution of Precision (DOP)

There exists a matrix, H, which relates the states to the observables by taking the partial derivatives of the measurements with respect to the unknowns. This design matrix is sized n x 4, where n is the number of observables and 4 unknowns (x, y, z, dT), as seen in Equation 2.2, below.

$$H = \begin{bmatrix} \dfrac{dP_i}{dx_r} & \dfrac{dP_i}{dy_r} & \dfrac{dP_i}{dz_r} & \dfrac{dP_i}{cdT} \\ \dfrac{dP_j}{dx_r} & \dfrac{dP_j}{dy_r} & \dfrac{dP_j}{dz_r} & \dfrac{dP_j}{cdT} \\ . & . & . & . \\ . & . & . & . \\ \dfrac{dP_n}{dx_r} & \dfrac{dP_n}{dy_r} & \dfrac{dP_n}{dz_r} & \dfrac{dP_n}{cdT} \end{bmatrix}$$

(2.2)

where

P = pseudorange

x = x position unknown

y = y position unknown

z = z position unknown

dT = receiver clock error unknown

c = speed of light

The diagonal elements of the co-factor matrix, Q_x, represent the geometric strength of the satellite constellation, or how evenly spread out the satellite sources are with respect to the user. This is known as Dilution of Precision (DOP). Several different DOP's (Equations 2.4 to 2.8) can be formulated by taking different diagonal elements from the co-factor matrix shown in Equation 2.3.

$$Q_x = (H^T H)^{-1} = \begin{bmatrix} D_{11} & D_{12} & D_{13} & D_{14} \\ D_{21} & D_{22} & D_{23} & D_{24} \\ D_{31} & D_{32} & D_{33} & D_{34} \\ D_{41} & D_{42} & D_{43} & D_{44} \end{bmatrix} \qquad (2.3)$$

$$GDOP = \sqrt{D_{11} + D_{22} + D_{33} + D_{44}} \qquad \text{(Geometric DOP)} \qquad (2.4)$$

$$PDOP = \sqrt{D_{11} + D_{22} + D_{33}} \qquad \text{(Position DOP)} \qquad (2.5)$$

$$HDOP = \sqrt{D_{11} + D_{22}} \qquad \text{(Horizontal DOP)} \qquad (2.6)$$

$$VDOP = \sqrt{D_{33}} \qquad \text{(Vertical DOP)} \qquad (2.7)$$

$$TDOP = \sqrt{D_{44}} / c \qquad \text{(Time DOP)} \qquad (2.8)$$

2.8.2 User-equivalent range error (UERE)

The accuracy of the pseudorange value is quantified by the UERE. It is essentially the summation of all error sources that affect the pseudorange. Please refer to Table 2.2, above for the Standard Positioning Service (SPS) UERE.

2.8.3 Positioning Error

The overall positioning accuracy is the product of the satellite/user geometry (otherwise known as the DOP) and UERE. Please see Equation 2.9, below.

$$Position\ Error = DOP \times UERE \qquad\qquad (2.9)$$

Chapter 2 discussed the basics of GPS technology. However, in order to acquire full knowledge of all the technology used in this research, UWB fundamentals and reasons why it is complementary to GPS, need to be explained. This is done in the following chapter.

CHAPTER 3: ULTRA WIDEBAND

In the previous chapter, GPS principles were described. This chapter concentrates on introducing UWB technology and then concludes by exploring why it is useful for UWB to be integrated with GPS. The reader should have a clear understanding of the benefits of doing this following the chapter.

3.1 HISTORY

UWB originated in the 1960's and was first studied by Dr. Gerald F. Ross when he looked into time domain electromagnetics. Other researchers, such as Harmoth at Catholic University of America, Robins at Sperry Rand Corporation and van Etten of the United States Air Force, also led the way in the conception of modern UWB technology (Barrett 2000 & Barrett 2001). Only with the advent of sampling oscilloscopes and sub-nanosecond (baseband) pulse generation, could impulse UWB responses be observed, integrated and measured (Barrett 2001).

In the 1970's, Ross applied these new methods to radar and communication technologies. As result, the first UWB communication technique was patented with the replacement of the sampling oscilloscope by a newly created sensitive baseband pulse receiver (Ross 1973). By 1974, the first ground penetrating radar, invented by Morey at the Geophysical Survey Systems Corporation, was also created. And by the late 1980's, Ross had over 50 patents in UWB, with applications in communications, radar, and positioning systems (Reed 2005).

Up until 1989, this technology was known as baseband, carrier-free, impulse technology. The US DoD coined the term Ultra wideband as a method to transmit information through the use of impulse signals (Fontana 2006).

In 1993, Scholtz at the University of Southern California discovered a method for multiple access for UWB communication systems. Because of this, UWB communication systems were now also able to support wireless networks. This important innovation paved the way for numerous researchers to study UWB indoor and outdoor

propagation, signal effects of various materials, and antenna responses to impulse signals (Scholtz 1993).

Since the 1990's, numerous organizations and corporations, such as Time Domain Corporation, Multispectral Solutions, Federal Communications Commission (FCC), Federal Aviation Administration (FAA), National Telecommunications and Information Administration (NTIA), and Defense Advanced Research Projects Agency (DARPA), to name a few, spent exhaustive efforts in researching the effects of UWB signals on existing narrowband systems.

With the assistance of the aforementioned groups and more, the FCC issued a First Report and Order in 2002, on the operation of UWB signals within the spectrum (FCC 2002).

3.2 DEFINITION

UWB pulses are very short. They range from a few tens of picoseconds to a few nanoseconds and usually last only a few cycles of an RF carrier wave. Since the pulses are short, the energy is spread across a large bandwidth resulting in a low power density. Having a large bandwidth allows UWB to produce very fine time resolution. UWB waveforms are very broadband and it is sometimes very difficult to determine the "centre" frequency. This is why it was initially called "carrier-free" (Fontana 2006). Currently, there are several definitions of UWB with the most common being:

- ♦ Greater than 20% of centre frequency or 500 MHz bandwidth regardless of frequency (Reed 2005)
- ♦ Modulation methods that vary pulse timing and not carrier frequency, phase and/or amplitude (Reed 2005)

UWB signals still obey Maxwell's Equations, as well as the laws of physics.

The two most common UWB signal structures are known as impulse UWB and multicarrier UWB.

3.3 IMPULSE UWB

Impulse radio uses a sequence of baseband pulses to convey information, as opposed to using a modulated sinusoidal carrier as more conventional communication systems do. Because the duration of these pulses are typically in the nanoseconds range, their transmitting bandwidth is on the order of gigahertz.

In Equation 3.1, below, an impulse UWB pulse train is shown without distortion and the channel is noiseless with infinite SNR. The transmit signal $s(t)$ is a sum of all pulses, i, in the pulse train. Theoretically, there is no limit to the number of pulses in the pulse train and i is used to represent the ith pulse. In reality, the transmitted pulse is distorted by the circuitry, antenna and other causes.

$$s(t) = \sum_{i=-\infty}^{\infty} A_i(t) p(t - iT_f) \tag{3.1}$$

where

$s(t)$ = transmit signal as seen by the receiver

$A_i(t)$ = amplitude of the ith pulse

$p(t)$ = received pulse shape with normalized energy

T_f = frame repetition time

i = the ith pulse

The most common pulse shape when describing impulse UWB is the Gaussian pulse and its first and second derivatives. Another popular pulse shape is the sinusoidal modulated Gaussian pulse, which may be more suited for commercial purposes because it can be more practical to implement based on FCC's emission rules. Please refer to Figure 3.1, below, for the Gaussian pulselet and its derivatives.

Gaussian Pulses

(a) Gaussian pulse

(b) First derivative of Gaussian pulse

(c) Second derivative of Gaussian pulse
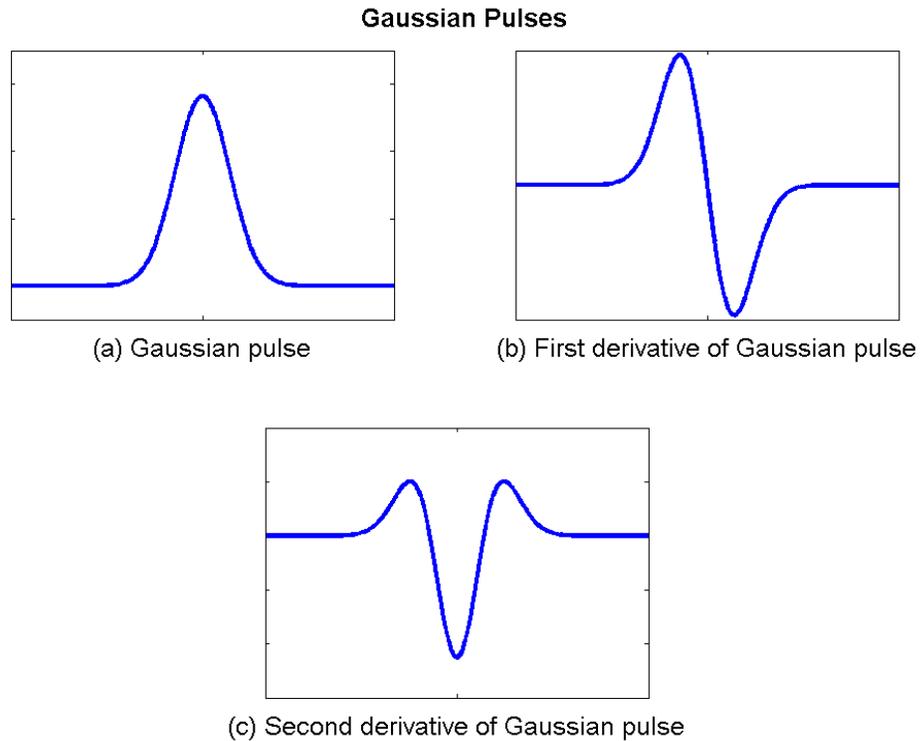
Figure 3.1: (a) Gaussian pulse in time domain; (b) the first derivative of the Gaussian pulse, also known as the Gaussian pulselet; and (c) the second derivative of the Gaussian pulse

Impulse UWB signals are pulse shaped to limit output at certain frequencies based on FCC emission rules. Gaussian pulses and their derivatives are often easy to produce and analyze, however they are not practical to use because they do not always fit into the FCC mask. Multi-carrier UWB may be better suited for FCC emission limits, as seen in Figure 3.2, below.
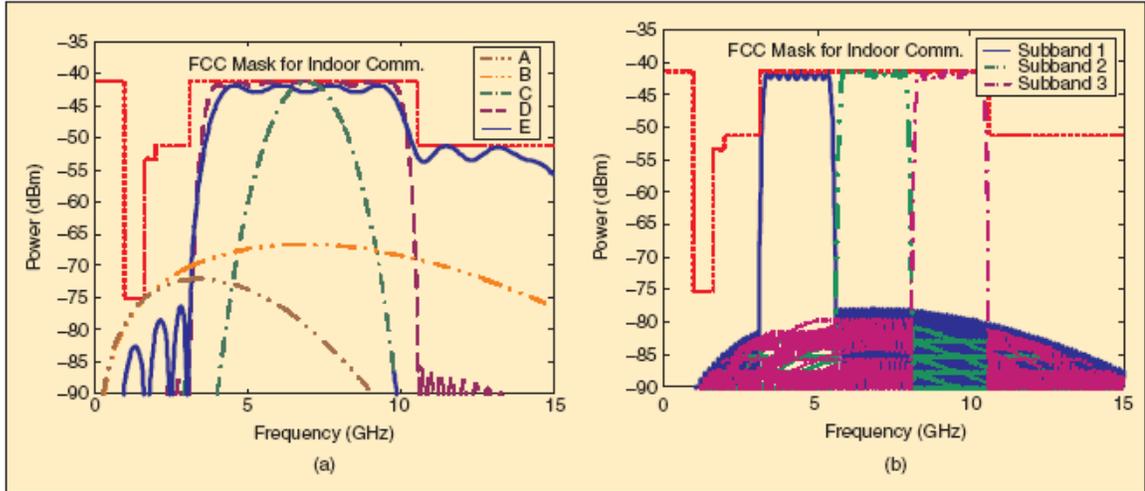
▲ 15. (a) Baseband pulse shapers and the FCC mask for indoor communications. A–Gaussian monocycle with $T_p = 0.37$ ns; B–Gaussian monocycle with $T_p = 0.19$ ns; C–a pulse shaper in [98]; D&E–pulse shapers in [99]; (b) Multiband UWB using baseband pulse shapers.

Figure 3.2: (a) Impulse UWB Gaussian pulses fitting into the FCC mask; and (b) Multi-carrier UWB sub-carrier pulses fitting into the FCC mask (from Yang and Giannakis 2004)

3.3.1 Modulation Schemes

There are several possible modulation schemes for impulse UWB signals; however, the discussion is limited to two of the more common schemes.

3.3.1.1 Pulse Amplitude Modulation (PAM)

Pulse Amplitude Modulation consists of a binary bit stream consisting of a series of -1 or +1. Equation 3.2, below, represents PAM with binary bit stream amplitude.

$$s(t) = \sum_{i=-\infty}^{\infty} d_i(t) p(t - iT_f)$$

(3.2)

where

$s(t)$ = transmit signal as seen by the receiver

$d_i(t)$ = binary bit stream amplitude of the pulse

$p(t)$ = received pulse shape with normalized energy

T_f = frame repetition time

A graphical representation of a PAM pulse train is shown in Figure 3.3, below.
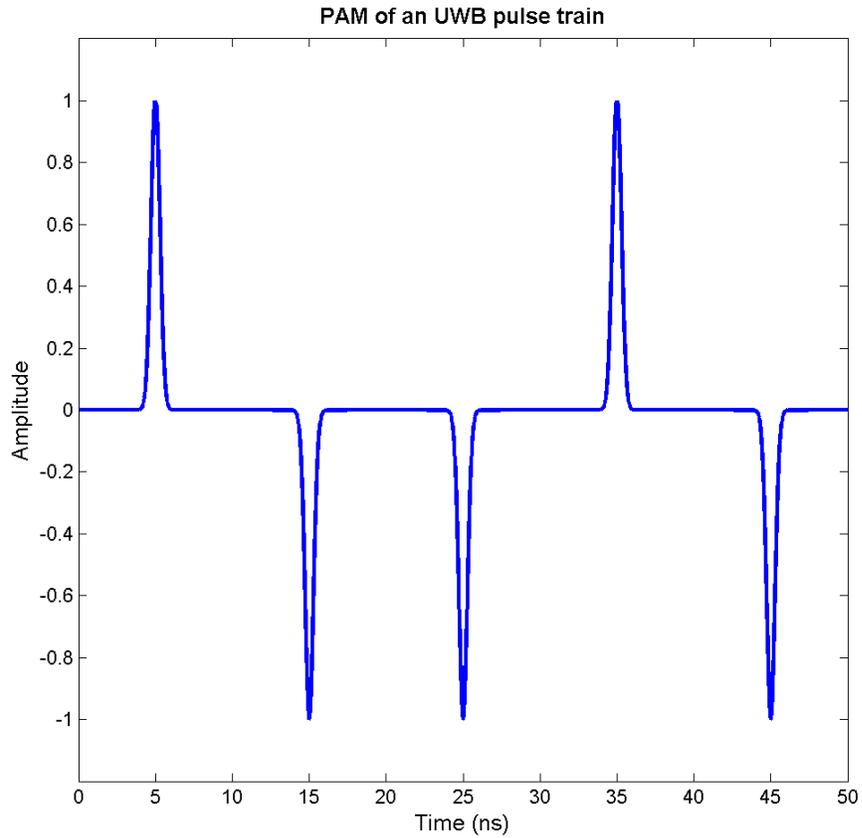
Figure 3.3: Pulse Amplitude Modulation of an UWB pulse train

3.3.1.2 Pulse Position Modulation (PPM)

Pulse Position Modulation consists of equal pulse amplitudes within the pulse train. However, certain pulses are either shifted slightly before or after its position in a regularly spaced pulse train. PPM can be formulated with Equation 3.3, below.

$$s(t) = \sum_{i=-\infty}^{\infty} Ap(t - iT_f - \delta d_i(t))$$ (3.3)

where

$s(t)$ =   transmit signal as seen by the receiver

A	$=$	amplitude of the pulse
$p(t)$	$=$	received pulse shape with normalized energy
T_f	$=$	frame repetition time
δ	$=$	base time increment
$d_i(t)$	$=$	time modulation for the pulse

An example of PPM is shown in Figure 3.4, below.
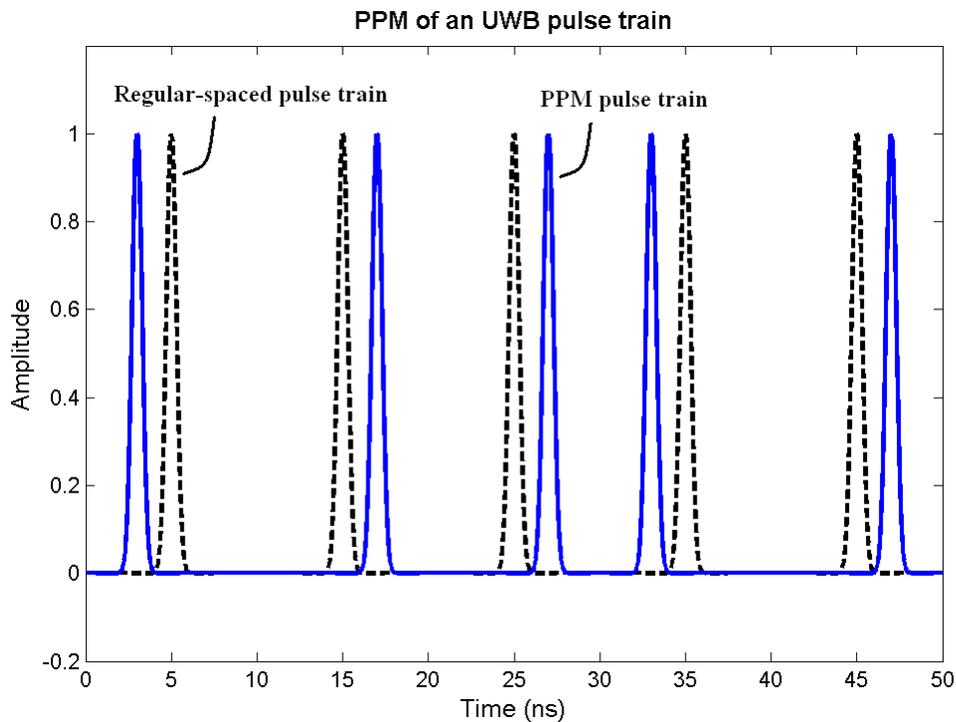
Figure 3.4: Pulse Position Modulation (PPM) of a UWB pulse train. The black dashed line is a regularly spaced pulse train, while the blue solid line represents the PPM of the same pulse train.

3.4 MULTI-CARRIER UWB

Multicarrier UWB signals, on the other hand, use a set of subcarriers. These subcarriers are streams of data that run in parallel but on different frequencies and combine to form a single data stream. Each of these subcarriers must be overlapping, but also non-interfering with one another. So, creating these multi-carrier UWB signals requires more effort, but can be done with real time Fourier transforms.

Multi-carrier UWB is represented in equation form, in Equation 3.4, below.

$$s(t) = A \sum_r \sum_{n=1}^{N} b_n^r p(t - rT_p) e^{(j2\pi n f_o (t - rT_p))} \tag{3.4}$$

where

$s(t)$	=	transmit signal as seen by the receiver
r	=	transmission interval
N	=	number of subcarriers
b_n^r	=	transmission symbol in the rth interval over nth subcarrier
f_o	=	fundamental frequency or $(T_p)^{-1}$
T_p	=	symbol duration

One of the major advantages of multicarrier UWB signals are their ability to minimize interference because the subcarriers can be chosen to avoid interference with bands used by other systems sharing the spectrum (Reed 2005). Furthermore, multicarrier UWB systems tend to have better time/range resolution, giving enhanced multipath mitigation. These systems also use the spectrum more efficiently, resulting in higher bit rate communications.

3.4.1 MULTIPLE ACCESS SCHEMES - Orthogonal Frequency Division Multiplexing (OFDM)

Orthogonal Frequency Division Multiplexing (OFDM) is becoming increasingly popular for multicarrier UWB modulation because it allows for subcarriers to precisely overlap, but at the same time, not interfere with each other. Multicarrier UWB OFDM also allows for gaps in certain frequency bands of subcarriers. Multiple users can be accommodated by giving each user a set of subcarriers. In transmission, each subcarrier is split into a train of pulses. These pulses are sent to the user, which then reassembles the train of pulses to recreate each subcarrier (Saberinia and Tewfik 2002).

3.5 PROPAGATION EFFECTS

3.5.1 Free Space Loss

The standard Friis transmission formula for spreading loss is

$$P_r = \frac{P_t G_t G_t \lambda^2}{(4\pi d)^2}$$ (3.5)

where

P_r =   received power

P_t =   transmit power

G_t =   transmit antenna gain

λ =   wavelength of signal

d =   distance

It is important to note that even though Equation 3.5, above, implies that spreading loss is dependent on wavelength and frequency, spreading loss is actually frequency independent. The wavelength term is due to an antenna effect and not signal path. Buehrer et al (2004) showed that path loss is indeed frequency independent by measuring the pulse shape of the signal at different distances. As expected, the pulse shape remained constant with distance. The same result was attained when a second antenna was used. For further details, please refer to Reed (2005) and Buehrer et al (2004).

3.5.2 Line-of-Sight (LOS) and Non-Line-of-Sight (NLOS) Path Loss

Signal propagation is typically not in a free-space environment. Obstacles such as trees, buildings, or people, can greatly affect received signal strength. Diffraction, attenuation and fading are frequency dependent and should be taken into account when the signal is propagating through a non-free-space environment. Attenuation varies between material and also the frequency of the signal, and can range from less than 1 dB to over 12 dB. Please refer to Figure 3.5, below, illustrating attenuation amounts for common indoor materials.

(a) Drywall, Chip Wood, Wooden Door, and Office Partition

(b) Glass, Brick Wall, Plywood, Block Wall
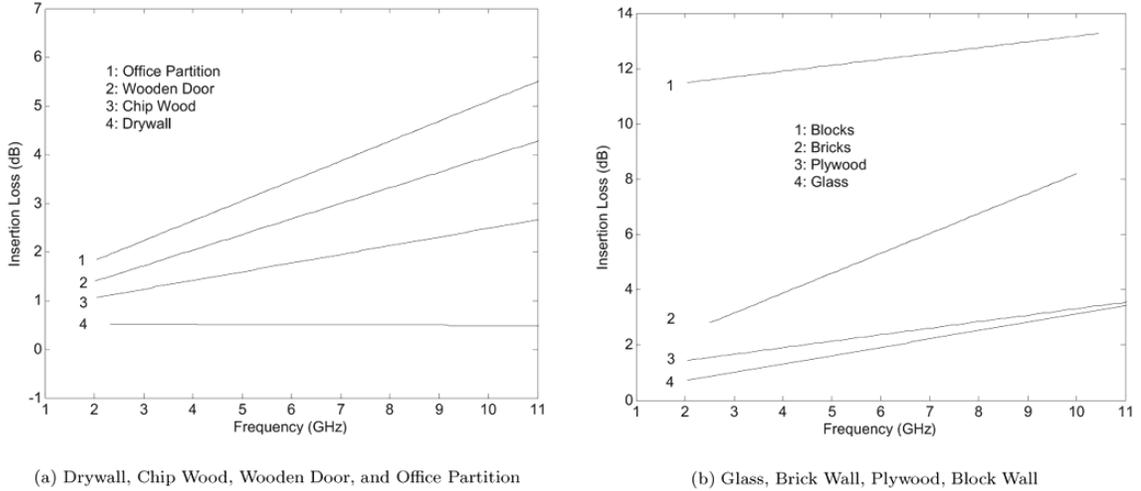
Figure 3.5: Attenuation loss for UWB through typical indoor building materials (from Reed 2005)

3.5.3 Cramer-Rao Lower Bound (CRLB)

There are several techniques to determine a range including TOA, and time difference of arrival (TDOA).

For an estimate of how well the TOA can determine a range, the variance of this method can be found using the Cramer-Rao Lower Bound (CRLB). The CRLB places a lower bound on the variance of the estimate and gives a measure of the best possible performance by the system. Without derivation, the CRLB is

$$\sigma_{\hat{\tau}}^2 = \frac{1}{8\pi^2 \beta_f^2 SNR} \qquad (3.6)$$

where

$\sigma_{\hat{\tau}}^2$ = variance error of the estimate

β_f = received signal bandwidth

SNR = signal-to-noise

From Equation 3.6, above, it can be seen that the SNR and bandwidth of the signal have an inverse linear and an inverse quadratic effect on the ranging accuracy, respectively.

Since UWB utilizes such a large bandwidth, ranging accuracy, as proven by the CRLB, is relatively precise because of the inverse quadratic effect (Reed 2005).

3.5.4 Two-Way Ranging

The UWB radios used in this thesis use a form of two-way ranging, where one radio sends a request and the other radio responds to the request. In Figure 3.6, below, Device A sends a range request message to Device B. After a known reply time ("t_{replyB}"), Device B responds to the range request message. The transmission time between Device A and B is illustrated as t_p in Figure 3.6. Clock errors, in regards to the specific UWB radios used in this thesis, are discussed in Section 5.6.
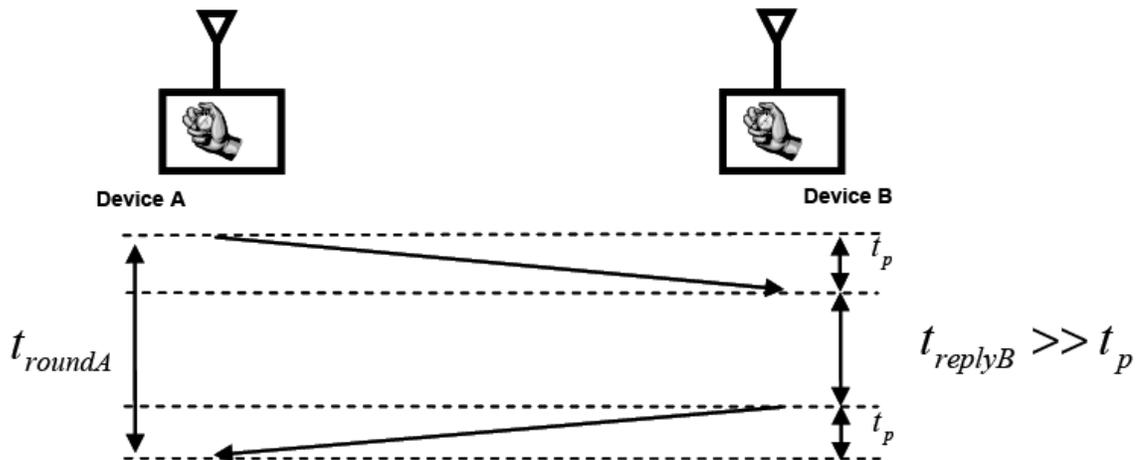
Figure 3.6: Two-way ranging of two devices. A range request message is sent from Device A to Device B. After a known delay (t_{replyB}), a response is sent back from Device B to Device A (from IEEE 802-15.4a 2007)

3.6 ULTRA WIDEBAND MERITS

UWB has several advantages compared to narrow-band ranging technologies. However it also has some disadvantages. These are described below.

3.6.1 Advantages

♦ With power spread over large bandwidth, frequency selective fading from materials/multipath is mitigated (Hoffman et al 2001)

♦ Minimal multipath cancellation effects

♦ Low energy density gives minimal interference to nearby systems and minimal RF health hazards

♦ Ranging – very fine range resolution

Multipath cancellation happens when a multipath signal arrives at the receiver partially or totally out of phase with the direct signal. The result is a reduced amplitude response. With short duration pulse signals, direct signals come and go before indirect signals arrive. This is why there are fewer multipath effects with UWB signals (Fontana 2006).

Since pulse duration is inversely related to bandwidth, short pulses mean that the bandwidth is quite large. With power spread over a large spectrum, the energy density (transmitted Watts of power per unit Hertz of bandwidth) is also low. Further, this will help prevent other systems from detecting UWB pulses.

3.6.2 Disadvantages

UWB, like other RF technologies, is still subject to the laws of physics for RF signals. Hence, it suffers from disadvantages similar to those of other RF technologies, such as trade-offs in SNR versus bandwidth, etc (Fontana 2006).

Another issue with UWB is its accuracy in ranging. While the UWB radios can provide relatively good accuracy in LOS baseline conditions, performance degrades linearly with distance and even more with non-line-of-sight (NLOS) measurements.

Finally, UWB measurements seem to be affected by a scale factor and bias, which is dependent on each specific radio pair used to measure the range. The scale factor and

bias must be determined for each radio pair used and must be calibrated or removed prior to using UWB data. Analysis of UWB range accuracy is discussed in Chapter 5.

3.7 FCC APPROVAL/NARROWBAND INTERFERENCE

UWB interference has long worried the GPS community. So, on September 1, 1998, the FCC began to study this problem by issuing a public Notice of Inquiry on UWB. In response to this Notice of Inquiry, the FCC received more than a thousand documents from numerous organizations hoping to revise Part 15 rules, which would allow for the unlicensed use of UWB technology. The FCC's response to this study was to allow UWB to operate over already used frequencies, rather than to cut out specific parts of the spectrum just for UWB use. However, UWB power levels must be low enough to ensure that operation would not cause performance degradation in existing devices. UWB's low power spectral density ensured minimal interference with existing users. Specific applications and user restrictions have been outlined in the FCC's First Report and Order (Reed 2005).

3.7.1 Equivalent Isotropically Radiated Power (EIRP)/PEAK Limits

FCC regulations divide UWB usage and set its rules based on three categories: communication and measurement systems, vehicular radar systems and imaging systems. Each category has its own designated spectral mask, while no modulation scheme restrictions have been put in place. Figure 3.7, below, shows FCC spectral mask limits for the three UWB categories.
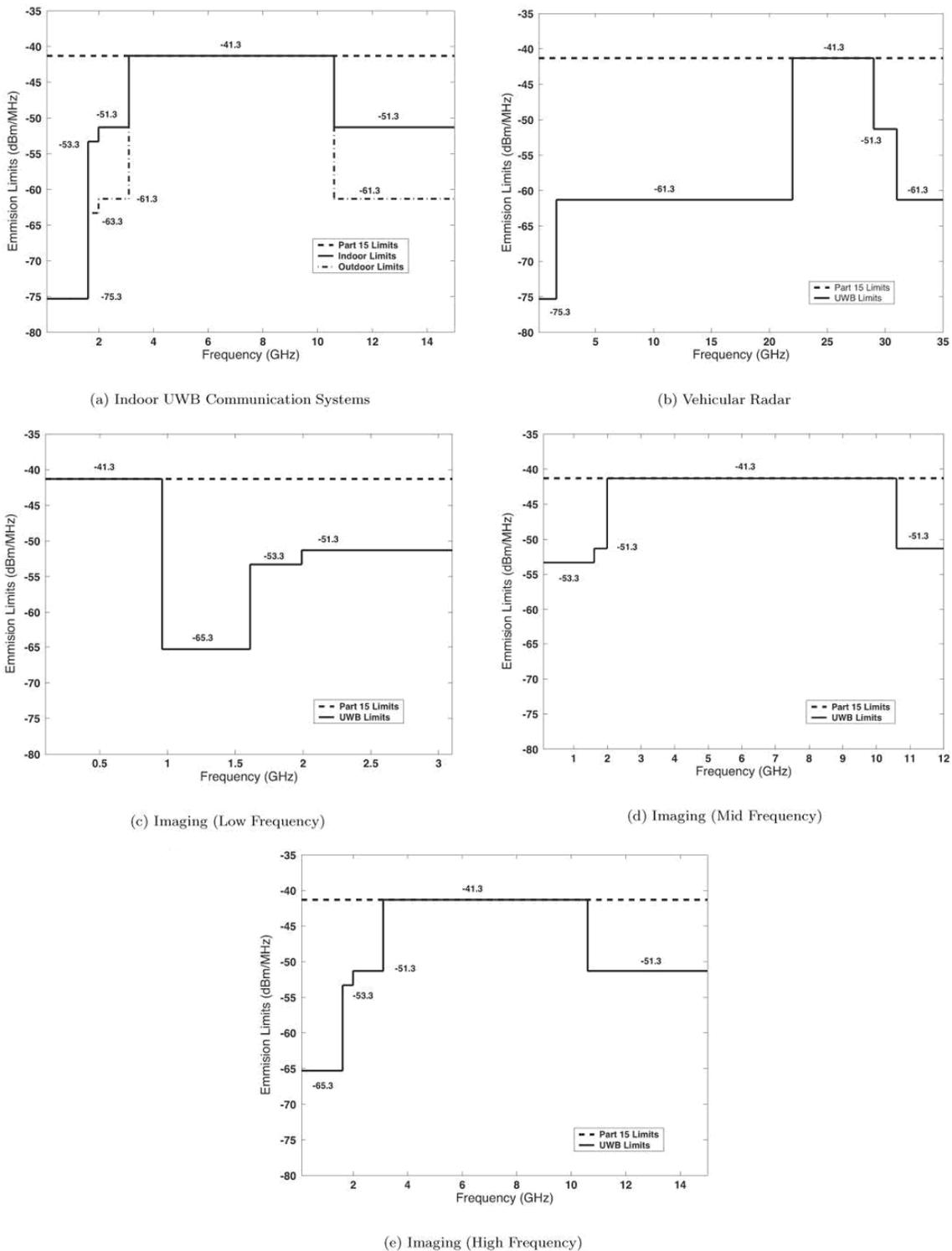
Figure 3.7: FCC Part 15 Spectral Mask for UWB for different applications (from FCC 2008)

Imaging systems encompass all ground penetrating radar, through-wall imaging, surveillance, and medical systems.

Vehicular radar systems are sensors placed on vehicles that detect objects on the ground. These systems use the bandwidth between 22 GHz and 29 GHz. A specific restriction is that the center frequency for these systems must exceed 24.075 GHz. Further, any signals sent above 30 degrees with respect to the horizontal must have its transmit energy level reduced by 25 dB.

Communication and measurement systems include wireless personal area network (WPAN), asset location applications, and more. These are further separated into indoor and outdoor categories. Indoor devices should not be used outdoors, while outdoor devices must be handheld devices.

For further details on FCC limits and restrictions on UWB devices, please refer to FCC (2008).

3.8 APPLICATIONS

There are numerous applications where UWB can give significant advantages, in terms of cost and performance. One of the main motivations was for high data rate applications, such as Wireless Personal Area Networks (WPAN), for short range data transfer.

The most common WPAN application is the de-cluttering of cables for multiple high-speed devices. Some at-home devices, such as televisions, CD and DVD players, projectors, printers, scanners, keyboards, etc, may use several cables. The use of so many cables is cumbersome and can pose safety concerns. Hence, UWB is a wireless, high-data rate connection alternative between several devices (Siwiac 2002).

People and asset tracking using UWB has enabled organizations and companies to efficiently monitor staff and equipment. Optimized management of staff, worker safety and security, and efficient tracking of inventory/equipment are just a few examples of how UWB can be used to save both time and money.

UWB is also increasingly being used for public safety personnel in rescues because this type of technology can help "see through" walls. This is particularly useful in hostage situations or fire/debris disaster areas. Not only is UWB being used for rescue operations, but its "see through" technology is being used for medical imaging inside of people and animals (Staderini 2002).

And more recently, UWB signals are being investigated for use as accurate and precise positioning systems. While research into this area is in its infancy, the potential for UWB positioning and navigation is growing because of UWB's ability for fine time/range resolution and robust performance in high multipath environments.

Other important applications include Obstacle Avoidance Radars for commercial aviation, Intrusion Detection Radars, Industrial RF Monitoring Systems, Unmanned Aerial Vehicle (UAV) and Unmanned Ground Vehicle (UGV) Data links, Tactical Handheld Radios, and more (Fontana 2006).

Finally, it is important to note that different UWB applications will use different parts of the spectrum. The type of application determines which part of the spectrum is used. This is why UWB advocates insist that the FCC should allow UWB signals to operate within a wide spectrum, even if it overlaps with important sections of the spectrum, such as the GPS spectrum (Reed 2005). In practice however, UWB transmission has been generally limited to a range of 3.1 GHz to 10.6 GHz, specifically to avoid interference with GPS and other essential services operating below 3.1 GHz (Time Domain 2008).

3.9 FUTURE DIRECTION

The FCC has allowed UWB technology to continue to develop under its First Note and Order issued in 2002. Two particular concerns for interference are GPS and air traffic control systems. However, rules and regulations stated in the First Note and Order may change as more extensive research into UWB is conducted.

An upcoming application of UWB is in medical imaging. By sending extremely short pulses into a person, UWB pulses would be able to detect movement of internal organs from a distance away from the patient. Other irregularities in the body, such as tumours, may also potentially be detected and UWB may be a cheaper alternative than CT or X-ray scans. Work is currently also being done to use UWB pulses to identify cancer cells (Bond et al 2003).

Location aware communications is a hybrid of communication and radar systems. From tracking firefighters in rescue operations, to soldiers in the battlefield, to students and staff in buildings, this new form of personnel tracking offers improvement to both safety and productivity. Assets, such as equipment or retail products, can also be tracked in an effort to thwart theft. Finally, location aware communication systems may even be extended for security applications, where intruders can be carefully monitored and tracked within the UWB network geographical area (Reed 2005).

Finally, UWB can also be used for channel sounding. Using its short pulses, it's possible to distinguish multipath signals and provide an improved understanding of the signal itself, multipath and other propagation effects.

3.10 GPS-UWB INTEGRATION

3.10.1 Motivation

Using UWB as a means of ranging and positioning is a promising area of research. Using UWB to augment GPS extends the capability of positioning and navigation in places where GPS typically falters; this is typically in indoor or hostile signal environments. UWB, on the other hand, is able to provide highly accurate ranges in these signal conditions. One setback that UWB positioning has is that it can only report relative positions, as opposed to the absolute positions that GPS offers. For these reasons, GPS and UWB are complementary systems. Combining these sensors for positioning draws the benefits from both, while diminishing the shortcomings of each separately. Work into this subject is in its initial stage, but preliminary results from several groups look promising, as discussed in a literature review in Section 3.10.3.

3.10.2 UWB Interference with GPS

While the FCC has set emission rules on UWB signals, there is still a fear of interference with GPS and other systems. For most cases, interference should not happen because the frequency band in which UWB operates is outside of the GPS band, however, there may possibly still be instances where having multiple UWB radios set up may increase the risk of GPS interference. An example of this would be "UWB hotspots" created by a host of UWB devices set up for indoor home entertainment networking purposes. And according to Marsh (2005), it is estimated that 98% of UWB use will be for such WPAN/wireless local area network (WLAN) use. Having a GPS receiver in the proximity of UWB hotspots may raise interference issues.

One particular simulation done by Nekoogar (2006) was to determine the density of UWB devices needed in the proximity of a GPS receiver, in order to cause interference to the receiver.
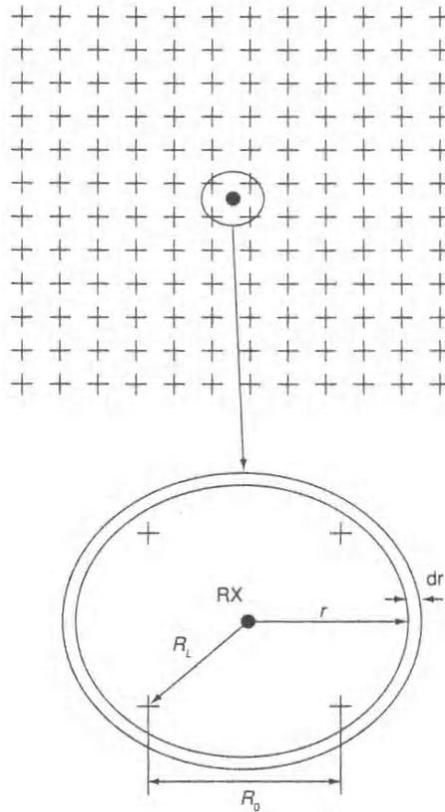
Figure 3.8: A dense network of UWB devices (shown as crosses) with one victim GPS receiver in the middle (shown as the black dot). This is representative of a possible UWB hotspot found in an urban area (from Nekoogar 2006).

Nekoogar (2006) calculates the total interference power at the GPS receiver, which is a function of the density of UWB devices, bandwidth of the receiver, wavelength, power spectral density of UWB, free-space distance and a path loss coefficient.

It is determined that with a density of 300 UWB sources per square km, GPS receiver acquisition would be difficult, while it would be difficult to track satellites at a UWB density of 1500 per square km (Nekoogar 2006).

Despite previous interference concerns from several companies and organizations, such as the FAA, Tem Innovations, US GPS Industry Council, American Airlines, the General Aviation Manufacturers Association, Stanford University, and United Airlines, UWB technology has been allowed to develop under rules set forth in the FCC's 2002 First

Report and Order (Nekoogar 2006). As UWB technology matures and interference worries diminish, the FCC may change its rule on UWB emissions in the future, but for now, the FCC seems content with current rules and regulations.

3.10.3 Current Research

UWB ranging used as an augmentation to GPS is a very new topic. As result, there are currently a limited number of groups and publications on this topic. UWB-GPS integration is still in early development, but several groups have come up with innovative methods to integrate the measurements and promising results have been seen.

Gonzalez et al (2007) uses a particle filter to combine GPS and UWB measurements in an indoor/outdoor track. Although UWB measurements are intermittent when the rover unit is far from the UWB beacon, improvements in positioning are still observed when the measurements are integrated. Tan and Law (2007) also show improvement with the addition of UWB measurements to GPS. However, accuracy is also a function of the location of the UWB beacons. And with UWB-GPS combined measurements, the estimation is found to be less sensitive to the initial guess of the position. Finally, Opshaug and Enge (2002) through simple simulation only have predicted horizontal improvements of 15% and 25% for an UWB-GPS over GPS-only and UWB-DGPS over DGPS-only, respectively. Nonetheless, these quantified results are based on simulation and thus, still need to be proven with the use of real data.

3.10.4 UWB-GPS Applications

UWB-GPS integration may result in numerous important applications. Because of UWB's ability to make measurements in high multipath environments, combining UWB with GPS allows for indoor navigation and positioning of anything from assets to people. From fire rescue, to tracking of personnel and equipment in companies, UWB augmentation with GPS is a means to increase safety, productivity and surveillance in the workplace. For outdoor applications, with a proper UWB network, positions can be made in urban canyons, valleys and even under heavy foliage. Surveys can be done in

forests or construction sites, where measurements from GPS or a total station may be difficult to obtain.

At this point, both GPS and UWB technologies have been fully described in relation to this thesis. Reasons and possible complications for UWB-GPS integration have also been discussed. In the following chapter, methods and equipment used to perform the actual integration are described.

CHAPTER 4: ESTIMATION METHODS AND EQUIPMENT

This chapter introduces implementation techniques and estimation methods of how GPS and UWB observations are used to produce a position solution. A basic review of least-squares is first given, followed by a detailed description of an alternative filter (to the standard Kalman filter) that is used to produce the results. Finally, all equipment that is used to collect data for this research concludes this chapter.

4.1 LEAST-SQUARES AND KALMAN FILTERING

The Kalman filter is a method of estimating the current state of a linear dynamic system corrupted by white noise. Using the Kalman filter, a user can incorporate previous measurements into current estimate to arrive at a more accurate position, velocity and time (PVT) estimate. This is assuming that the user's motion and clock errors can be modeled well enough over time. Least-squares can only deal with information from the current epoch and as result, can only estimate state variables from the same epoch. Least-squares is a special case of Kalman filtering. Furthermore, prediction of the future states of dynamic systems cannot be done with least-squares, unlike Kalman filtering.

4.2 INTEGRATION OF SENSOR INFORMATION

Another common use of the Kalman filter is combining two or more sensors' information together to output one single PVT solution. Sensors that are commonly added to GPS measurements include inertial sensors, dopplerometers, altimeters, speedometers, ultra wideband ranges, and more. Furthermore, the filter can continue to estimate a PVT solution when a GPS outage occurs. The overall solution is also seen to be "smoothed" over. For more details regarding the Kalman filter or its equations, please refer to Grewel (2001).

4.2.1 Loosely-Coupled Integration

In loosely-coupled integration, the PVT solutions of two or more sensors are first calculated by their own respective Kalman filters and then the solutions are combined to form a new solution. The advantage of loosely-coupled integration is the simplicity in the method, robustness (if one sensor fails, a solution is still maintained), processing time

and redundancy. A significant disadvantage is that a GPS solution is not possible when the user observes less than four satellites.

4.2.2 Tightly-Coupled Integration

In tightly-coupled integration, the measurements of two or more sensors are combined together and then put through one single Kalman filter to arrive at a single PVT solution. Tightly-coupled integration has all of loosely-coupled integration's benefits, plus generally higher accuracy, improved system performance by having one single Kalman filter and the ability to estimate a solution when the user observes less than four satellites. A disadvantage with this method is the increased state vector size, which leads to longer processing times.

Combined UWB-GPS solutions in this thesis have been estimated using tightly-coupled integration.

4.3 WEIGHTED LEAST-SQUARES

Least-squares is a method of finding a solution for an over-determined linear system. The goal of least-squares is to find the solution that results in a minimum value for the sum of squared residuals. The underlying assumption is that errors are normally distributed. The solution for a linear least-squares problem is unique.

Without proof, the state estimate $\hat{x}$ is

$$\hat{x} = (H^T P H)^{-1} H^t P l \tag{4.1}$$

where

$\hat{x}$ = vector of parameters

H = design matrix relating the observables to the parameters

P = weight matrix

l = vector of observations

For non-linear problems, linearization of the problem needs to be done through Taylor series expansion. A Jacobian design matrix needs to be calculated. Non-linear least-squares requires an initial guess of the unknowns and is an iterative process. The solution for a non-linear least-squares problem is not unique.

Without proof, the corrections to the initial approximate parameters are

$$\tilde{x} = (H^T PH)^{-1} H^T Pw \qquad (4.2)$$

where

$\tilde{x}$ = vector of corrections to the parameters

w = misclosure vector (difference between the actual and computed observations)

The initial guess of the parameters is then corrected by the $\tilde{x}$ term.

4.3.1 Vector of states/unknowns, $\hat{x}$

In basic GPS, 4 parameters are estimated: 3 position states and a receiver clock term, as shown in the following equation

$$\hat{x} = \begin{bmatrix} x \\ y \\ z \\ dT \end{bmatrix} \qquad (4.3)$$

where

x = x position unknown

y = y position unknown

z = z position unknown

dT = receiver clock error unknown

For single difference GPS RTK, the number of unknowns become 4 + n for one single epoch, where n is the number of satellites. Please refer to equation 4.4, below

$$\hat{x} = \begin{bmatrix} x & y & z & cdT & N^1 & N^2 & N^3 & N^4 \end{bmatrix}^T \text{ for 4 satellites} \tag{4.4}$$

where

N^i = ambiguity for i^{th} satellite

4.3.2 Weight Matrix, P

The corresponding weight matrix, P, which describes the variance-covariance between the states is

$$P = \sigma^2 C_x^{-1} \tag{4.5}$$

where

σ^2 = a priori variance factor

C_x = variance-covariance matrix of the unknowns

When all errors have the same variance and are uncorrelated, then $C_x = I$.

With single difference GPS RTK, the size of the P matrix would be $(4 + n)$ by $(4 + n)$ for one epoch, where n is the number of satellites. The matrix would describe the variance-covariance values for the 3 position, 1 receiver clock, and satellite ambiguity parameters.

4.3.3 Misclosure vector, w

This vector is the difference between the actual observations and the computed observations.

$$w = f(x,l) \tag{4.6}$$

or $\quad w^0 = f(x^0,l)$ using the initial guess of the parameters

4.3.4 Vector of Observations, l

For GPS, the vector of observations contains the satellites observations. For code DGPS, the vector would only contain a pseudorange from each satellite. For GPS RTK, the

vector would contain a pseudorange and carrier-phase measurement from each satellite, as follows:

$$l = \begin{bmatrix} pseudorange1 \\ . \\ pseudorange4 \\ carrier-phase1 \\ . \\ carrier-phase4 \end{bmatrix} \text{ for 4 satellites} \qquad (4.7)$$

With UWB augmented to GPS, the vector would look like

$$l = \begin{bmatrix} pseudorange1 \\ . \\ pseudorange4 \\ UWB\_range1 \\ UWB\_range2 \\ UWB\_range3 \\ carrier-phase1 \\ . \\ carrier-phase4 \end{bmatrix} \text{ for 4 satellites and 3 UWB ranges} \qquad (4.8)$$

4.3.5 Design Matrix H

The design matrix relates the observations to the parameters. The dimension of the matrix is n x m, where n is the number of observations and m is the number of parameters. For GPS, a typical design matrix would resemble Equation 4.9, below.

$$H = \begin{bmatrix} \dfrac{dl_i}{dx_r} & \dfrac{dl_i}{dy_r} & \dfrac{dl_i}{dz_r} & \dfrac{dl_i}{dcdT} \\ \dfrac{dl_j}{dx_r} & \dfrac{dl_j}{dy_r} & \dfrac{dl_j}{dz_r} & \dfrac{dl_j}{dcdT} \\ . & . & . & . \\ \dfrac{\dot{dl}_n}{dx_r} & \dfrac{\dot{dl}_n}{dy_r} & \dfrac{\dot{dl}_n}{dz_r} & \dfrac{\dot{dl}_n}{dcdT} \end{bmatrix}$$ (4.9)

where

c = speed of light

Since

$$l = Pseudorange = \sqrt{(x_{sat} - x_i)^2 + (y_{sat} - y_i)^2 + (z_{sat} - z_i)^2} + cdT + \varepsilon$$ (4.10)

then Equation 4.9 becomes

$$H = \begin{bmatrix} \dfrac{dl_i}{dx_r} & \dfrac{dl_i}{dy_r} & \dfrac{dl_i}{dz_r} & 1 \\ \dfrac{dl_j}{dx_r} & \dfrac{dl_j}{dy_r} & \dfrac{dl_j}{dz_r} & 1 \\ . & . & . & . \\ . & . & . & . \\ \dfrac{\dot{dl}_n}{dx_r} & \dfrac{\dot{dl}_n}{dy_r} & \dfrac{\dot{dl}_n}{dz_r} & 1 \end{bmatrix}$$

For single difference GPS RTK, the design matrix would have the following structure

$$H = \begin{bmatrix} \dfrac{dl_i}{dx_r} & \dfrac{dl_i}{dy_r} & \dfrac{dl_i}{dz_r} & 1 & 1 & 0 & 0 & 0 \\ . & . & . & 1 & 0 & 1 & 0 & 0 \\ & & & 1 & 0 & 0 & 1 & 0 \\ \dfrac{\dot{dl}_{i+3}}{dx_r} & \dfrac{\dot{dl}_{i+3}}{dy_r} & \dfrac{\dot{dl}_{i+3}}{dz_r} & 1 & 0 & 0 & 0 & 1 \end{bmatrix} \quad \text{for 4 satellites}$$ (4.11)

where the first 4 columns represent the 3 positions and 1 clock state, while the last 4 columns represent each satellite's ambiguity term

4.3.5.1 Special Case 1: GPS & UWB

In this thesis, UWB ranges are added into the filter as additional ranges. The only difference is that the UWB range equation does not contain a clock term, as seen in equation 4.12, below.

$$U = \sqrt{(x_{known} - x_i)^2 + (y_{known} - y_i)^2 + (z_{known} - z_i)^2} + \varepsilon \qquad (4.12)$$

So, $\dfrac{dU}{cdT} = 0$ and the design matrix becomes

$$H = \begin{bmatrix} \dfrac{dP_i}{dx_r} & \dfrac{dP_i}{dy_r} & \dfrac{dP_i}{dz_r} & 1 \\[2mm] \dfrac{dP_j}{dx_r} & \dfrac{dP_j}{dy_r} & \dfrac{dP_j}{dz_r} & 1 \\[2mm] \cdot & \cdot & \cdot & \cdot \\[1mm] \cdot & \cdot & \cdot & \cdot \\[2mm] \dfrac{dP_n}{dx_r} & \dfrac{dP_n}{dy_r} & \dfrac{dP_n}{dz_r} & 1 \\[2mm] \dfrac{dU_a}{dx_r} & \dfrac{dU_a}{dy_r} & \dfrac{dU_a}{dz_r} & 0 \\[2mm] \dfrac{dU_b}{dx_r} & \dfrac{dU_b}{dy_r} & \dfrac{dU_b}{dz_r} & 0 \\[2mm] \dfrac{dU_c}{dx_r} & \dfrac{dU_c}{dy_r} & \dfrac{dU_c}{dz_r} & 0 \end{bmatrix} \qquad (4.13)$$

where the bottom 3 rows in the matrix of equation 4.13, above, correspond to UWB range observations.

4.3.5.2 Special Case 2: UWB-only

Under hostile or indoor conditions, GPS occasionally suffers from complete satellite outages. This scenario will be presented in Section 6.3.4 when a UWB-GPS rover is

brought indoors. GPS requires a minimum of 4 observations to estimate the 3 positions and 1 receiver clock term. Because UWB does not have this clock term, it is able to maintain a position solution with only 3 ranges. The filter that is used to process GPS-only or GPS & UWB measurements can handle these instances by fixing the clock term when GPS is absent. In this case, the design matrix looks like

$$H = \begin{bmatrix} \dfrac{dU_a}{dx_r} & \dfrac{dU_a}{dy_r} & \dfrac{dU_a}{dz_r} & 0 \\ \dfrac{dU_b}{dx_r} & \dfrac{dU_b}{dy_r} & \dfrac{dU_b}{dz_r} & 0 \\ \dfrac{dU_c}{dx_r} & \dfrac{dU_c}{dy_r} & \dfrac{dU_c}{dz_r} & 0 \\ 0 & 0 & 0 & 1 \end{bmatrix} \tag{4.14}$$

where the first 3 columns are the 3 position states and the last column being the fixed clock state.

Further, with UWB-only processing, the misclosure term for the clock is set to 0 m and the measurement noise value is set to 1 m.

4.4   SQUARE-ROOT   FILTERING   USING   THE   BIERMAN-THORNTON ALGORITHM

The Kalman filter is the standard method for estimating a kinematic GPS carrier phase float solution. However, in the early developments of the Kalman filter, it was evident that there were instances which caused the Kalman filter to become unstable and diverge. To overcome such instability, a class of Kalman filters known as square-root filters was developed.

Square-root filtering using modified Cholesky factors, also commonly known as the Bierman-Thornton Unit Upper Triangular and Diagonal (UD) algorithm, is an alternative to the standard Kalman filter. This factorization not only generates a more stable filter, but this approach also results in notable computational savings and increased machine

precision. With the augmentation of an additional sensor using tightly-coupled integration, the size of the matrices in the filter increases leading to increased processing times and computation burden. As a bonus, this implementation results in a float solution that fits more naturally into the processing scheme used by the Least-Squares AMBiguity Decorrelation Adjustment (LAMBDA) method of ambiguity resolution which requires access to the UD factorization of the covariance matrix of the float ambiguities. However, resolving the integer ambiguities is beyond the scope of this thesis.

4.4.1 Kalman Filter Issues

The class of Kalman filtering known as square-root filtering first appeared in the 1960's. Computational issues, such as numerical stability, roundoff errors and asymmetry of the covariance matrix of the states, P, can all lead to filter divergence and these were the reasons for the development of square-root filtering. These issues were much more problematic in the past than they are today with development of faster computers and the routine use of double precision arithmetic. Still, there are instances where divergence has been reported from numerical instability and ill-conditioned cases (Grewel 2001).

4.4.2 Error Propagation within the Kalman Filter

The standard Kalman filter can be represented by two loops, the estimation loop, which computes the state estimate $\hat{x}$, and the gain loop, which calculates the covariance of the state estimate P. Kalman gain, K, is estimated in the gain loop, but acts as an error correction feedback in the estimation loop. As long as the gain is accurate, this feedback into the estimation loop should correct for errors in the state estimate that are caused from roundoff errors, noise and *a priori* estimation errors. However, no such feedback exists in the gain loop and so, any errors, such as from computer roundoff, accumulate and go unchecked in the computation of the state variance-covariance. Furthermore, there are about twice as many computer roundoff operations in the gain loop, compared to the estimation loop of the Kalman filter (Grewel 2001). Calculation of the variance-covariance of the states is the part of the Kalman filter where more stable factorization methods will be most beneficial due to the lack of gain loop feedback as previously explained.

4.4.3 Factorization Methods

There are several factorization methods of the variance-covariance matrix of states:

    1) Products

        a)   Triangularization (QR decomposition)

           i) Givens rotations

           ii) Householder transformations

        b)   Gram-Schmidt orthonormalization

    2) Square-root and UD filters

        a)   Carlson-Schmidt algorithm

           i) Cholesky factors

        b)   Bierman-Thornton algorithm

           i) Modified Cholesky factors

    3) Others

Currently, the preferred method of factorization is the Bierman-Thornton UD factorization (Grewel 2001). This method uses modified Cholesky factors of the state variance-covariance matrix. It is classified as a square-root filter, but technically, there are no square-root operations in the implementation.

4.4.4 Modified Cholesky Factors

Factorization of a matrix is the process of breaking down a matrix into a set of matrices. In the case of Bierman-Thornton UD factorization, the variance-covariance matrix, P, is broken down into a set of three matrices. As long as the variance-covariance matrix is positive definite, the factorization of UDU^T of the matrix can be represented by Equation 4.15, below.

$$\begin{pmatrix} p_{11} & p_{21} & p_{31} \\ p_{12} & p_{22} & p_{32} \\ p_{13} & p_{23} & p_{33} \end{pmatrix} = \begin{pmatrix} 1 & u_{12} & u_{13} \\ 0 & 1 & u_{23} \\ 0 & 0 & 1 \end{pmatrix} \begin{pmatrix} d_{11} & 0 & 0 \\ 0 & d_{22} & 0 \\ 0 & 0 & d_{33} \end{pmatrix} \begin{pmatrix} 1 & u_{12} & u_{13} \\ 0 & 1 & u_{23} \\ 0 & 0 & 1 \end{pmatrix}^T \qquad (4.15)$$

This UDU^T factorization replaces the need to propagate the state variance-covariance matrix in the Kalman filter. The state variance-covariance matrix is never explicitly computed since the UDU^T factors are always propagated in each computational step.

4.4.5 Sequential Processing

The UD filter is only capable of incorporating scalar observations, meaning that the observations must be uncorrelated for the solution to be rigorous. GNSS double-differenced phase observations are inherently mathematically correlated, which suggests why a UD carrier-phase float filter has not been reported in previous literature. This limitation can be overcome by diagonalizing the observation covariance matrix; thus, decorrelating the components of the matrix. Although not initially intuitive, forming arbitrary linear combinations of the observations will not affect the integer nature of the estimated ambiguities provided we continue to estimate ambiguities corresponding to the original double-differences. For example, the design matrix, H, prior to decorrelation of the measurements has the form

$$H = [H^* \quad \lambda I] \tag{4.16}$$

where H^* are the usual double-difference direction cosines. The decorrelation procedure results in a factorization of measurement noise, R, into $U_R D_R U_R^T$ factors and design matrix H is replaced with

$$H' = U_R^{-1} H = [U_R^{-1} H^* \quad \lambda U_R^{-1}] \tag{4.17}$$

Notice that the right hand side of the new design matrix, in Equation 4.17, is no longer a wavelength scaled identity matrix, but a wavelength scaled inverse Cholesky factor. This shows that the original double difference ambiguities continue to be estimated even after measurement decorrelation. Further details of the measurement decorrelation procedure are discussed later in the chapter.

With the observations uncorrelated, sequential processing of the measurements is done. One of the major advantages of one-at-a-time processing is that it allows for flexibility in the size of matrices in the filter. For example, with simultaneous processing of all measurements at one time epoch for the conventional Kalman filter, the filter must produce a suitable design matrix and covariance matrix of measurement noise to fit all potential combinations of measurements. Consequently, the filter must also be able to perform corresponding operations with varying matrix dimensionality. With sequential processing, the filter can skip measurements that are not available, only processing those that are - one at a time. Essentially, most of the processing is an addition or a multiplication of scalar values.

4.4.6 LAMBDA

Centimetre-level accuracy can only be achieved when the ambiguities of a GPS double difference solution have been estimated. Without knowing the integer estimate of the ambiguities, only sub-metre level accuracy can be attained (ie. RTK float solution). LAMBDA, or Least-squares AMBiguity Decorrelation Adjustment, is an integer estimate of GPS double difference ambiguities (de Jonge & Tiberius 1996). Although LAMBDA is not performed in this thesis, it is planned for future work. This is one of several reasons why the Bierman-Thornton algorithm is chosen over standard Kalman filtering.

The first step in the LAMBDA algorithm is to decorrelate the double differenced ambiguities before the actual integer estimate of ambiguities is done. The decorrelation requires that the variance-covariance matrix of the ambiguity states be broken down into LDL^T (or equivalently UDU^T factors), which the Bierman-Thornton algorithm does.

To ensure the usefulness of this factorization, the state vector and variance-covariance matrix must be arranged so that position states are estimated first, followed by ambiguity states (de Jonge et al 1996) as shown in Equation 4.18.

$$\hat{x} = [\hat{b} \quad \hat{a}]^T \tag{4.18}$$

$$P_{\hat{x}} = \begin{bmatrix} P_{\hat{b}} & P_{\hat{b}\hat{a}} \\ P_{\hat{b}\hat{a}} & P_{\hat{a}} \end{bmatrix} \qquad (4.19)$$

where

$\hat{x}$ = states

$\hat{b}$ = position states

$\hat{a}$ = are ambiguity states

P = variance-covariance matrix of the states

In Bierman-Thornton, P is factored into UDU^T matrices. Noticing that $P_{\hat{x}}$ in Equation 4.19 contains $P_{\hat{a}}$ in the lower right partition of the matrix, the factorization of $P_{\hat{x}}$ will result in $U_{\hat{a}}$ and $D_{\hat{a}}$ factors of the ambiguity states. These $U_{\hat{a}}$ and $D_{\hat{a}}$ factors, already inherently calculated through the Bierman-Thornton algorithm, are exactly what is passed onto LAMBDA.

So, it is easy to see how the Bierman-Thornton algorithm, when applied to a GPS double differenced float solution, naturally fits into the LAMBDA ambiguity resolution algorithm. This gives an overall efficiency in the process of going from a float solution to a fixed solution.

There are further computational savings through the fact that Bierman-Thornton only factorizes the variance-covariance matrix only once when the number of ambiguity states is constant. The factors U and D are propagated through the filter. The variance-covariance matrix is only factorized again if there are changes to the makeup ambiguity states. As for LAMBDA, factorization of the variance-covariance matrix of the ambiguity states happens at every epoch if the variance-covariance matrix is not already decorrelated. This redundant factorization is unnecessary and can be avoided by using Bierman-Thornton UD factorization.

4.4.7 Bierman-Thornton Algorithm

$$\hat{\mathbf{x}}_k^-, \mathbf{P}_k^-$$

Compute Kalman gain:
$$\mathbf{K}_k = \mathbf{P}_k^- \mathbf{H}_k^T (\mathbf{H}_k \mathbf{P}_k^- \mathbf{H}_k^T + \mathbf{R}_k)^{-1}$$

Prediction:
$$\hat{\mathbf{x}}_{k+1}^- = \mathbf{\Phi}_k \hat{\mathbf{x}}_k$$
$$\mathbf{P}_{k+1}^- = \mathbf{\Phi}_k \mathbf{P}_k \mathbf{\Phi}_k^T + \mathbf{Q}_k$$

Updating:
$$\hat{\mathbf{x}}_k = \hat{\mathbf{x}}_k^- + \mathbf{K}_k (\mathbf{z}_k - \mathbf{H}_k \hat{\mathbf{x}}_k^-)$$

Compute updated variance matrix:
$$\mathbf{P}_k = (\mathbf{I} - \mathbf{K}_k \mathbf{H}_k) \mathbf{P}_k^-$$
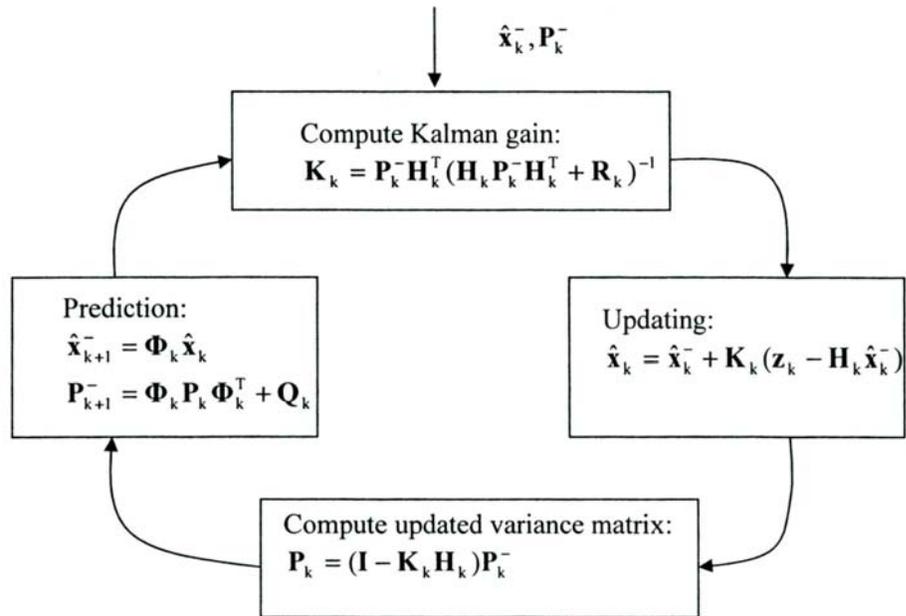
Figure 4.1: Standard Kalman filter algorithm (from Gao & Sideris 2005)

$$\hat{\mathbf{x}}_k^-, \mathbf{P}_k^-$$

Compute Kalman gain:
$$\mathbf{K}_k = (\mathbf{U}_k^- \mathbf{D}_k^- \mathbf{U}_k^{-T}) \mathbf{H}_k^T (\mathbf{H}_k (\mathbf{U}_k^- \mathbf{D}_k^- \mathbf{U}_k^{-T}) \mathbf{H}_k^T + \mathbf{R}_k)^{-1}$$

Prediction:
$$\hat{\mathbf{x}}_{k+1}^- = \mathbf{\Phi}_k \hat{\mathbf{x}}_k$$
$$(\mathbf{U}_{k+1}^- \mathbf{D}_{k+1}^- \mathbf{U}_{k+1}^{-T}) = (\mathbf{\Phi}_k \mathbf{U}_k) \mathbf{D}_k (\mathbf{U}_k^T \mathbf{\Phi}_k^T) + \mathbf{Q}_k$$

Updating:
$$\hat{\mathbf{x}}_k = \hat{\mathbf{x}}_k^- + \mathbf{K}_k (\mathbf{z}_k - \mathbf{H}_k \hat{\mathbf{x}}_k^-)$$

Compute updated variance matrix:
$$(\mathbf{U}_k \mathbf{D}_k \mathbf{U}_k^T) = (\mathbf{I} - \mathbf{K}_k \mathbf{H}_k)(\mathbf{U}_k^- \mathbf{D}_k^- \mathbf{U}_k^{-T})$$
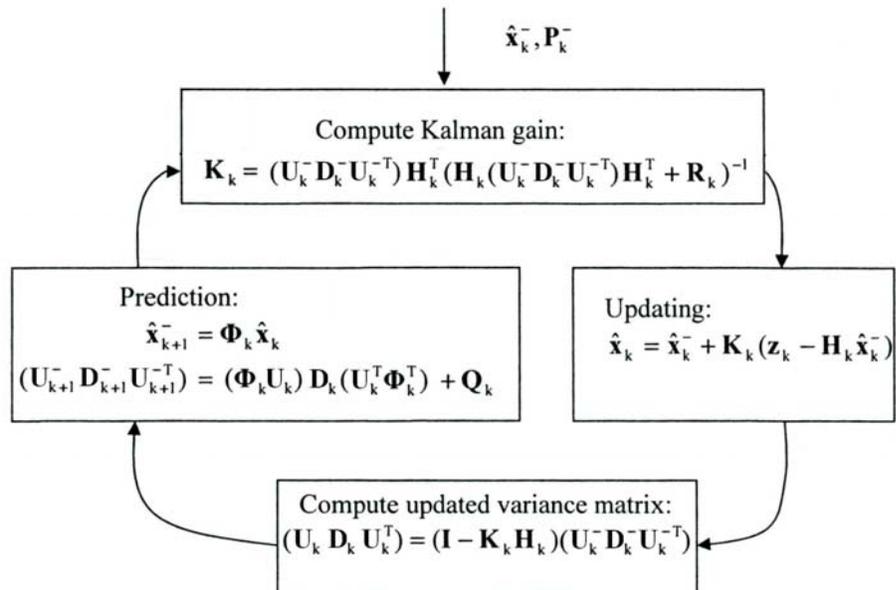
Figure 4.2: Square-root filter using Bierman-Thornton UD factorization

4.4.7.1 Bierman Observational Update

The standard Kalman filter loop is shown in Figure 4.1. The Bierman observational update algorithm begins with the updating of the variance-covariance matrix of the states, P, which is seen in Figure 4.2, above. For convenience, this updating of the variance-covariance matrix, P, is repeated again in Equation 4.20.

$$P_k = P_k^- - P_k^- H_k^T (H_k P_k^- H_k^T + R_k)^{-1} H_k P_k^-$$
(4.20)

If the measurements are decorrelated, then the measurements can be processed sequentially. So, if

$$\beta = H_k P_k^- H_k^T + R_k, \qquad \text{(where } \beta \text{ is a scalar)}$$

$$P_k^- = U^- D^- U^{-T}, \text{ and}$$

$$P_k = U^+ D^+ U^{+T},$$

then substituting β, P_k^- and P_k into equation 4.20 yields

$$U^+ D^+ U^{+T} = U^- D^- U^{-T} - \beta^{-1} U^- D^- U^{-T} H_k^T H_k U^- D^- U^{-T}$$
(4.21)

Regrouping some of the terms in equation 4.21 gives

$$U^+ D^+ U^{+T} = U^- [D^- - \beta^{-1}(D^- U^{-T} H_k^T)$$

$$(D^- U^{-T} H_k^T)^T] U^{-T}$$
(4.22)

Noticing that the square bracketed term in equation 4.22 is symmetric, then it too can be factored into UDU^T as shown in Equation 4.23.

$$[D^- - \beta^{-1}(D^- U^{-T} H_k^T)(D^- U^{-T} H_k^T)^T] = \overline{U}\,\overline{D}\,\overline{U}^T \tag{4.23}$$

Substituting Equation 4.23 back into Equation 4.22 gives

$$U^+ D^+ U^{+T} = U^- \overline{U}\,\overline{D}\,\overline{U}^T U^{-T}$$
$$= (U^- \overline{U})\overline{D}(U^- \overline{U})^T \tag{4.24}$$

So, the Bierman observational update solution is $U^+ = (U^- \overline{U})$ and $D^+ = \overline{D}$. These factors are carried forward into the state variance-covariance prediction step, shown below as the Thornton temporal update.

4.4.7.2 Thornton Temporal Update

The conventional state variance-covariance prediction step is as follows

$$P_{K+1}^- = \Phi_K P_K \Phi_K^T + Q_K \tag{4.25}$$

If the solution of the Bierman observation update is substituted into Equation 4.25, then

$$P_{K+1}^- = \Phi_K (U^+ D^+ U^{+T})\Phi_K^T + Q_K$$
$$= (\Phi_K U^+)D^+ (\Phi_K U^+)^T + Q_K \tag{4.26}$$

If the process noise matrix, Q_k, is not diagonal, it may be beneficial to diagonalize Q_k by factorizing Q_k into UDU^T terms and then making the following substitutions:

$$Q_k = D_k$$
$$G' = GU_k$$

Diagonalizing Q_k will reduce the net computational complexity.

4.4.7.3 Sequential Processing

Sequential processing can only be done if the measurements are decorrelated. The decorrelation of the measurements is a simple process, but must be done on GPS double differenced observations since they are inherently correlated. To decorrelate the measurements, the measurement noise matrix, R, must be factored into the form $R = U_R D_R U_R^T$. Then, the following substitutions are made:

$$R' = D_R$$

$$H' = U_R^{-1} H$$

$$z' = U_R^{-1} z$$

where

R = measurement noise

H = design matrix

z = vector of measurements

The measurements are now uncorrelated and have unit variance.

Once the decorrelation is done, sequential processing of the measurements can be done. We return to the computation of the Kalman gain, but now, $HPH^T + R$ is a scalar value since H is 1xn, P is nxn, and H^T is nx1, so hence, HPH^T is 1x1 in dimension. It is important to note that H is the row vector corresponding to the measurement being done, and similarly, R is the diagonal element corresponding to the current measurement.

$$K_{nx1} = P_{nxn} (H^T)_{nx1} [H_{1xn} P_{nxn} (H^T)_{nx1} + R_{1x1}]^{-1} \qquad (4.27)$$

Updating the estimates sequentially, we have

$$\hat{x}_{nx1} = \hat{x}_{nx1}^- + K_{nx1} (z_{1x1} - H_{1xn} \hat{x}_{nx1}^-) \qquad (4.28)$$

Finally, the variance-covariance matrix can be updated,

$$P_{nxn} = (I_{nxn} - K_{nx1}H_{1xn})P_{nxn}^{-} \tag{4.29}$$

Equations 4.27 to 4.29 are repeated for each measurement in that time epoch.

4.4.8 Bierman-Thornton Results

Numeric results between the standard Kalman filter and Bierman-Thornton algorithm are identical. However, the Bierman-Thornton algorithm produces a more stable filter performance, as well as increased machine precision and notable computational savings. Table 4.1, below, shows the operation counts, measured in flops, for the Bierman-Thornton execution.

Table 4.1: Operation Counts for Procedures within the Bierman-Thornton algorithm (from Grewel & Andrews 2001)

Procedure	Operation Counts (flops)	Notes
$P = UDU^T$	$\dfrac{2}{3}m^3 + \dfrac{1}{2}m^2 - \dfrac{5}{6}m$	Matrix is mxm
$U \rightarrow U^{-1}$	$\dfrac{1}{6}m^3 - \dfrac{1}{2}m^2 + \dfrac{1}{3}m$	Matrix is mxm
Measurement Decorrelation	$\dfrac{2}{3}l^3 + l^2 - \dfrac{5}{3}l + \dfrac{1}{2}l^2 n - \dfrac{1}{2}ln$	H-matrix is lxn
Sequential Processing	$\dfrac{2}{3}l^3 + l^2 - \dfrac{2}{3}l + \dfrac{1}{2}l^2 n + 2l$ $+ n\dfrac{1}{2}ln^2$	P-matrix is nxn l-measurements
Bierman Algorithm	$2n^2 + 7n + 1$	P-matrix is nxn
Thornton Algorithm	$n(n-1)(4n+3p-1)/2$ $+ p(p-1)(3n+p+4)/6$	P-matrix is nxn Q-matrix is pxp

For example, the computational saving by implementing measurement decorrelation and sequential processing is

$$\frac{1}{3}l^3 - \frac{1}{2}l^2 + \frac{7}{6}l - \ln + 2l^2n + \ln^2 \text{ flops} \qquad (4.30)$$

where

l = number of measurements

n = number of states

Please refer to Grewel & Andrews (2001) for further details on operation count calculations.

The float solution obtained from the estimation, results in a state variance-covariance matrix in a form easily adaptable to LAMBDA. Because the variance-covariance matrix of the ambiguity states is of the form UDU^T, these factors can be directly passed onto LAMBDA for integer ambiguity estimation.

4.4.9 Concluding Remarks on Square-Root Filtering

Using the Bierman-Thornton UD square-root filtering algorithm has several advantages over the conventional Kalman filter. By implementing a few straight forward changes to the standard filter, square-root filtering allows for a more stable filter with less chance of divergence from known issues like computer roundoff and asymmetrical state variance-covariance matrices. In addition, this algorithm intrinsically factorizes the variance-covariance matrix into a unit triangular and diagonal matrix. Because this filter provides only a float solution, other algorithms, such as LAMBDA, will need to be used to solve for the integer ambiguities. The resulting unit triangular matrix from the square-root filter can be directly used into LAMBDA since the first step in this procedure is to decorrelate the ambiguity states into UDU^T or LDL^T factors. The overall process of going from a float solution to a fixed solution is resultantly more efficient. Furthermore, factorization of the variance-covariance matrix of the ambiguity states is only done once and the UD factors are propagated through the filter. The factorization only happens

again if the ambiguity states change. This contrasts with LAMBDA, where factorization of the ambiguity states happens at every epoch regardless of changes in the ambiguity states or not. This further adds to the computational benefit and efficiency of the Bierman-Thornton method.

Please note that LAMBDA and ambiguity resolution is not done in this thesis; however, it is listed as one of the items that need to be accomplished for future work (Section 8.1) and hence, is one of the reasons in choosing this implementation method.

4.5 EQUIPMENT

This following section reviews equipment used in tests described in Chapters 5-7.

4.5.1 Trimble R8 GNSS Receivers

For all tests in this research involving GPS, Trimble R8 GNSS multi-channel, multi-frequency receivers are used. These receivers are capable of receiving multiple signals from multiple navigation systems (such as GPS L2C, GPS L5, GLONASS L1/L2, etc); however, only GPS L1 signals are used for this research. For details regarding Trimble R8 GNSS receivers, please refer to Trimble (2008).

4.5.2 Multispectral Solutions (MSS) Ranging Radio system

One of the sets of UWB radios used is from Multispectral Solutions (MSS). These radios use round trip time-of-flight to accurately measure the distance between two or more radios. Please refer back to Section 3.5.4 for an explanation regarding two-way raging. With one single range measurement, accuracies of 0.152 m can be attained; however, with multiple readings, accuracy can be improved to up to 0.038 m. The manufacturer stated LOS ranging capability is 600+ m with 0.30 m accuracy when the radios are 1 m off the ground. However, when modified to comply with Commerical Part 15 regulations, the demonstrated measurement performance is 50+ m for omni-directional antennas and 300+ m with gain antennas (Foster 2007). Figure 4.3, below, is a picture of MSS UWB radios.

Figure 4.3: Multispectral Solutions (MSS) UWB radios

4.5.3 Time Domain (TD) PulsON 210 Radios

The other set of UWB radios used for this research are the Time Domain (TD) PulsON 210 development kit radios as shown in Figure 4.4, below. The technical specifications for the UWB radios are listed in Table 4.2.

Table 4.2: Technical Specifications of Time Domain PulsON 210 UWB radios (after Time Domain, 2005)

System Type:	Impulse UWB	Network Configuration:	Application dependent
Pulse Shape:	Gaussian Monocycle	Implementation:	SiGE
Modulation Scheme:	PPM/PAM	Data Rate:	9.6 Mbps @ 20 m
Band Plan:	3.1-10.6 GHz	Range:	Up to 140 m
Error Correction Coding Scheme:	N/A	Total Power Dissipation:	550 mW
Spreading Scheme:	Time Hopping & Integration	Bit Error Rate:	10^{-9}
MAC Layer:	Time Hopping, PN Codes		

Figure 4.4: Time Domain PulsON 210 UWB Radios

4.5.4 Time Synchronization of Different Sensors

As with all two-way ranging systems, it is necessary to have time synchronization between all systems. Before GPS measurements and UWB ranges can be compared and integrated, both systems need to be logging in the same time frame. For all tests, both systems use GPS time. This is not a problem for the Trimble R8 receivers as the receivers' time is automatically synchronized with GPS time via the satellites, but the data logged from the UWB radios have to be time synchronized with GPS time. To accomplish this, the time on a laptop is connected to the GPS receiver and then subsequently, laptop time is synchronized with GPS time. Since the UWB radio logs its data into the laptop, the UWB data is time matched with the synchronized GPS laptop time.

4.5.5 UWB-GPS Co-Axial Mount

To connect the UWB radio and the GPS receiver onto the same platform, a UWB-GPS antenna mount was built. The mount prototype is designed so that the phase centers of both systems are vertically co-linear. Further, to ensure minimal multipath, attenuation or other unwanted propagation effects from the mount, it is made of clear, hard plastic material. The UWB-GPS mount is shown in Figure 4.5, below.

Figure 4.5: UWB-GPS co-axial mount

GPS, UWB and methods to integrate UWB-GPS have been described. While GPS is a well-studied technology and its characteristics including accuracy and precision, are well documented, UWB used for positioning, on the other hand, is a newer concept. Hence, the next chapter attempts to study certain UWB characteristics, including quantifying UWB accuracy and precision.

CHAPTER 5: UWB RANGE VERIFICATION

In this chapter, UWB range assessments are conducted on Time Domain (TD) and Multispectral Solutions (MSS) radios. Indoor and outdoor range tests are performed on both sets of radios. Attenuation, fading and multipath effects are studied. Once UWB range accuracy and reliability have been verified, single and multiple UWB ranges are then employed to augment and/or replace GPS, which will discussed in the following chapters.

5.1 INDOOR RANGE VERIFICATION TESTS

Indoor testing of the TD and MSS radios is conducted within the engineering buildings at the University of Calgary. Truth distances are measured three independent times using a tape measure. Once the tape measure distances are confirmed three times, a marker is placed on the floor. The UWB radios are placed at the marked locations and ranges are collected. UWB collected ranges are then compared to the truth ranges at various distances.

5.1.1 Time Domain UWB Radio Indoor Test

Both LOS and NLOS measurements are made for this test. LOS distances of 5 m, 10 m, 15 m, 20 m and 25 m are measured out three times using a tape measure and NLOS distances of 5 m are made through a door and piece of plywood. The piece of plywood is unglazed and 1.5 cm thick. LOS distances greater than 25 m are difficult to assess due to the limitation that TD radios' power source is an electrical cord (and extension cords when available) plugged into an electrical wall socket. Once these distances have been set out and marked on the floor, the UWB radios are placed on the markers and ranges are collected for approximately 10 minutes at each point.

5.1.1.1 Observations

The number of observations per every 100 s ranged from over 430 at 5 m to 109 at 25 m. Since measurement duration is slightly different at each point, the number of observations has been standardized to show the number of observations per every 100 s, as opposed to total number of observations which is dependent on measurement duration.

As seen in Figure 5.1, below, the number of observations logged is inversely proportional to range.
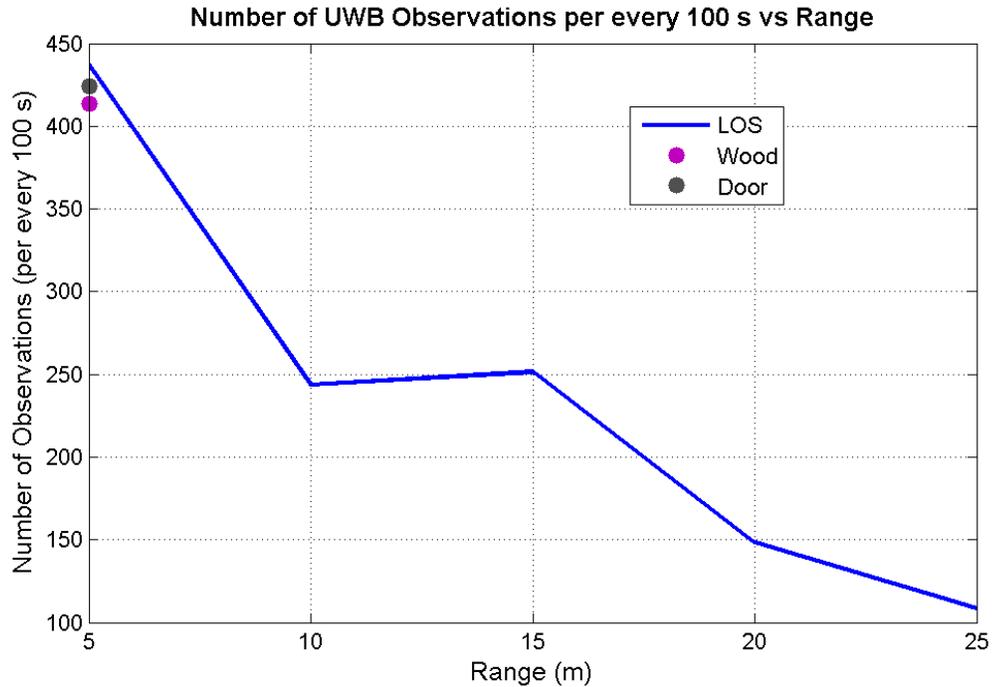
Figure 5.1: Number of measurements made by the TD radio per every 100 seconds plotted against range. The blue line indicates LOS measurements, while the purple and black dot represent measurements made through a piece of wood and door, respectively.

The reason for this is likely due to signal power decreasing or increasing attenuation as the distance between the two radios increases.

5.1.1.2 Outliers

Outliers in the measurements need to be removed prior to further analysis of the data. For static data, a 2σ (95% confidence interval) and 3σ (99% confidence interval) removal is sufficient for removing erroneous data. The first step is to calculate the mean and standard deviation of the sample and then compare each measurement to the 2σ value. If the absolute difference between the observation and average is more than two times the standard deviation, then the observation is removed.

Following this, a new average and standard deviation is calculated and now a 3σ value (99% confidence interval) is compared to each observation. If the absolute difference between the observation and the mean is outside the bounds of three times the standard deviation, then the observation is removed. This is repeated for each measurement distance.

Figure 5.2, below, shows a histogram of the ranges at each measurement distance prior to outlier removal. Blatant outliers are circled in red.
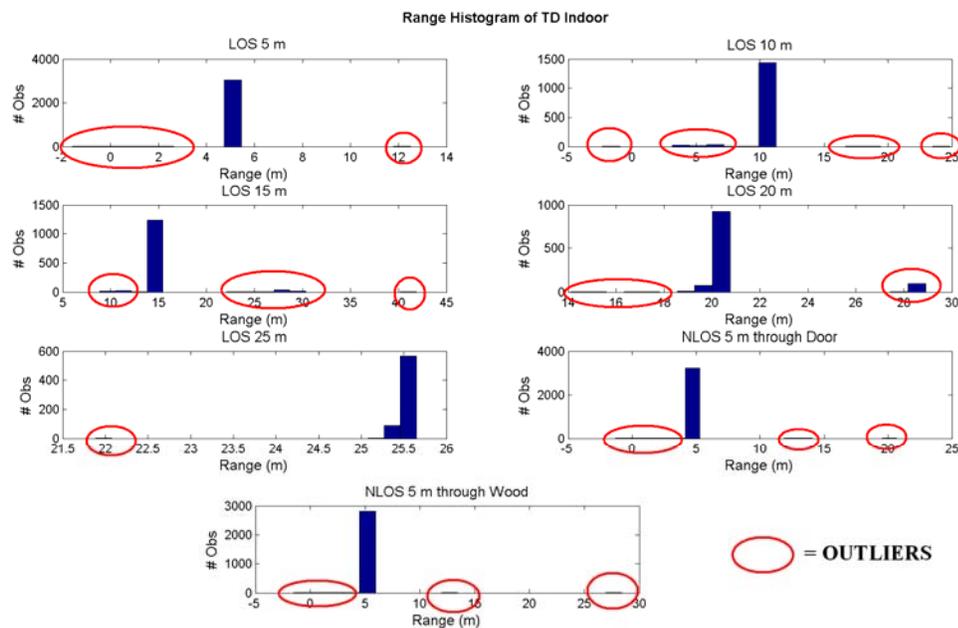
Figure 5.2: Range Histogram of Time Domain UWB radios indoors. The red circles are outliers.

The percentage of outliers range from just under 6% at 20 m, to over 14% at 25 m. Although there is a huge spike in the number of outliers at 25 m, the outlier results are not strong enough to infer a correlation trend. Please refer to Figure 5.3.
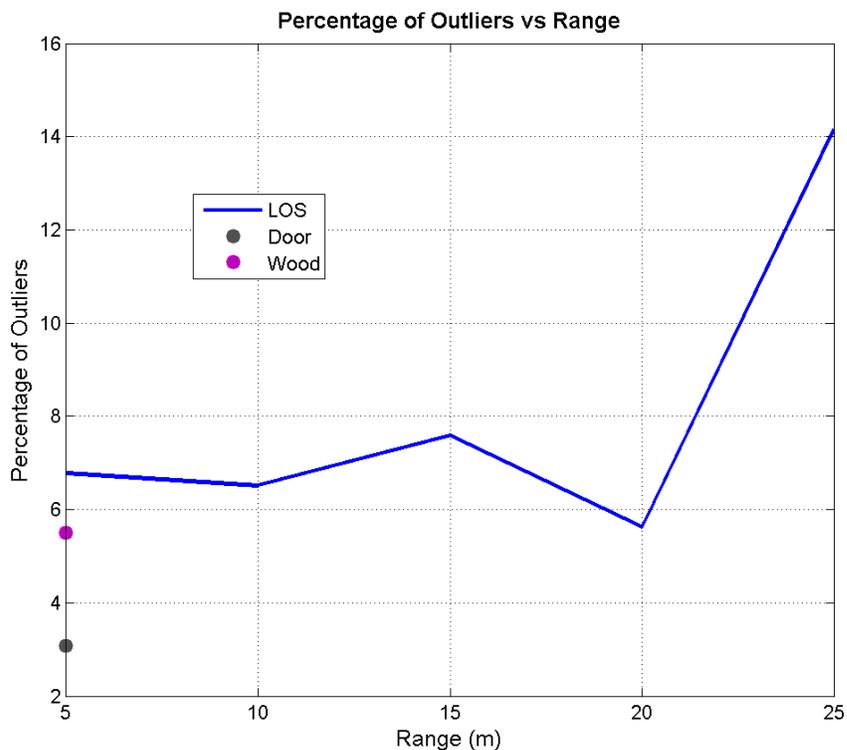
Figure 5.3: Percentage of outliers removed from the data for TD measurements.

5.1.1.3 Mean Error

The mean error is the difference between the true range and measured UWB range. As seen from the LOS measurements in Figure 5.4, below, as range increases, so do the errors. There is a definite bias and scale factor in the measurements. The bias is -0.054 m, while the scale factor is 8400 ppm. NLOS measurements have larger mean errors and this is expected because of greater attenuation.
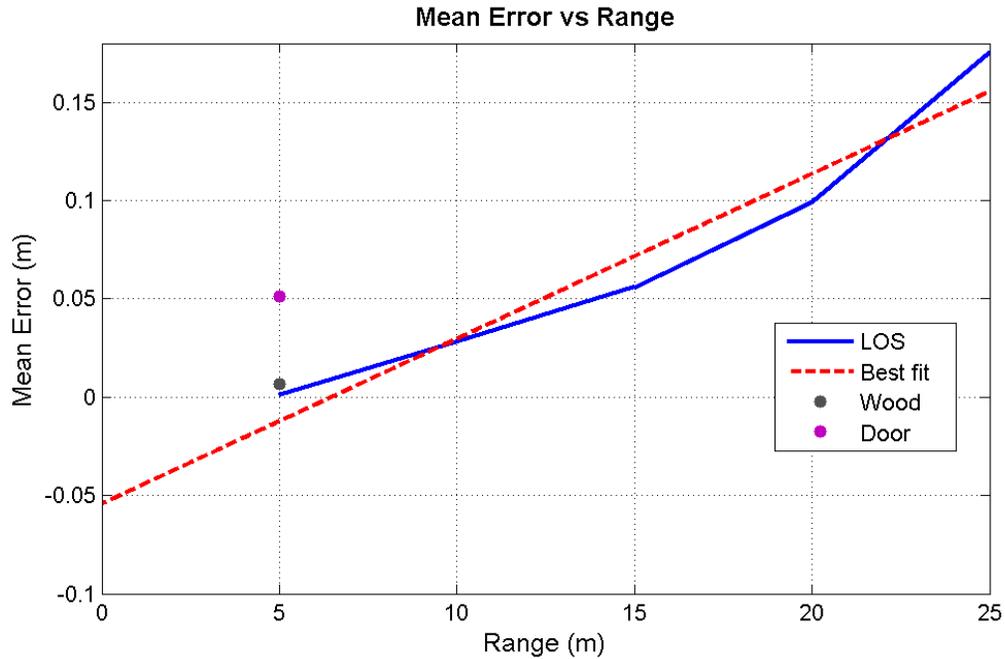
Figure 5.4: Mean errors for indoor TD radio measurements. Blue line results are LOS measurements, while the purple and black dots are NLOS measurements.

5.1.1.4 Mean Error Standard Deviation

The mean error standard deviation also follows a linear pattern. As range increases, standard deviation also increases. However, the results are still considered quite precise as the largest standard deviation value, at 25 m, is only 0.024 m. NLOS standard deviation values are negligibly larger than LOS standard deviation values at the same distance. Please refer to Figure 5.5, below.
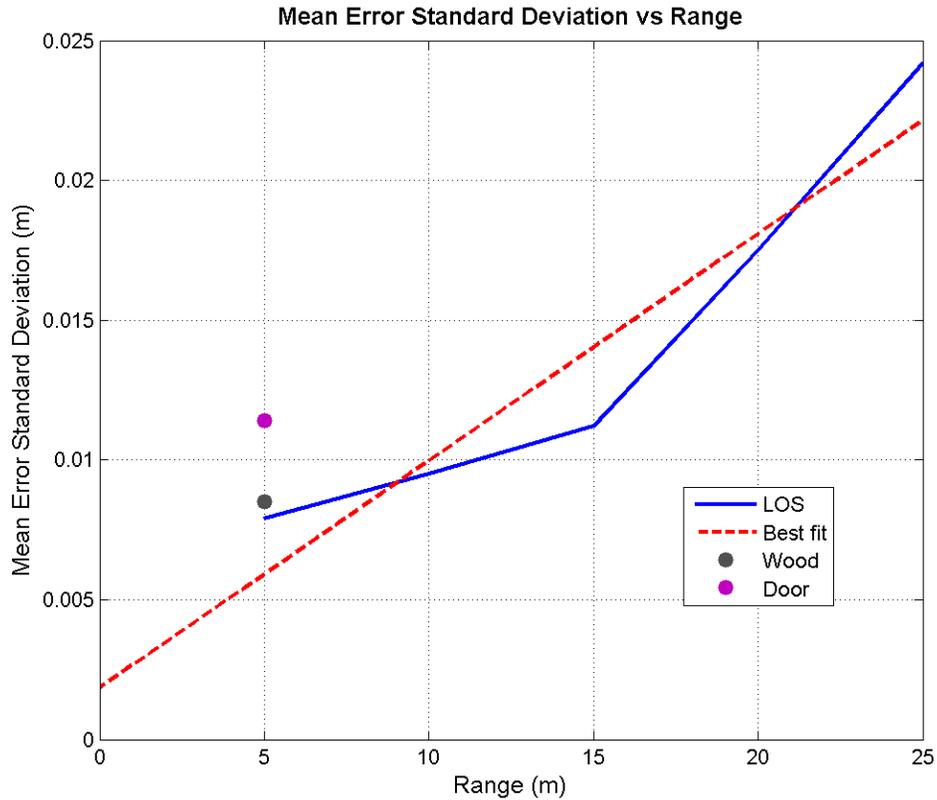
Figure 5.5: Mean error standard deviation values for TD indoor measurements. Measurements through the door and wood are NLOS.

5.1.2 Multispectral Solutions UWB Radio Indoor Test

To assess the accuracy of UWB measurements indoors, a LOS range test is conducted inside a hallway within the engineering complex at the University of Calgary. This hallway is selected because of its unique design as depicted in Figure 5.6, below. Multipath signals are expected within this hallway using standard narrowband systems.
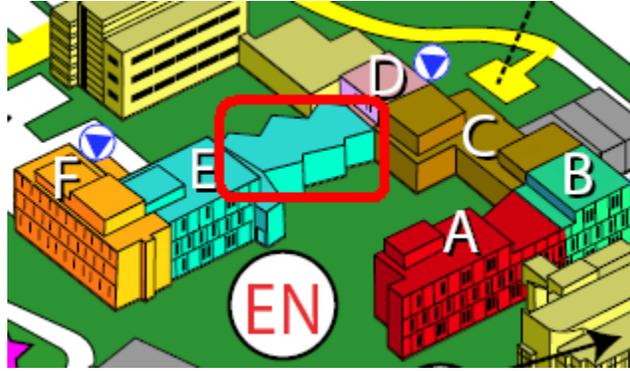
Figure 5.6: Indoor test hallway used for testing MSS radios (from University of Calgary 2008)

LOS measurements are taken at 5 m, 10 m, 15 m, 20 m, 25 m, 30 m, 35 m, 40 m, 45 m, 50 m and 55 m. A comparison is done between the measured UWB range and tape measure ranges. Tape measure distances are confirmed by measuring the same distance 3 times independently. A marker is placed at each distance. UWB radios are placed at each of the marked distances and measurements are taken for 1-2 minutes at 0.292 m above ground for each point. Each of the four MSS radios are labelled by numbers (ie. Radio 6, 7, 8 and 9). In this test, only radios 6 and 7 are used.

Unlike TD radios, MSS radios are easier to assess large LOS ranges because MSS radios' power source is an internal rechargeable battery. TD radios' power source is an electrical cord plugged into the electrical wall socket and hence, results in certain limitations.

5.1.2.1 Measurements

The number of measurements (standardized to every 100 s) collected at each distance varies from 1409 at 40 m to 1443 measurements at 55 m. As opposed to indoor measurements from TD radios, these MSS radios show no strong correlation between number of observations and range, as shown in Figure 5.7, below.
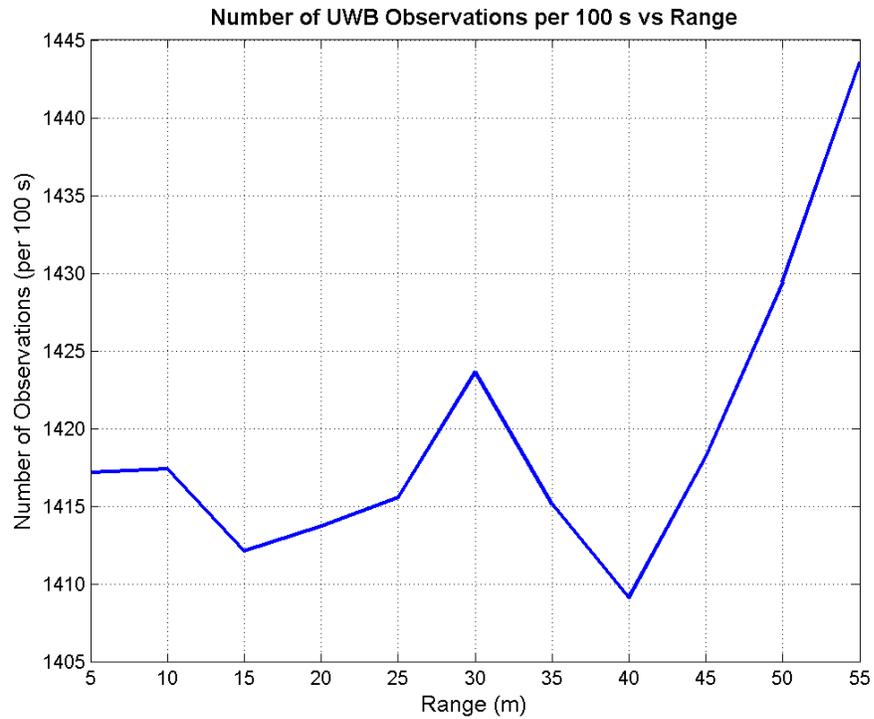
Figure 5.7: Number of measurements (per 100 s) versus distance for indoor MSS radios

5.1.2.2 Outliers

In Figure 5.8, below, a histogram of the ranges prior to outlier removal is shown at each distance. Despite a bias, the measurements generally resemble a normal distribution. Each bin size in the histogram represents 0.01 m.
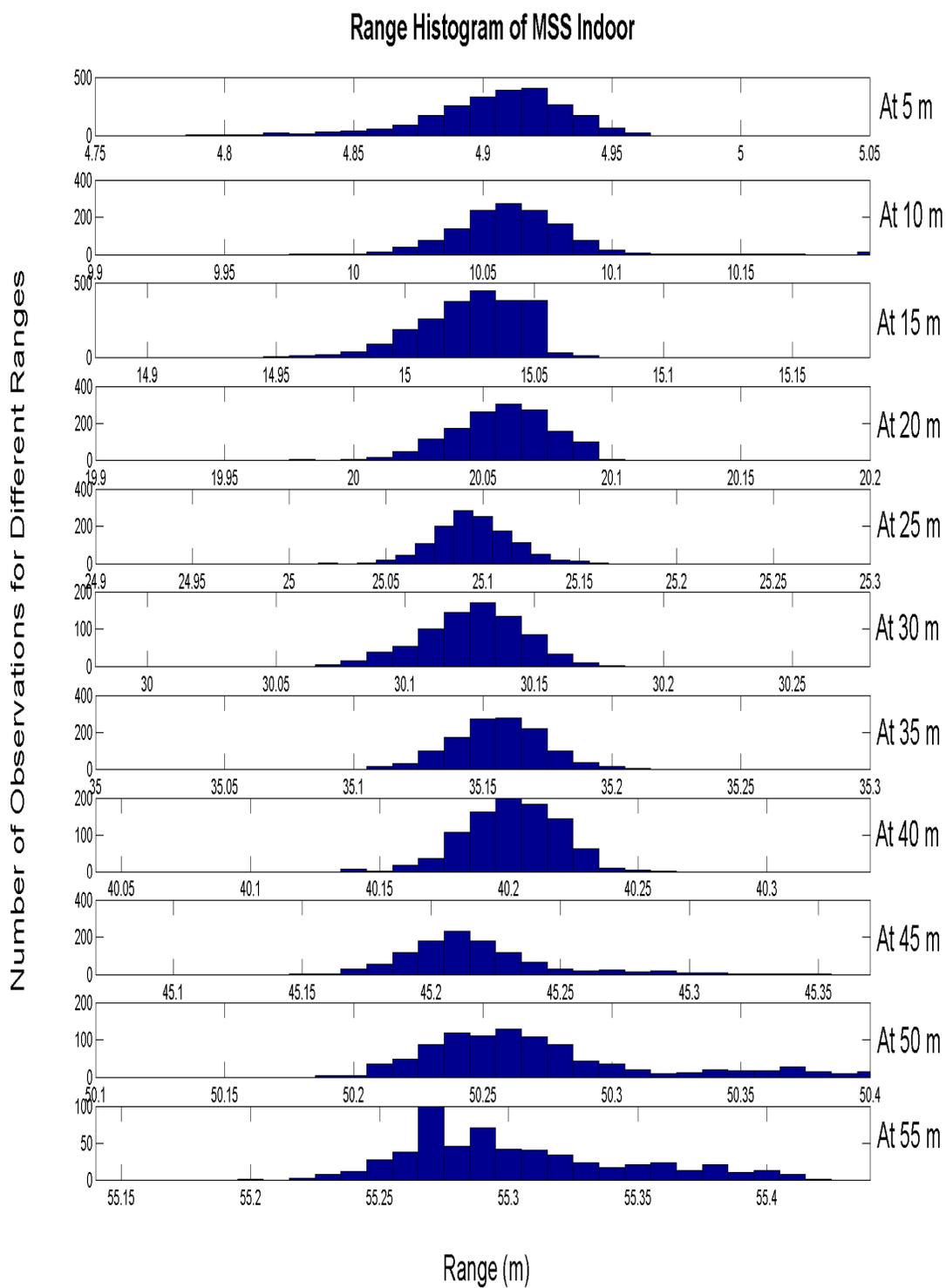
Figure 5.8: Range histogram for MSS radios, indoors

The percentage of outliers varies from 0% at 5 m and 35 m, to 1.15% at 10 m. No correlation is found between number of outliers and distance, as seen in Figure 5.9, below.
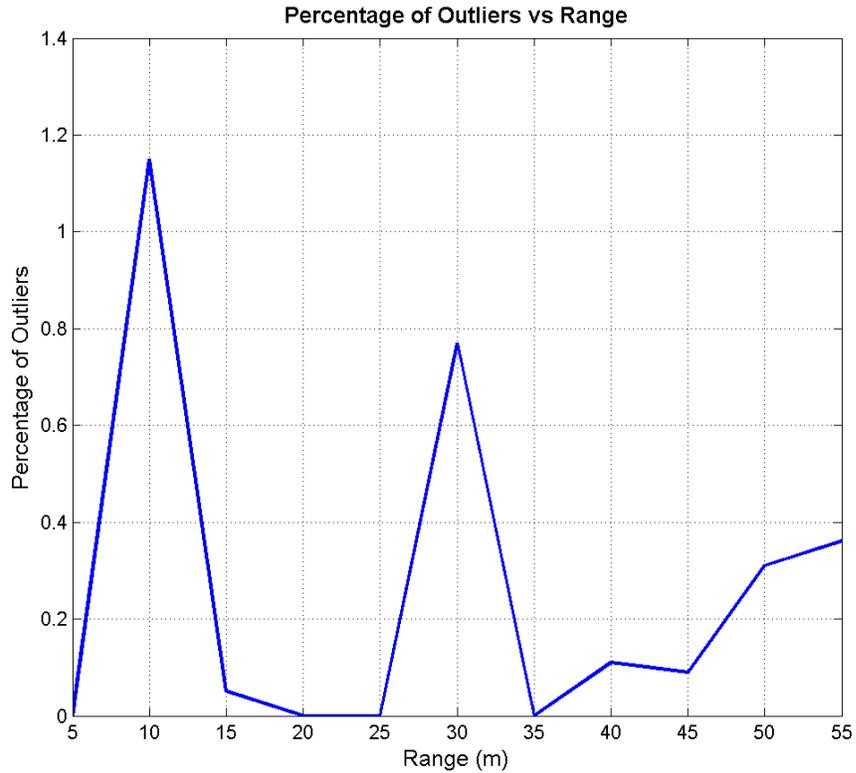
Figure 5.9: Number of outliers versus distance for indoor MSS radios

Outliers are detected and removed in the same method as how TD UWB measurement outliers were detected. For the method of detection and removal, please refer back to Section 5.1.1.2.

5.1.2.3 Mean Error

MSS radio data collected in the hallway indicates that the mean error is linearly dependent on distance. At 55 m, the mean error is slightly over 0.30 m. In Figure 5.10, below, the actual results after outlier removal are shown in blue, while the best fit line is drawn overtop in red.
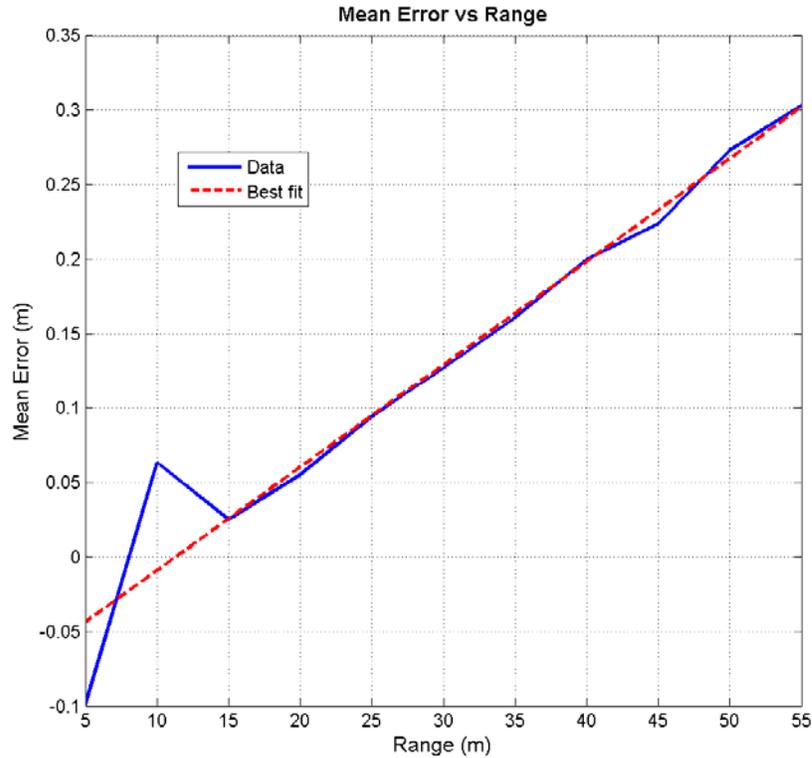
Figure 5.10: Mean error versus distance. The blue line is the actual result, while the red line is the best fit line.

It is also important to remember that these mean error results are from LOS conditions. In NLOS conditions, the mean error increases further. How much the error increases is dependent on the material that the signal passes through. It was shown by a group at Virginia Tech, that attenuation loss due to common materials, such as office partitions, wooden doors, chip wood, drywall, bricks, plywood and glass, can result in losses of 6 dB in power, while losses of up to 14 dB were reported for concrete blocks for signals in the frequency bandwidth of 2 GHz to 11 GHz (Muquibel & Safaai-Jazi 2003). This is discussed in Section 3.5.2.

Comparing mean error data with its best fit line in Figure 5.10, above, it can be clearly seen that the mean error matches up with the best fit line quite closely. This suggests that the radio is recording little multipath effects in most cases in a hallway where multipath would be expected from a narrowband system.

Despite the data showing no multipath effects, there is an obvious scale factor and bias that affects the data. The scale factor is 6900 ppm, while the bias is -0.078 m. These errors need to be accounted for and removed prior to further data analysis and integration with GPS data.

5.1.2.4 Mean Error Standard Deviation

By looking at Figure 5.11, below, there is no obvious correlation between the mean error standard deviation and range. Interestingly, this is different than what was seen with the mean error standard deviation of TD UWB radios in Section 5.1.1.4.
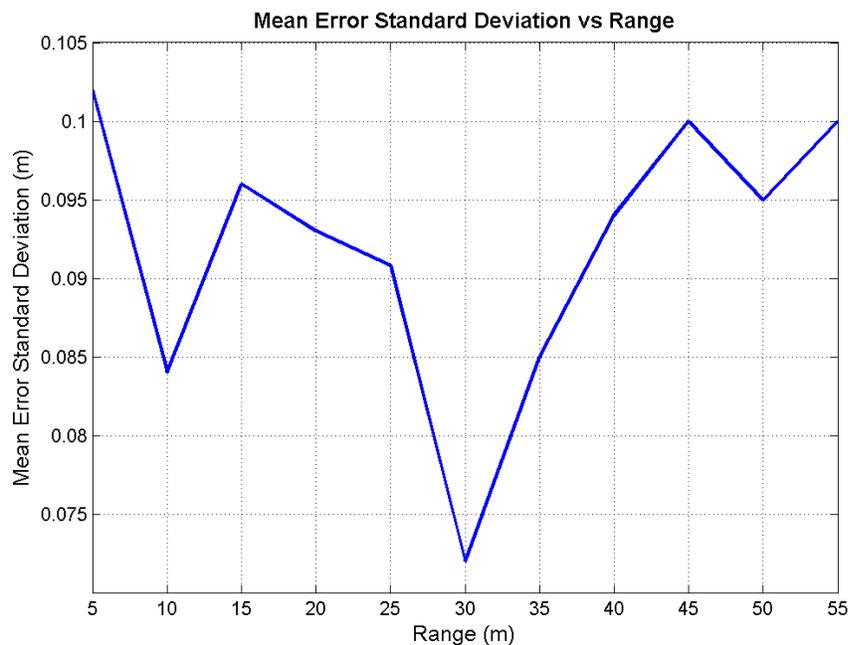
Figure 5.11: Mean error standard deviation values for indoor testing of MSS radio

5.2 OUTDOOR RANGE VERIFICATION TESTS

Outdoor testing of TD and MSS UWB radios is conducted at Shouldice Park in Calgary, Canada. Ranges are collected over several flat soccer fields, as seen in Figures 5.12 and 5.13, below.

Figure 5.12: Aerial view of Shouldice Park in Calgary, Canada (from Google Maps 2008)
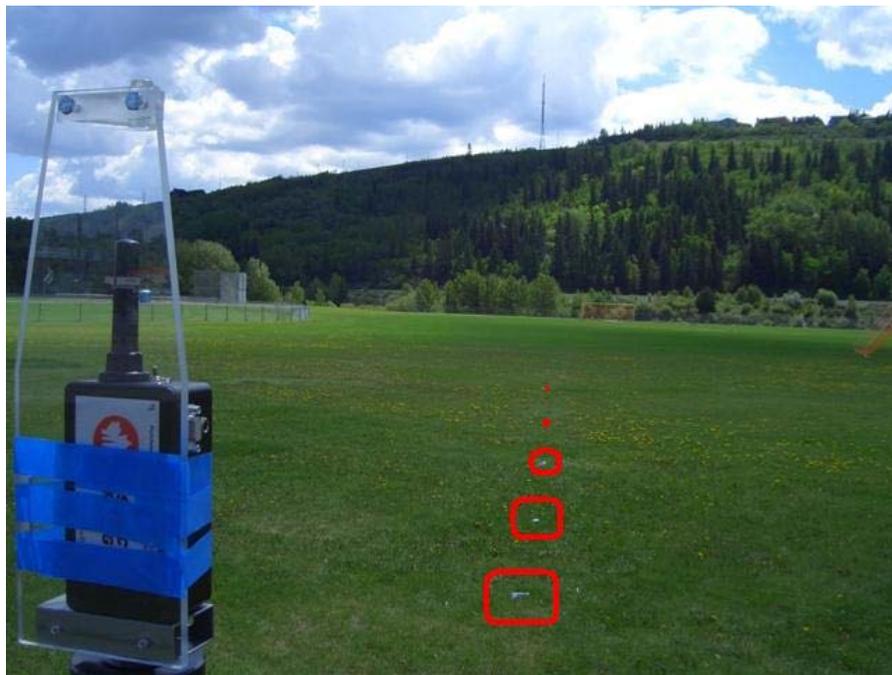
Figure 5.13: A soccer field at Shouldice Park in Calgary, Canada. Outdoor testing of TD and MSS UWB radios is done on the soccer field.

For both TD and MSS tests, truth ranges are measured out using a total station. Several different radio pairs are tested. Results for the tests taken at Shouldice Park for the TD and MSS radios are discussed in Section 5.2.1 and 5.2.2, respectively.

5.2.1 Time Domain UWB Radio Outdoor Test #1: Shouldice Park Test

Ranges are measured at 10 m, 20 m, 30 m, 40 m and 50 m using a total station. These ranges are assumed to be truth ranges since their accuracy is reported to be mm-level. The TD UWB radios are then placed at these truth distances and UWB ranges are taken.

5.2.1.1 Observations

Because the measurement duration at each point is not the same, they have been standardized to reflect number of measurements per 100 s. From Figure 5.14, below, there is positive correlation between the number of measurements and range. However, the correlation is very weak because from the distance of 10 m to 50 m, there is only an increase from 4.9 Hz to 5.1 Hz. This difference is quite negligible so the correlation is quite weak, as opposed to TD UWB ranging indoors.
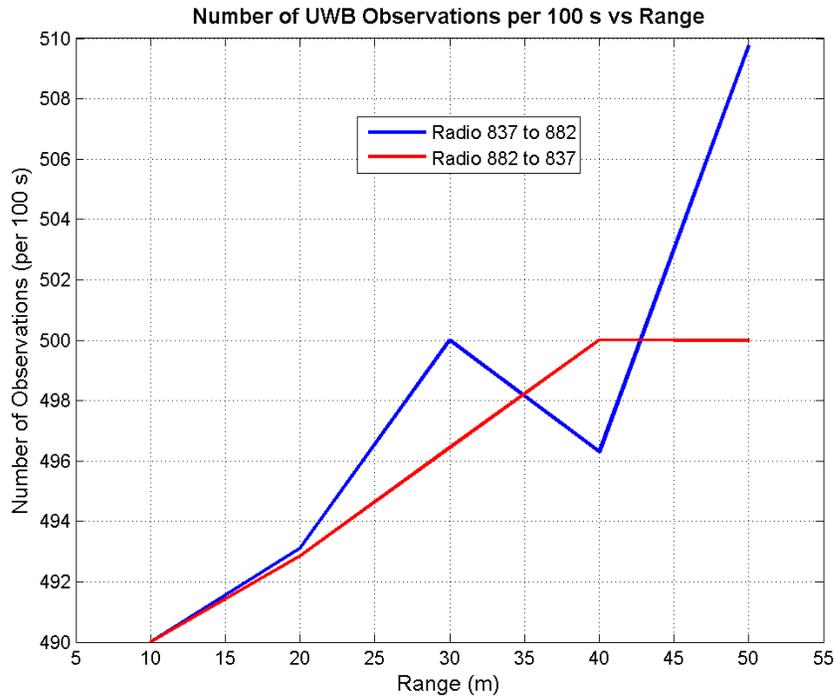
Figure 5.14: Number of observations made per 100 seconds for two combinations of TD UWB radios, outdoors

The general trend between the two radio combination pairs results in similar results and this redundancy confirms the result.

In total, there are 4 TD UWB radios and 4 MSS UWB radios used in this thesis. Each radio has a serial number attached to it. To distinguish between which radios are used in which tests, their serial numbers will also be stated. For example "Radio 837 to 882" means that the radio with serial number "837" is the requester, while the radio with serial number "882" is the responder. On the other hand, "Radio 882 to 837" indicates that the radio with serial number "882" is the requester and the radio with serial number "837" is the responder. This notation will be used for the remainder of the thesis. For an explanation of two-way ranging and why there is a requester and a responder, please consult Section 3.5.4.

5.2.1.2 Outliers

Figures 5.15 and 5.16, below, shows histograms of ranges prior to outlier removal for different measurement distances for Radio 837 to 882 and for Radio 882 to 837, respectively. There is no obvious correlation between range and outliers and most of the histograms seem to represent normal distribution. Each bin size in the histograms represents 0.01 m.
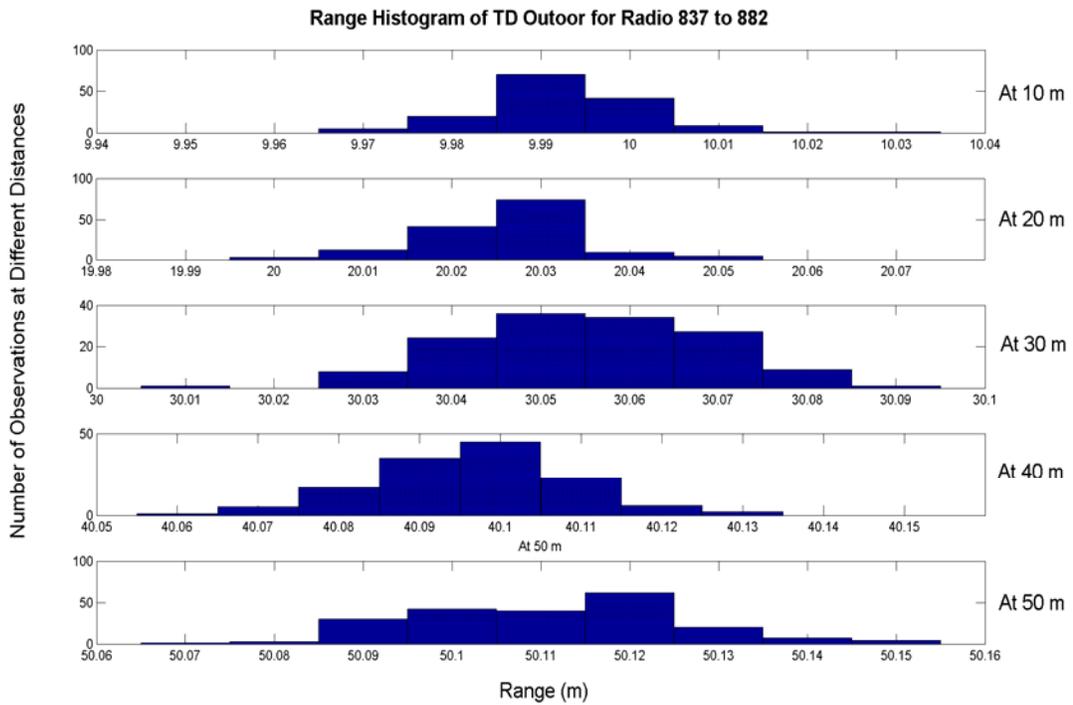
Figure 5.15: Range histogram between TD radios 837 to 882, outdoors
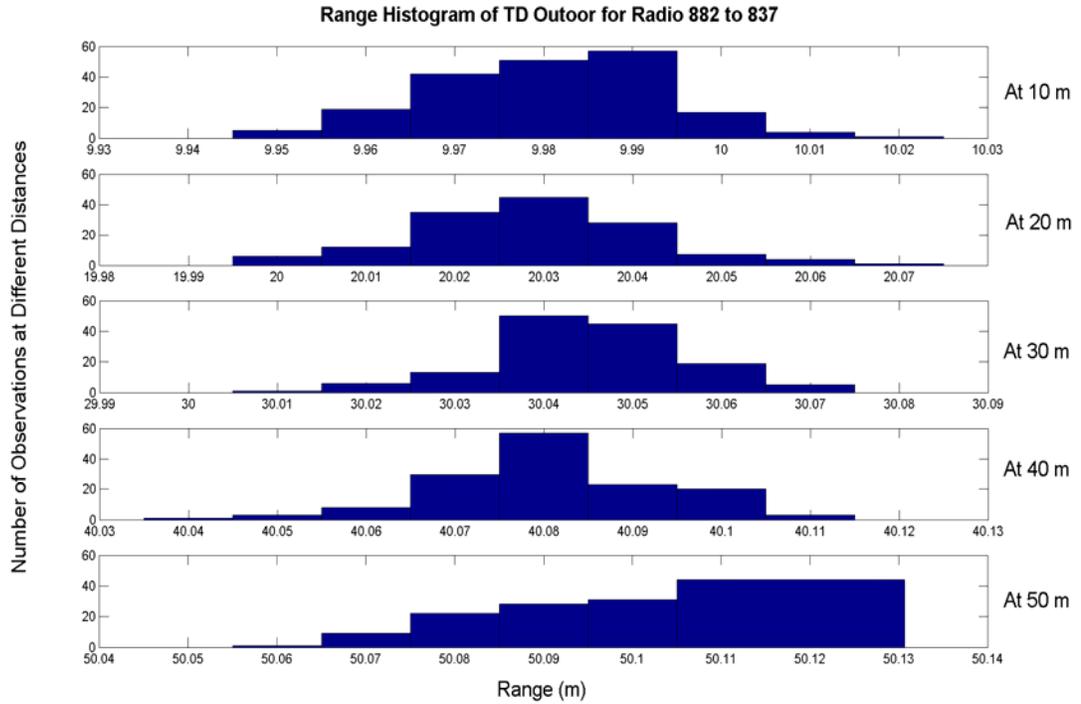
Figure 5.16: Range histogram between TD radios 882 to 837, outdoors

The number of outliers is at an acceptable level. There is no strong correlation between outlier versus range. Please refer to Figure 5.17, below. This result is expected and is consistent with other tests conducted with these radios. These outliers are removed and their detection method is described in Section 5.1.1.2.
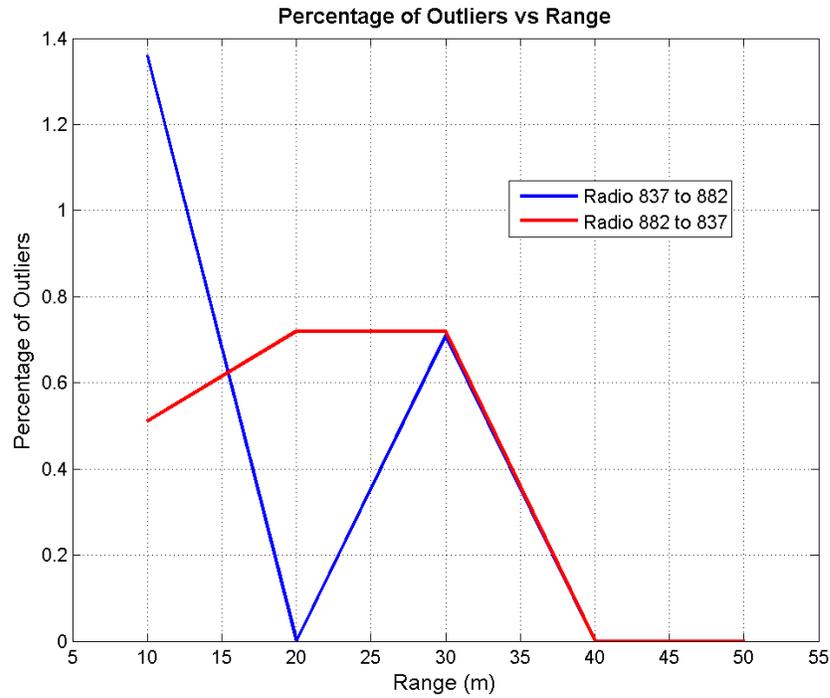
Figure 5.17: Percentage of outliers removed from data for two combinations of TD UWB radios, outdoors

5.2.1.3 Mean Error

The mean error for the TD radios in an outdoor setting show several things. Firstly, because the data closely follows the best fit line, there is minimal multipath. Secondly, there is a definite scale factor and bias. Lastly, the scale factor and bias are different between both radio pairings even though the same two radios are used. The scale factor and bias is greater when radio 837 is used as the requesting radio and the difference is likely due to different internal noise. Figure 5.18, below, shows the mean errors for the two radio combinations.
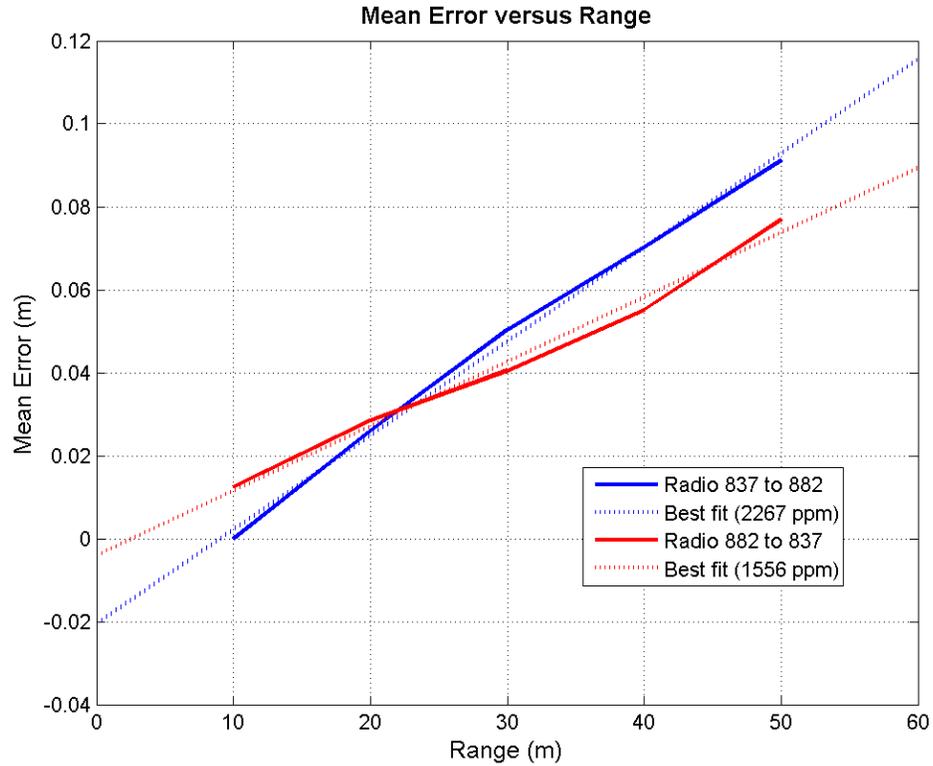
Figure 5.18: Mean error for two combinations of TD UWB radios, outdoors

5.2.1.4 Mean Error Standard Deviation

Mean error standard deviation also shows a positive correlation with range, as seen in Figure 5.19. However, this correlation is almost negligible as the range of standard deviation values is about 5 mm over a distance of 50 m.
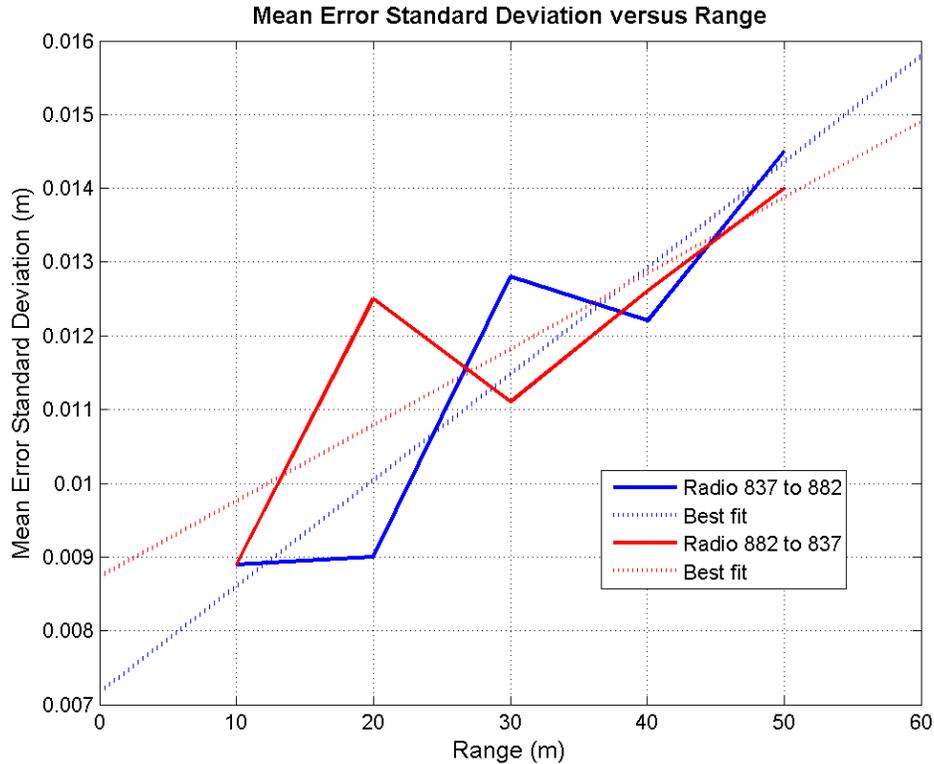
Figure 5.19: Mean error standard deviation for two TD UWB radio combination pairs, outdoors

5.2.2 Multispectral Solutions UWB Radio Outdoor Test

A similar test is done with the MSS radios. Testing is done at Shouldice Park in Calgary, Canada. Truth distances (mm-level accuracy) are marked out with a total station. MSS radios are placed on the marked out distances. Measurements are taken, and then subsequently compared to truth values. With TD radios, only two radios were available at the time of testing so only two radio combinations (ie. "Radio 837 to 882" and "Radio 882 to 837") are tested; however, with MSS radios, four radios are available and consequently, more radio pairings are available for this test.

For the pairs "Radio 6 to 7" and "Radio 7 to 6", measurements are taken at 10 m, 20 m, 30 m, 40 m, 50 m and 60 m, while for pairs "Radio 8 to 9" and "Radio 9 to 8", measurements are only taken at 10 m, 20 m and 30 m.

5.2.2.1 Observations

After standardizing the number of observations to 100 s, no correlation is found between the number of measurements and range. This can be explained by the fact that the radios are able to range to 120+ m. It is suspected that if a similar plot is made for ranges at 100 m to 150 m, a noticeable trend may be seen. This is because at that distance, a signal power decrease likely affects the ability of the radio to detect the signal. The radio detects the signal based on a threshold power level, so as the signal power approaches the threshold, fewer measurements are made. At a range of 10 m to 60 m, as done in this assessment, moving around within this range does not affect the number of measurements made since all measurements' signal power levels are significantly greater than the threshold. Please refer to Figure 5.20 and 5.21, below, for the number of observations plot for Radios 6, 7, 8 and 9.
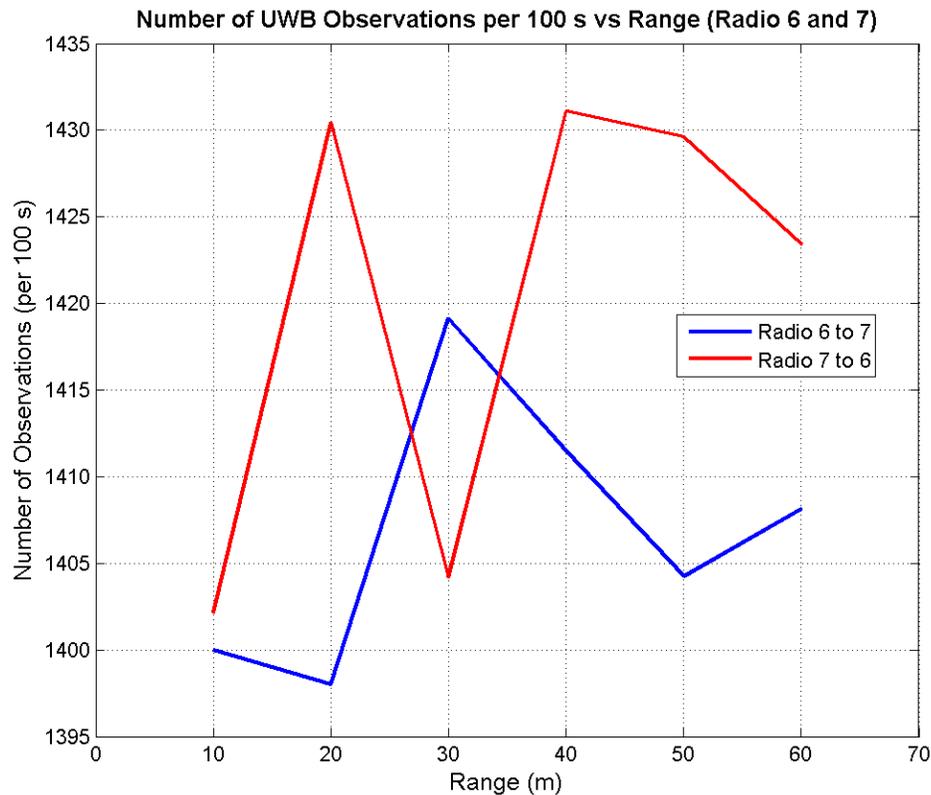
Figure 5.20: Number of observations made for MSS radios 6 and 7 per every 100 s, outdoors
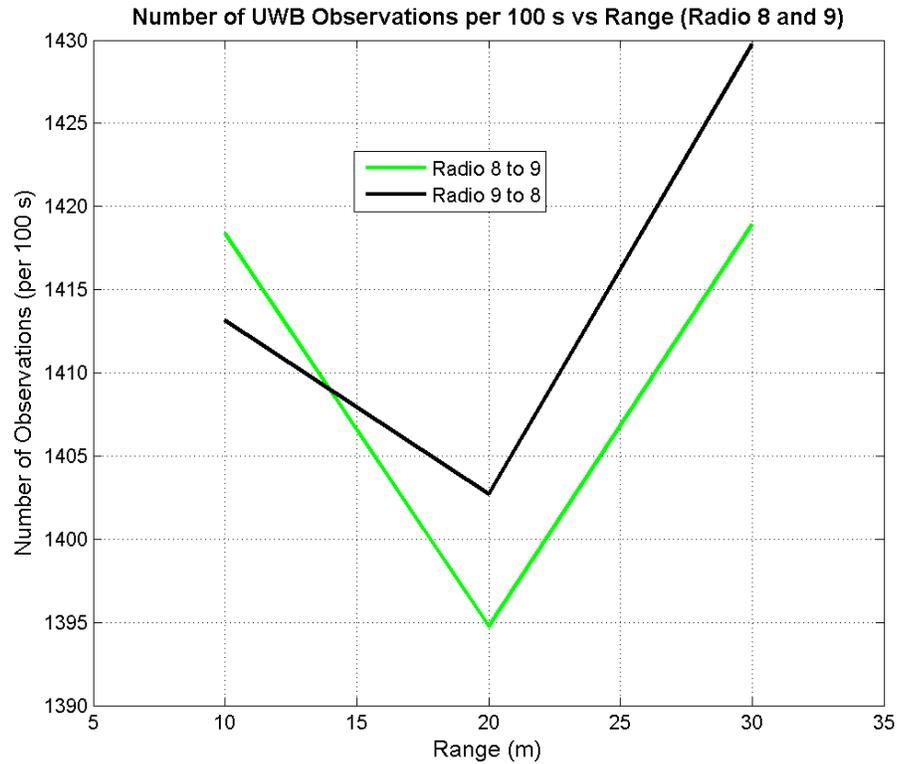
Figure 5.21: Number of observations made for MSS radios 8 and 9 per every 100 s, outdoors

5.2.2.2 Outliers

Figures 5.22, 5.23, 5.24 and 5.25, show the range histogram prior to outlier removal for "Radio 6 to 7", "Radio 7 to 6", "Radio 8 to 9" and "Radio 9 to 8", respectively. From visual inspection, there are few outliers in the data. Furthermore, the histogram plots generally show normally distributions (with the exception of "Radio 6 to 7" at 10 m). Each bin size in the following four plots represent 0.01 m.
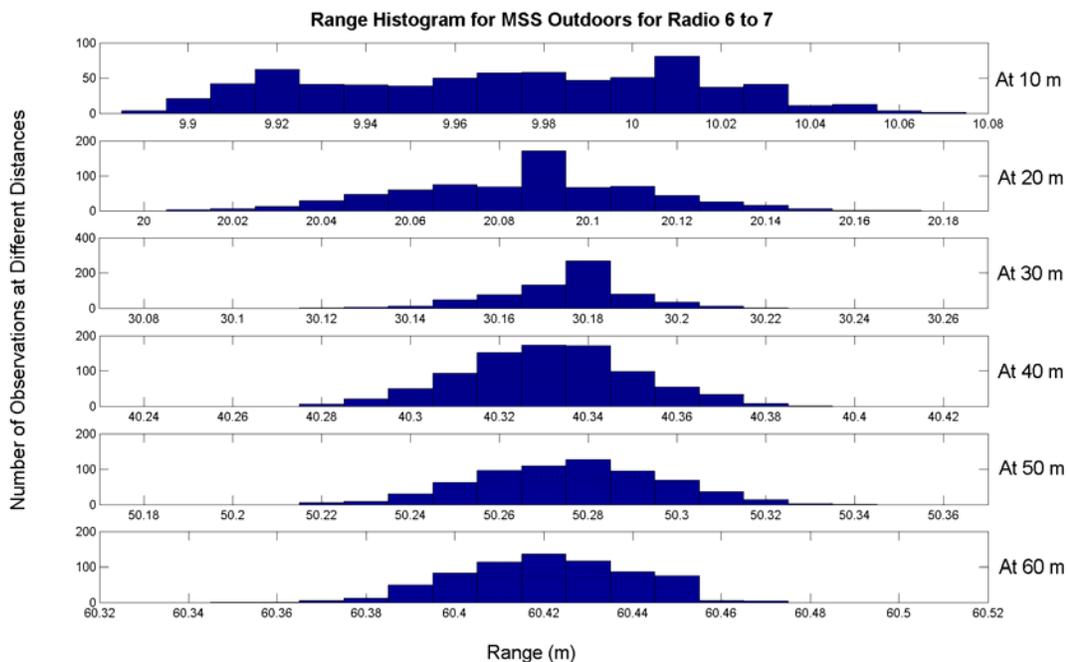
Figure 5.22: Range histogram of MSS radios 6 to 7 at different ranges, outdoors
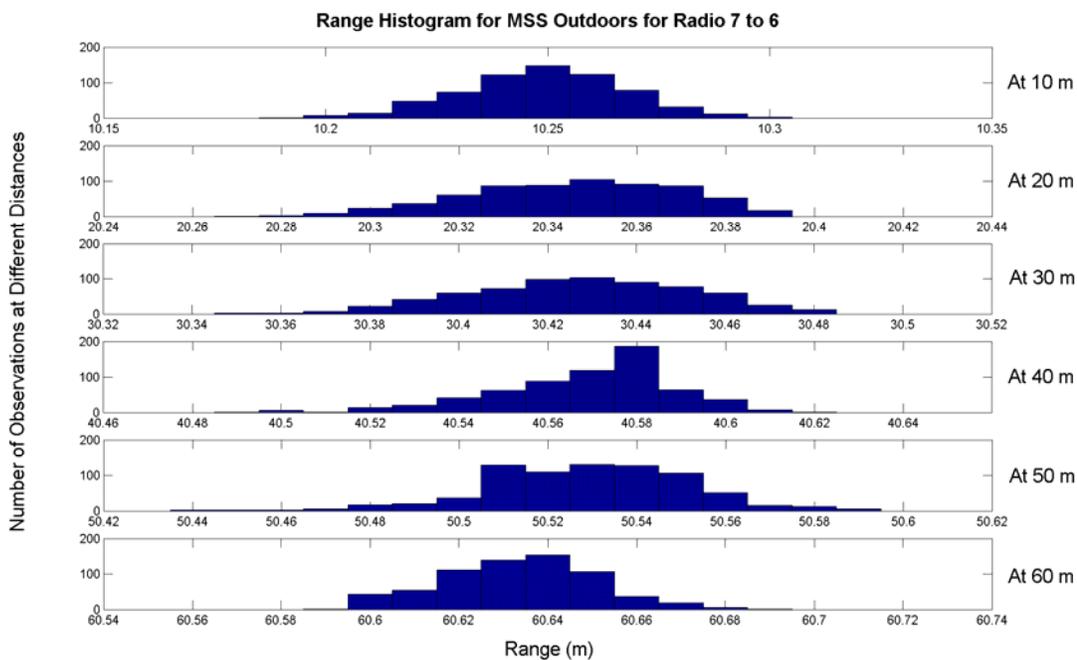
Figure 5.23: Range histogram of MSS radios 7 to 6 at different ranges, outdoors
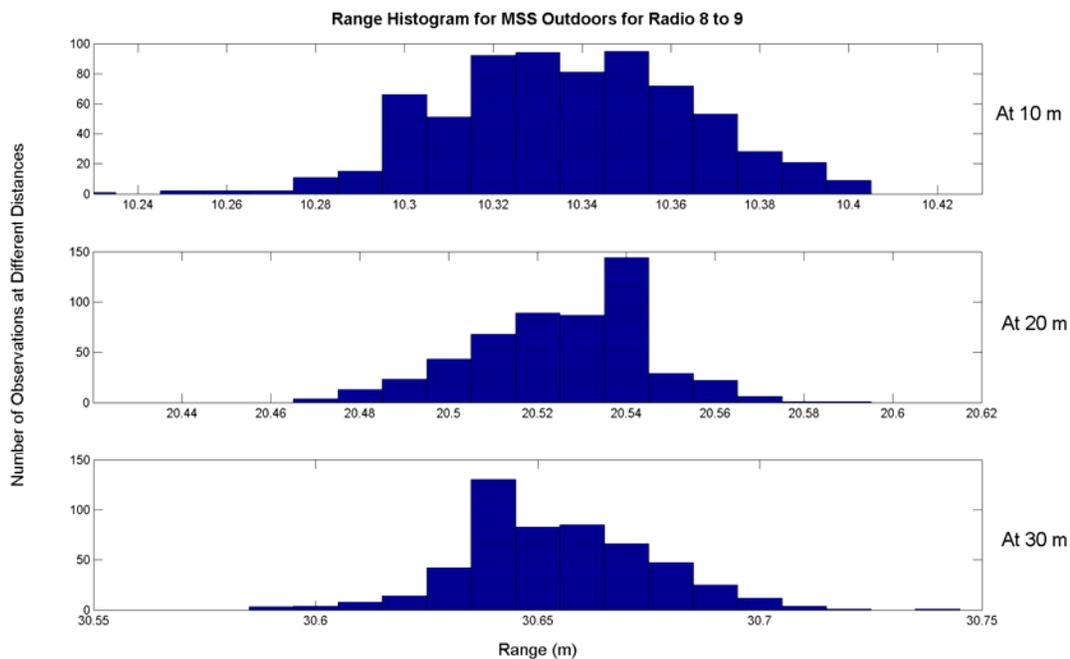
Figure 5.24: Range histogram of MSS radios 8 to 9 at different ranges, outdoors
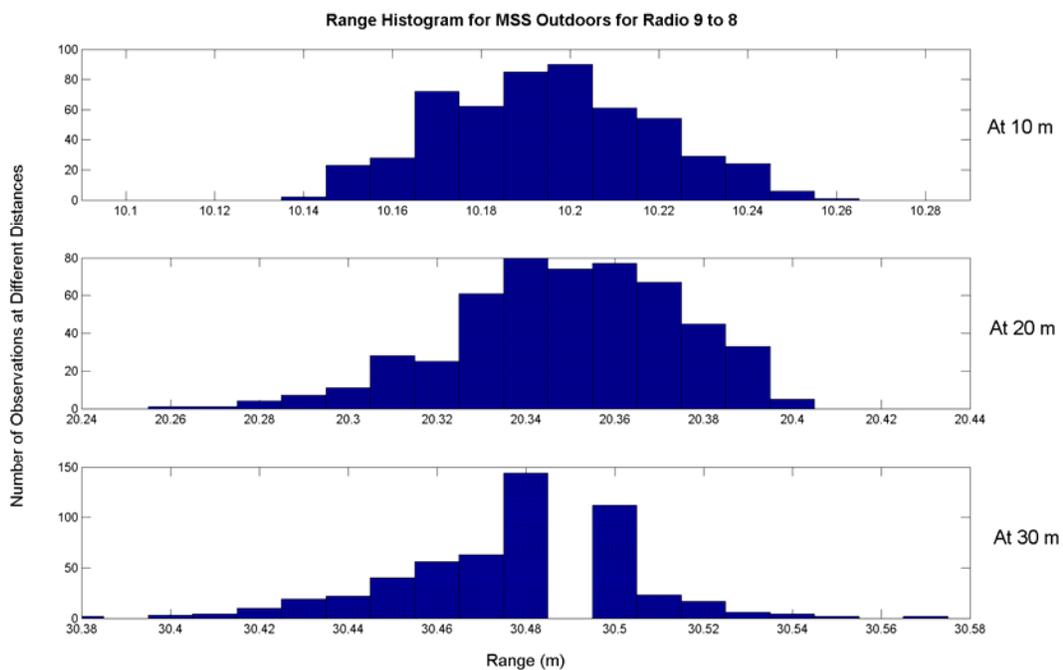
Figure 5.25: Range histogram of MSS radios 9 to 8 at different ranges, outdoors

There is no obvious correlation between outliers, radio pairs and range, as seen in Figures 5.26 and 5.27. Outlier detection is described in Section 5.1.1.2 and the outliers are removed.
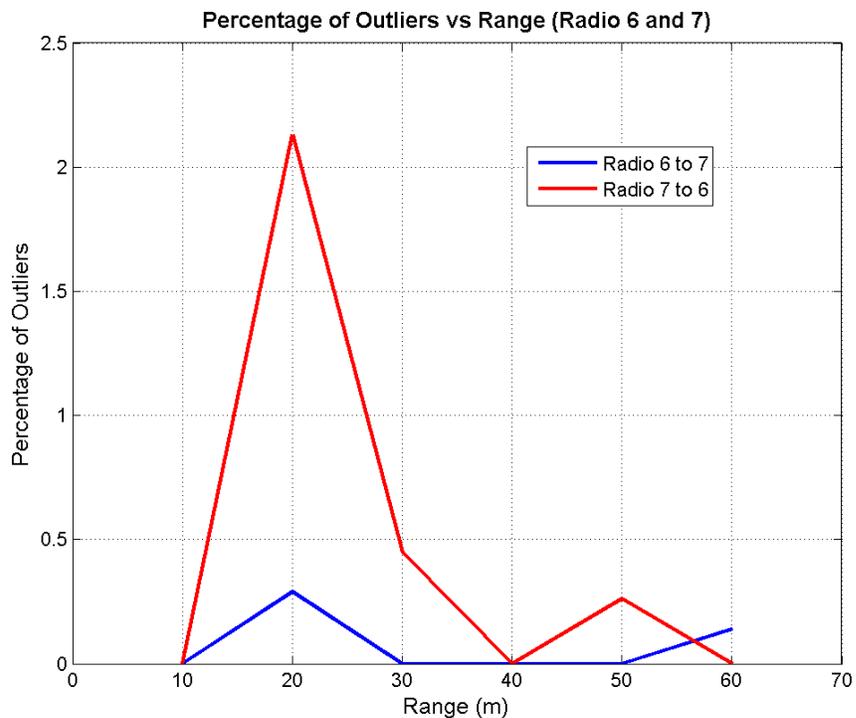
Figure 5.26: The percentage of outliers removed from MSS radios 6 and 7
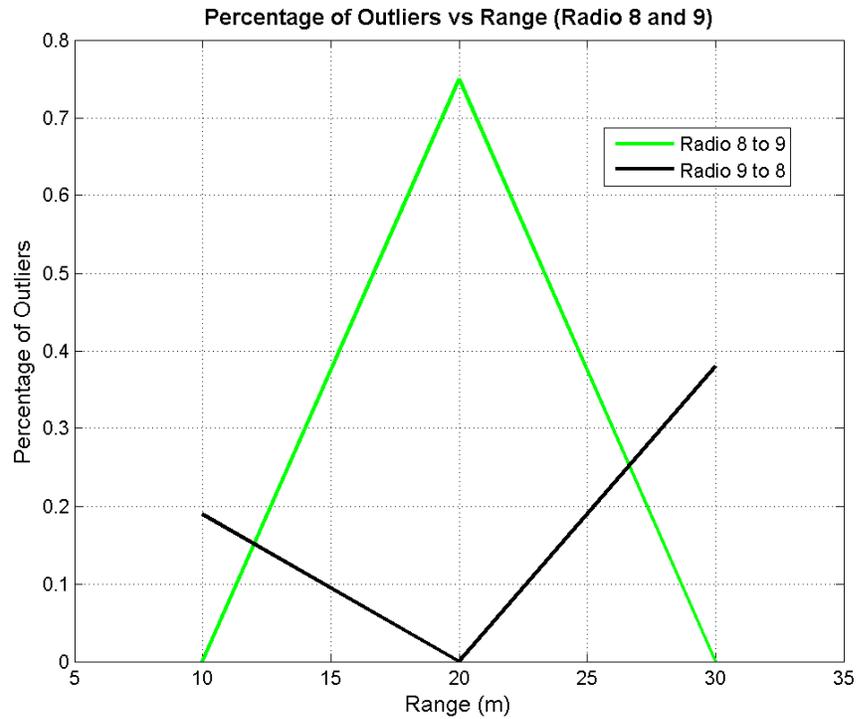
Figure 5.27: The percentage of outliers removed from MSS radios 8 and 9

5.2.2.3 Mean Error

In Figure 5.28, below, "Radio 6 to 7" and "Radio 7 to 6" both show a similar scale factor, but different bias. They show very similar trends at 40 m when the data spikes up above the best fit line, then down below the line at 50 m.
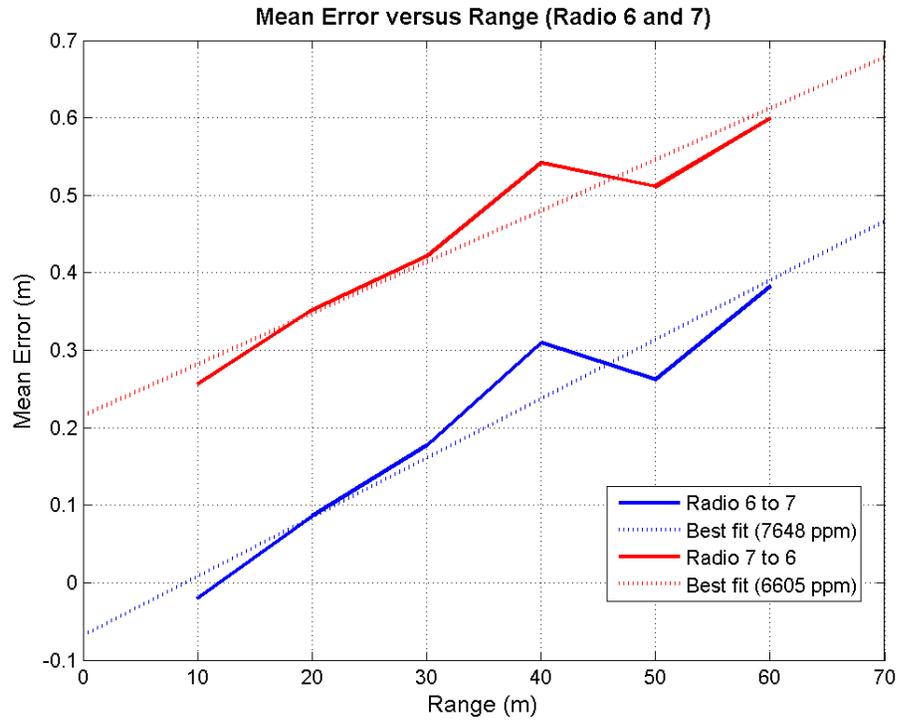
Figure 5.28: Mean error values for MSS radios 6 and 7 tested outdoors

"Radio 8 to 9" and "Radio 9 to 8" also exemplify similar mean error behaviour. Very minimal multipath can be inferred from Figure 5.29 because the data closely follows the line of best fit. Similar to the previous radio pairs, these two radio pairings share a similar scale factor with a different bias.
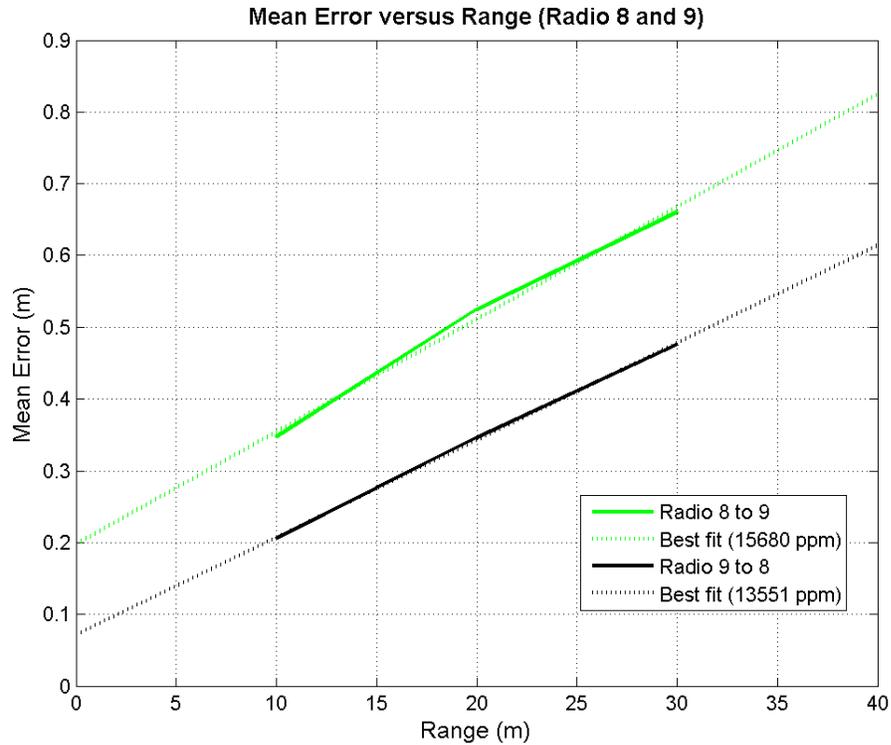
Figure 5.29: Mean error values for MSS radios 8 and 9 tested outdoors

Overall, comparing the four different radio pairings (in Figure 5.30, below), several observations can be made:

♦ different radio pairs have different scale factor and biases. A discussion on scale factor and bias will be presented in Section 5.6.

♦ some radios (either radio 8 or 9) have higher internal noise, resulting in significantly higher scale factor errors

♦ no multipath is seen and this is consistent with all radios

♦ all radios have a positive correlation between mean error and range
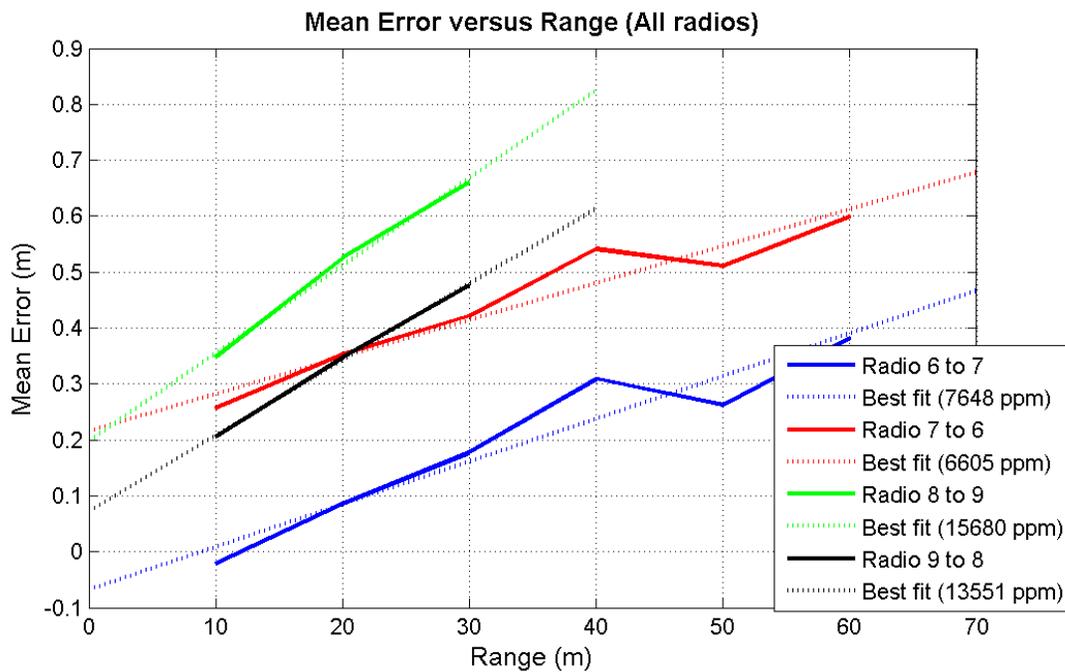
Figure 5.30: Mean error values for MSS radios tested outdoors

5.2.2.4 Mean Error Standard Deviation

Plotting the mean error standard deviations for the four radio pairs indicates no clear correlation with range, as seen in Figure 5.31, below.
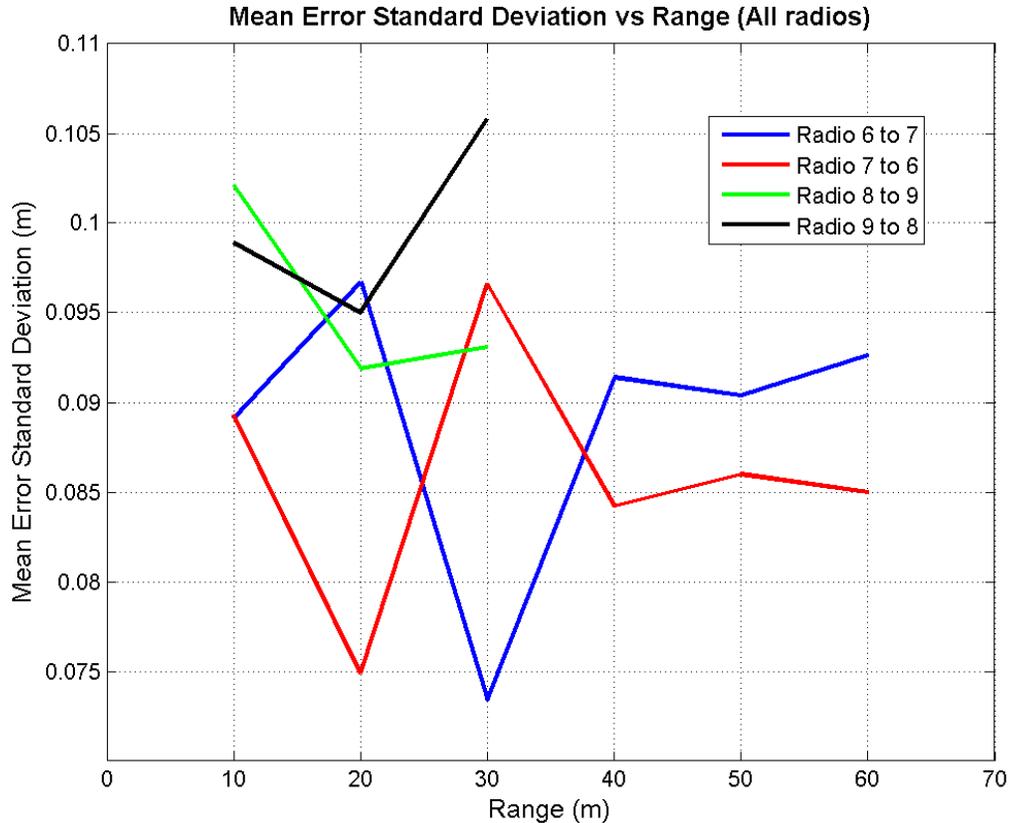
Figure 5.31: Mean error standard deviation for MSS radios outdoors

5.3 TIME DOMAIN: INDOOR VERSUS OUTDOOR

There is a large difference when comparing the number of measurements made versus range, in indoor and outdoor conditions. For indoor conditions, there is a strong negative correlation, while in outdoor testing, there is only a very weak positive correlation. In fact, for indoors, data logging decreases from 4.3 Hz to 1.1 Hz when the radio goes from 5 m to 25 m, respectively. For outdoors, data is consistently logged at a rate of about 5 Hz from a range of 10 m to 50 m. Indoor conditions do not indicate very much multipath; however, attenuation or signal loss is quite notable compared to outdoor ranging.

The mean error is three time as high for indoors, as it is outdoors. Indoor mean error is 8400 ppm, while outdoor mean error is 1556 ppm or 2267 ppm (depending on which radio pair used). This can be explained by the fact that indoor ranging suffers from a

higher degree of attenuation. Higher attenuation translates into lower received signal power. When the signal power level approaches the radio threshold's ability to detect, not only will fewer measurements be made, but also less accurate ranges may be logged compared to a strong, definite signal.

Mean error standard deviations for the indoor and outdoor case both show a positive correlation with range. Again, standard deviations for the indoor case increase at a greater rate with range.

5.4 MULTISPECTRAL SOLUTIONS: INDOOR VERSUS OUTDOOR

The number of observations and outliers do not show any correlation with range. The number of observations in Hz is quite consistent at just over 14 Hz.

Comparing mean errors between the indoor and outdoor case reveal that minimal multipath is observed in both cases. However, both are affected by a scale factor and bias. The radios used for the indoor case are radios 6 and 7. Radios 8 and 9 are not tested indoors. Comparing radios 6 and 7 indoors to the same set of radios outdoors, show fairly a similar scale factor with indoors being 6900 ppm and outdoors as 7648 ppm.

Mean error standard deviations in the indoor versus outdoor case both show no correlation with range, but rather a consistent value just under 0.1 m.

5.5 TIME DOMAIN VERSUS MULTISPECTRAL SOLUTIONS

TD radios seem to be much more affected by indoor environments versus outdoor conditions. Looking at the number of measurements made by TD and MSS radios, TD radios are drastically hampered when brought indoors. Attenuation affects TD radios indoors much more than multipath. MSS indoor/outdoor and TD outdoor measurements are not affected by attenuation or multipath.

The percentage of outliers is greater with TD radios. Depending on the application, the percentage of outliers in TD data can become significant. In the indoor case, > 14% of TD UWB radios data at 25 m was outliers. Negative ranges and large gross errors in the range have been observed in TD radio measurements. Proper outlier detection and removal is essential.

Comparing mean errors between both types of radios, there are two major differences:

- TD radios observe mean errors that are three times greater indoors, when compared to outdoor ranging
- MSS radios have significantly higher mean errors compared to TD radio measurements. TD radio mean errors are about 1556 ppm (outdoors) to 8400 ppm (indoors), while MSS radios' mean errors vary from 6605 ppm to 15680 ppm.

Mean error standard deviations are also different between both sets of radios:

- TD radios show a positive correlation between standard deviation and range, while MSS radios show a constant value
- TD radios are more precise than MSS radios because the standard deviation values are lower (around 5 cm for indoors and 2-3 cm for outdoors at ~50 m). MSS radio standard deviations are just under 10 cm for all scenarios.

Which radio to use depends on the tasks that need to be accomplished. MSS radios seem to be less affected by multipath and attenuation effects when indoors, so these radios might be a better choice when ranging indoors. If positioning outdoors, TD radios are the better alternative because they give more precise measurements with lower mean errors. However, mean errors in all radios are caused by a scale factor. This linear error, along with the bias, can be calibrated in post-processing and should be done prior to further analysis or data integration.

5.6 UWB MEASUREMENTS: SCALE FACTOR AND BIAS

The scale factor and bias in the measurements must not be ignored, especially with the MSS radios, which exemplify scale factors in excess of 15000 ppm, as seen in Figure 5.30. It will be shown in Section 6.3 that disregarding these errors results in a flawed position solution.

Previously in Figure 5.24, a bias of ± 0.2 m is seen in the MSS radios. This can be explained by the turn around time of the responding radio. Please refer back to Section 3.5.4 for a description of two-ray ranging.

The scale factor error is likely the result of several error sources:

♦ ranges are calculated in the receiver using vacuum light speed. Depending on the temperature and water vapour pressure, this can induce an error of up to 300 ppm

♦ oscillator drift of 20 ppm during signal time-of-flight

♦ a geometric delay error is introduced when signal power and amplitude decreases with a threshold detection receiver. As described in Ruotsalainen (1999), Ruotsalainen et al (2001), and Palojärvi (2003), as the signal power decreases due to spreading/path loss, the signal amplitude becomes lower and the time when the signal crosses the threshold value is delayed. This delay in detection time produces a geometric delay error, which is likely responsible for much of the scale factor error. Please refer to Figure 5.32, below.
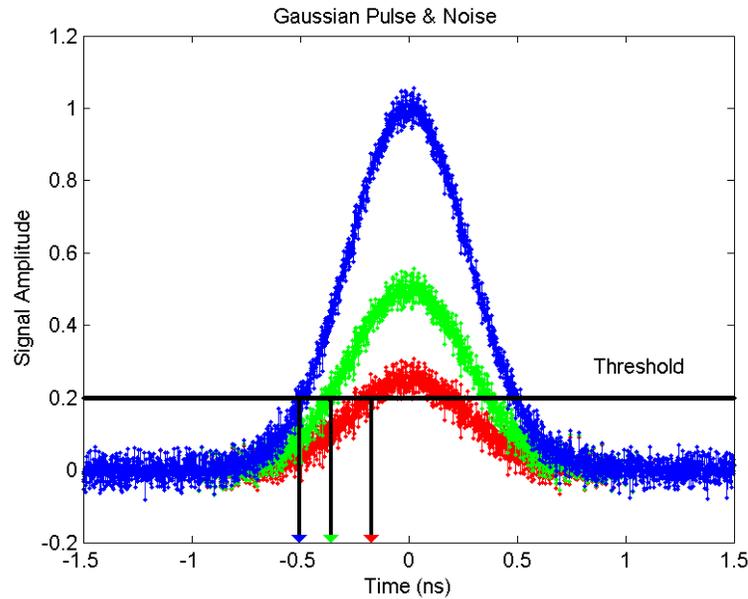
Figure 5.32: A geometric delay error is induced as signal power and amplitude decrease and as result, pass the threshold value at a delayed time

Because the bias is constant and scale factor is linear, this can easily be corrected for in the measurements. Alternatively, these errors could also be included as additional states in the Kalman filter.

UWB range accuracy and precision for both sets of radios have been studied. Multipath, attenuation, scale factor and bias effects are better understood as a result of this work. With UWB range characteristics known, the next step is to quantify UWB position accuracy with regards to GPS positioning prior to integration. This is described in the following chapter.

CHAPTER 6: ULTRA WIDEBAND AND CODE DGPS

Chapter 6 deals with the comparison and integration of UWB measurements with a code DGPS solution in varying signal environments. The main objective of this chapter is to show that with UWB measurements, good and reliable positioning accuracies can be attained in benign signal conditions, as well as maintained in hostile signal environments. Also, UWB can be used to augment or replace GPS under severely adverse GPS signal conditions.

The chapter is divided into three sections:

1) UWB-only positioning versus code DGPS-only positioning (Section 6.1)
2) One single UWB range measurement is used to augment a code DGPS solution (Section 6.2)
3) Multiple UWB ranges are used to augment to a code DGPS solution (Section 6.3)

6.1 UWB-ONLY POSITIONING VERSUS CODE DGPS-ONLY POSITIONING

For this assessment, two Trimble R8 GNSS receivers and four TD PulsON 210 (P210) UWB radios are used. Data collection takes place at the Schulich School of Engineering at the University of Calgary, shown in Figure 6.1, below.
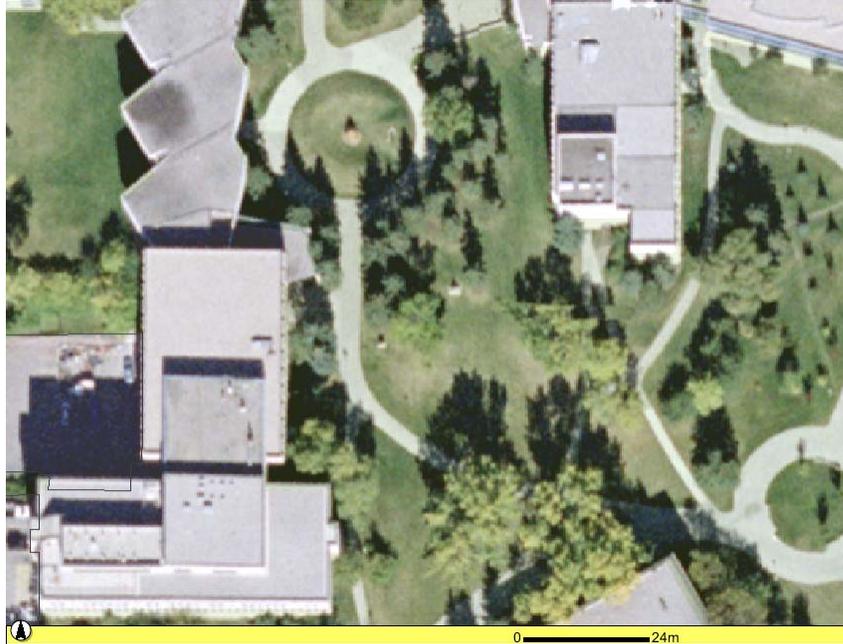
Figure 6.1: Aerial view of the engineering courtyard at the University of Calgary (from Google Maps 2008)

6.1.1 Setup

6.1.1.1 Base Station

One of the Trimble R8 GNSS receivers is used as a DGPS base station and is setup on a known point on top of the Faculty of Engineering building (herein called the "base station"). Please refer to Table 6.1 for base station coordinates and Figure 6.2, below, for the base station.

Table 6.1: Base station coordinates

	Known Coordinates
Latitude	51° 04' 45.94126"
Longitude	-114° 07' 58.29947"
Height (m)	1116.617

Figure 6.2: Trimble R8 GNSS receiver base station

The other GPS receiver, along with the four TD UWB radios are setup in the courtyard of the engineering complex approximately one hundred metres away, as shown in Figure 6.3.

Figure 6.3: TD UWB radio on a tripod

6.1.1.2 Stationary UWB Radio Points 1, 2 and 3

Each of three UWB radios are placed on different tripods set up in the courtyard. The positions of each tripod are previously surveyed using GPS. Trimble Geomatics Office (TGO) is used to compute their positions and in all three cases, a GPS RTK fixed solution is attained. The coordinates of the three tripods, as determined by TGO, are shown in Table 6.2, below.

Table 6.2: Coordinates of three stationary UWB radio points computed by TGO

UWB		TGO
1	Latitude	51° 04' 48.54561"
	Longitude	-114° 07' 56.04552"
	Height (m)	1099.295
2	Latitude	51° 04' 47.03546"
	Longitude	-114° 07' 55.22099"
	Height (m)	1097.473m
3	Latitude	51° 04' 47.70789"
	Longitude	-114° 07' 53.56467"
	Height (m)	1097.489

As seen in Figure 6.4, below, the three tripods are evenly placed on the outer boundaries of the test area to try to minimize HDOP values. These three UWB radios will remain stationary throughout the data collection and act as range request responders to the UWB-GPS rover, which is the range requester.
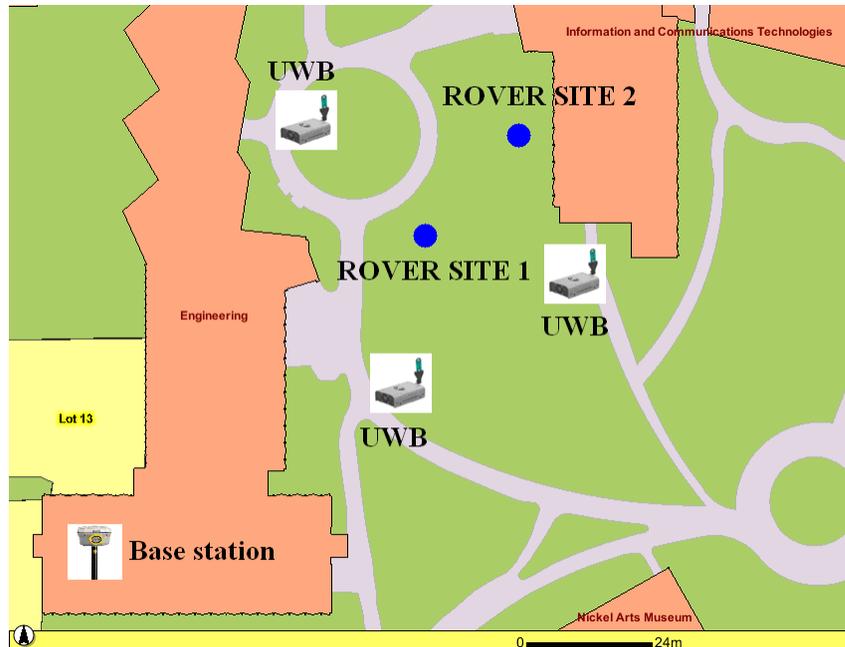
Figure 6.4: Digitized view of test area. One base station, three UWB radio tripods and two different rover locations for testing are shown (from University of Calgary 2008)

6.1.1.3 UWB-GPS Rover

The fourth UWB radio along with another GPS receiver (the "rover") is mounted on the UWB-GPS co-axial prototype on a rover pole, as seen in Figure 6.5, below. The UWB radio and GPS receiver are positioned so that their phase centers' are co-aligned. A co-axial mount was prototyped to achieve this. For details regarding the co-axial mount, please refer back to Section 4.5.5.

Figure 6.5: Trimble R8 receiver with a Time Domain UWB radio on a co-axial amount. The phase centers of both antennas are co-aligned vertically

Rover data is collected at two different locations throughout this experiment. The two locations are selected to replicate two varying signal environments. At the first location ("rover site 1"), the rover unit is placed in semi-clear signal conditions. Although this site is at some distance away from the surrounding buildings, there are a few tall pine trees surrounding part of the receiver's view of the sky. Attenuation is expected at this site. The second location ("rover site 2") is beside a two-storey engineering complex, as well as several tall pine trees. Signal masking (for one side of the sky), attenuation, multipath and fading are expected at rover site 2. Please refer back to Figure 6.4, for an illustration of where the rover sites are and Figure 6.1, for an aerial view of the test area showing the trees and building.

6.1.2 Procedure

The rover is set as a range message requester, while the other three stationary UWB radios are programmed as responders. All of the TD UWB radios are time synchronized to GPS time using the process described in Section 4.5.4.

Code DGPS measurements and UWB data are collected simultaneously on the rover pole (as seen in Figure 6.5, above) for 7-8 minutes at rover site 1 and 10 minutes at site 2 due to the fact that this is a more hostile signal location and a longer collection time may be beneficial.

6.1.3 Results

In comparing UWB-only positioning to code DGPS-only positioning, a reference solution is needed. The UWB-only and code DGPS-only solutions are meaningful (and can only be compared) if they are both differenced with the reference solution. The reference solution is a GPS RTK float solution computed with a four state extended Kalman filter with sequential measurement addition. The position and clock states are treated as random walk processes.

The UWB-only positioning solution is estimated using a 3-state square-root filter with east, north and up process noise set as 0.15 m/s, 0.15 m/s and 0.05 m/s, respectively. The position states are treated as random walk processes. The code DGPS-only solution uses a 4-state square-root filter with east, north, up, and clock offset process noise as 0.15 m/s, 0.15 m/s, 0.05 m/s and 100.0 m/s, respectively.

6.1.3.1 Rover Site #1

Rover site 1 is located near a few tall pine trees with a clear view of much of the sky. For details regarding this site and location of the site, please refer to Section 6.1.1.4 and Figure 6.4, respectively.

Figure 6.6, below, shows the UWB solution differenced with the known coordinates of the site. Despite a bias in the north and up directions, the differences are sub-metre level. Looking at the differences between code DGPS and RTK float in Figure 6.7, below, a bias still exists; furthermore, differences between the two solutions are several metres.
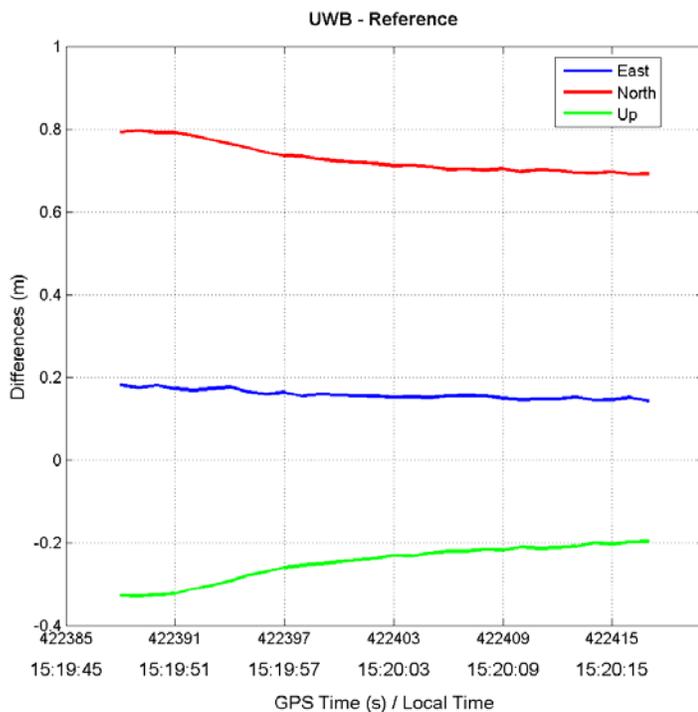
Figure 6.6: Difference between the UWB solution and GPS RTK float solution for rover site #1
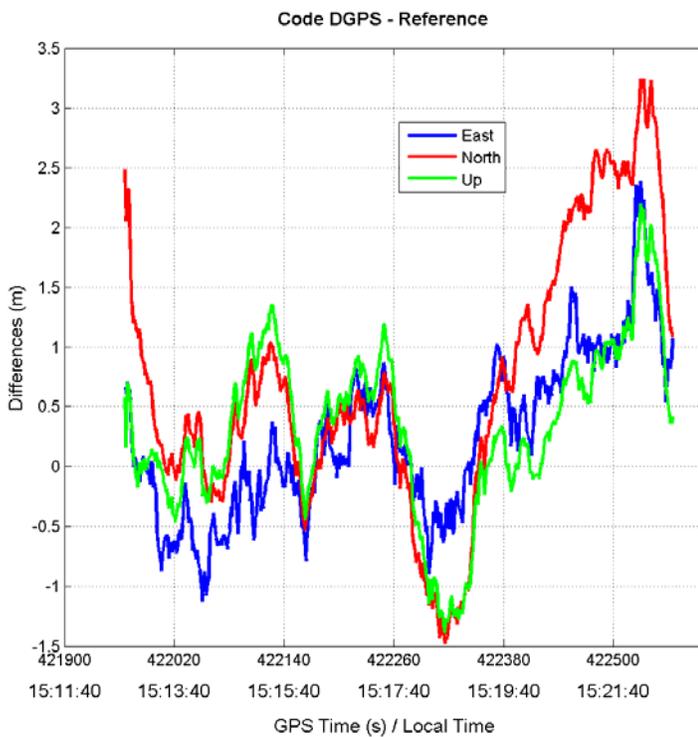
Figure 6.7: Difference between the code DGPS solution and GPS RTK float solution for rover site #1

Figure 6.8, below, shows the plane view of the UWB solution, code DGPS solution and RTK float solution laid overtop one another. Despite a scale factor and bias correction in the UWB measurements, a definite bias can still be seen compared to the RTK float reference solution. Another important observation is that the code DGPS solution is far less precise than UWB positions. UWB positions are almost always within 10 cm in precision, but as seen from the figure, code DGPS solution precision is in the metre-level.
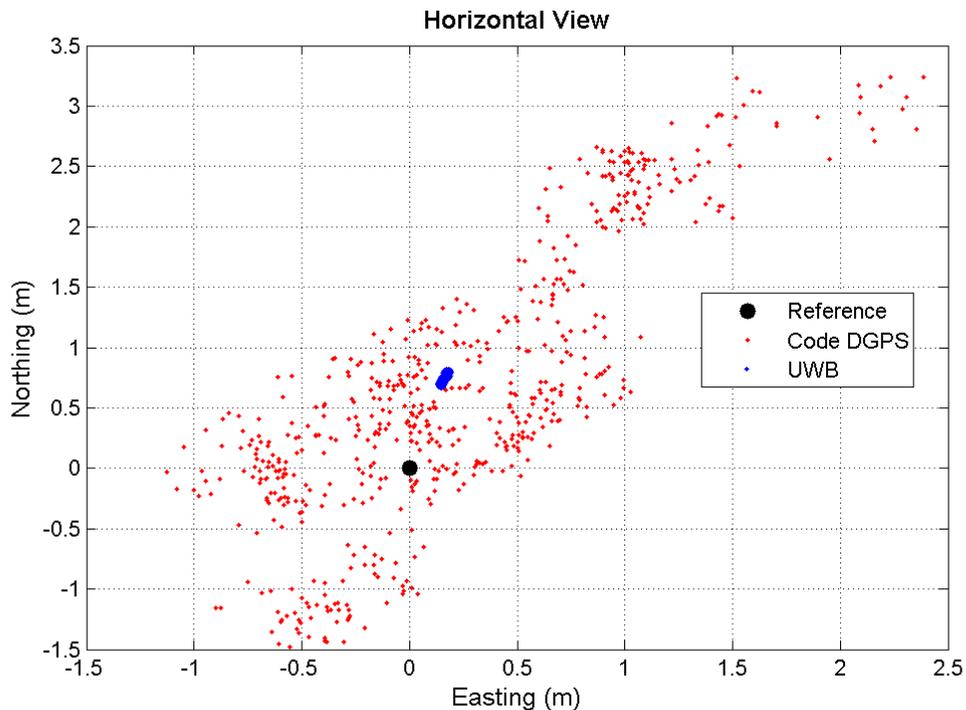
Figure 6.8: Plane view for the UWB, code DGPS, and GPS RTK float position solutions for rover site #1

UWB-only positioning looks to be more accurate and precise than code DGPS-only positioning. UWB reported sub-metre level accuracies with fairly precise measurements, whereas code DGPS-only positioning demonstrated metre-level accuracy and precision. UWB scale factor and bias errors have been corrected for, even though a bias is still observed.

6.1.3.2 Rover Site #2

This site is located in between a two-story building and tall pine trees. Hostile signal conditions are expected. For more information regarding this site and its location, please refer to Section 6.1.1.4 and Figure 6.4, respectively.

Differences between the UWB-only solution and RTK float, seen in Figure 6.9, below, indicate sub-metre level accuracy with a bias. The code DGPS differenced with RTK float solution gives accuracies of over 1 m with less bias compared to the UWB solution and is shown in Figure 6.10.
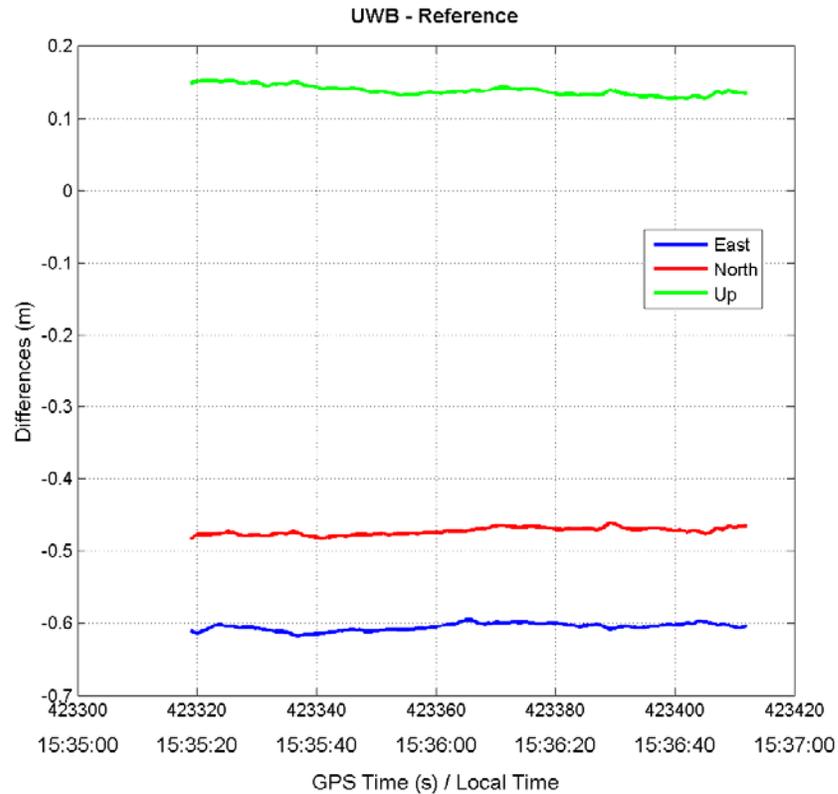
Figure 6.9: Difference between the UWB-only solution and GPS RTK float solution for rover site #2
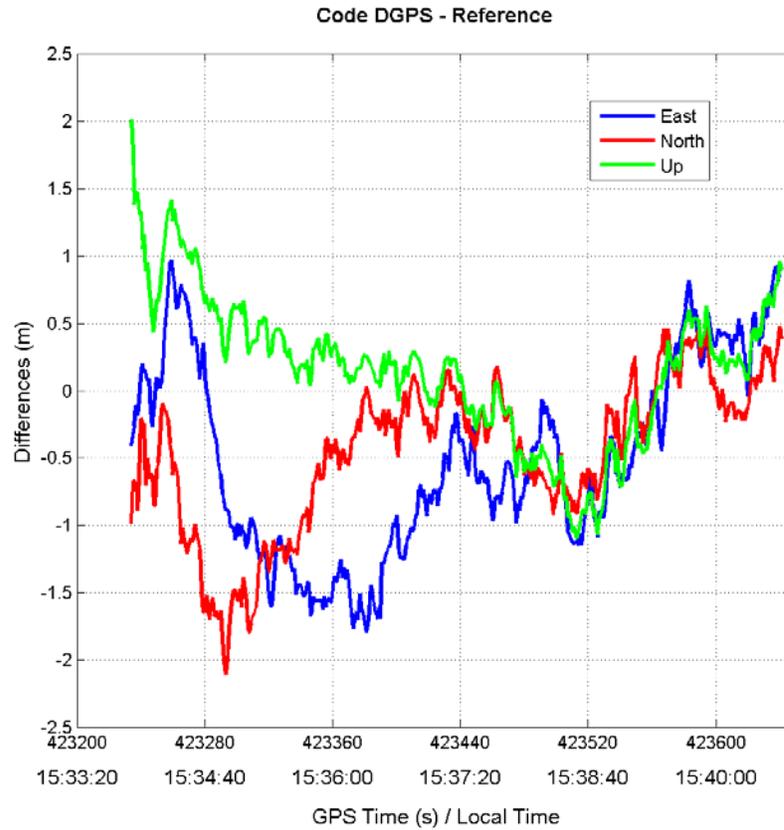
Figure 6.10: Difference between the code DGPS solution and GPS RTK float solution for rover site #2

Figure 6.11, below, shows the plane view of the three solutions: UWB-only, code DGPS-only and RTK float. The most precise solution is from UWB measurements, while code DGPS shows metre-level precision.
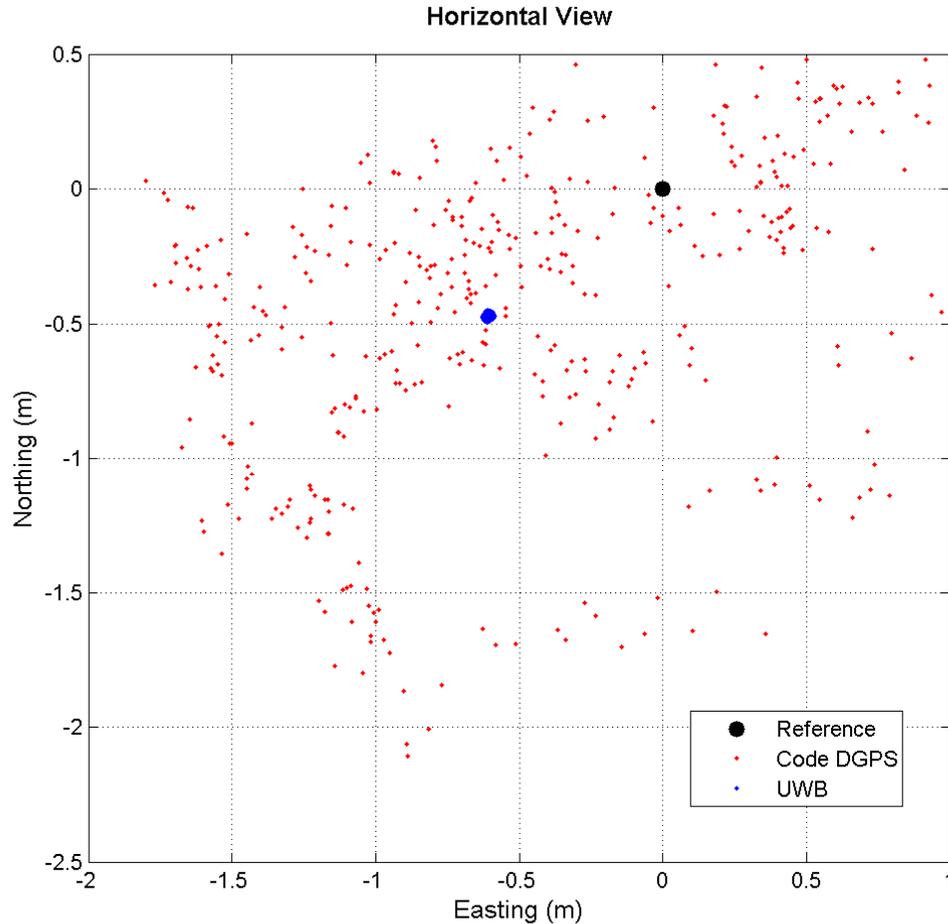
Figure 6.11: Plane view for the UWB, code DGPS, and GPS RTK float position solutions for rover site #1

Results from rover sites 1 and 2 produce several conclusions:

- ♦ UWB-only positions result in sub-metre level accuracies
- ♦ UWB provides centimetre-level precision
- ♦ The code DGPS solution gives metre-level accuracies and precision

6.2 SINGLE UWB RANGE AUGMENTATION TO CODE DGPS

In the previous section, comparing UWB and code DGPS solutions indicated that UWB provides more accurate and precise measurements than just code DGPS alone. Using the same dataset, one single UWB range is used to augment the code DGPS solution and

results are presented below. The setup and procedure, described in Section 6.1.1 and Section 6.1.2, are applicable to this investigation and are not repeated in this section.

The solution is estimated using a 4-state square root filter with elevation mask set at 13 degrees and a C/N_0 mask of 25.0 dB-Hz. The process noise values are set to 0.15 m/s, 0.15 m/s, 0.05 m/s and 100.0 m/s for east, north, up and clock offset. The position and clock states are treated as random walk processes.

6.2.1 Rover Site #1

At rover site 1, the UWB radio's measurements from reference point 2 (from Table 6.2) are added into the Kalman filter at GPS time 422100. For the entire assessment at this rover site, the same UWB radio is used.

6.2.1.1 Standard Deviation

In Figure 6.12, below, estimated standard deviations of the east component of the solution are shown. The single UWB range & code DGPS solution is shown with red, while the code DGPS-only solution is shown for reference in blue. It can be seen that as the UWB measurement is added in at GPS time 422100, the standard deviation drops to a lower value. Although this effect is more prominent in the east direction, it is also observed in the north and up directions in Figures 6.13 and 6.14, below. All UWB & code DGPS standard deviation convergence values are sub-metre, which confirms the results attained from the UWB-only versus code DGPS-only investigation in the previous section of this chapter.
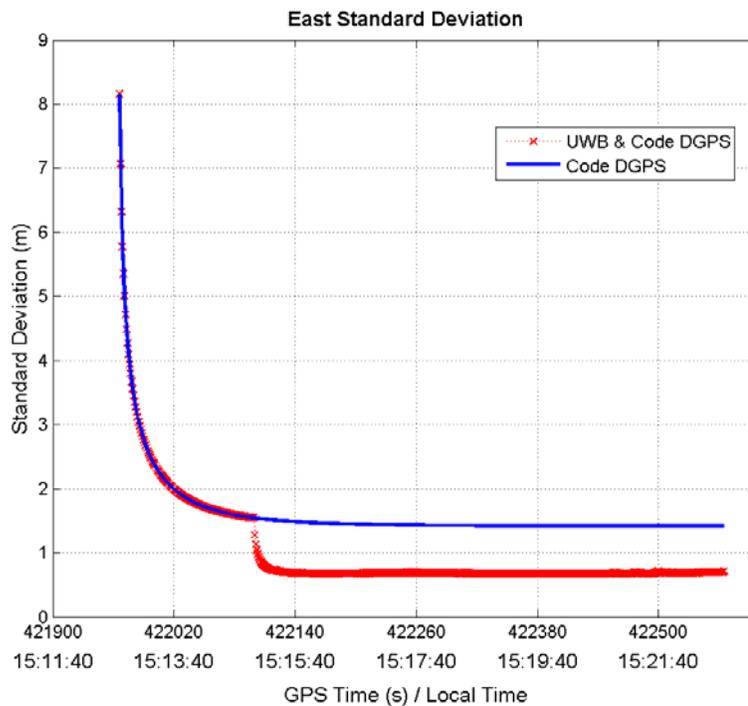
Figure 6.12: East standard position for single range UWB augmented to code DGPS, compared to code DGPS alone, for rover site #1
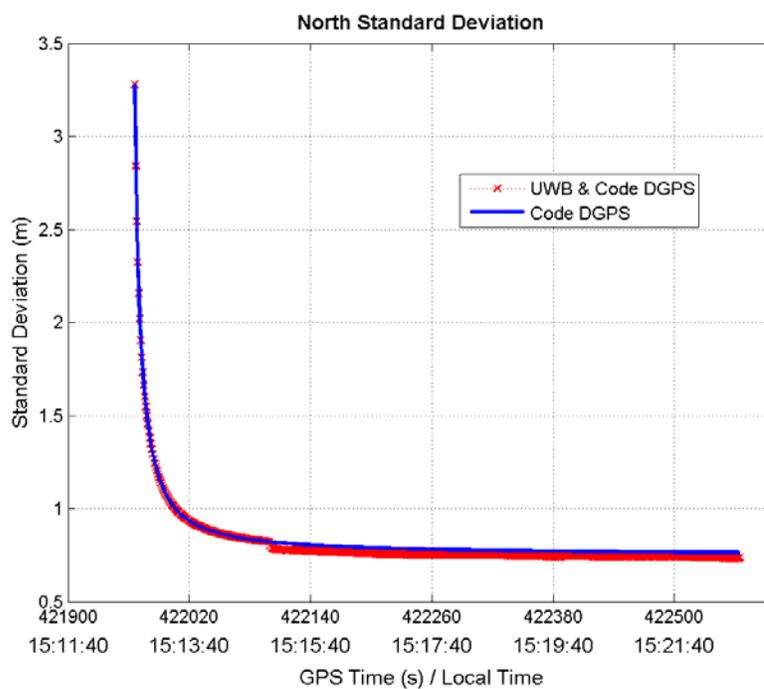
Figure 6.13: North standard position for single range UWB augmented to code DGPS, compared to code DGPS alone, for rover site #1
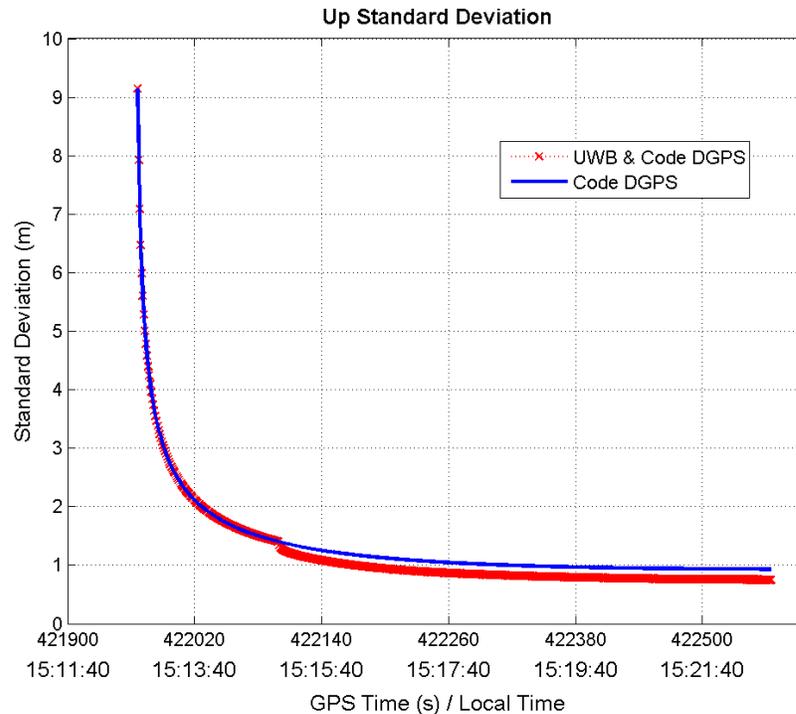
Figure 6.14: Up standard position for single range UWB augmented to code DGPS, compared to code DGPS alone, for rover site #1

The reason why there is more pronounced improvement in the east direction is because code DGPS-only standard deviation convergence values for north and up are already close to or below 1 m. So, adding in UWB measurements (which are shown to provide sub-metre precision) still results in standard deviation values of just below 1 m. On the other hand, the code DGPS-only east standard deviation value is shown to converge to approximately 1.5 m, as seen in Figure 6.12, above. So, adding in UWB measurements in that direction brings standard deviation down more than in the north and up directions.

6.2.1.2 Dilution of Precision

Figures 6.15 and 6.16, below, show the HDOP and VDOP values for the single range UWB & code DGPS solution (red plots) and the code DGPS-only solution (blue plots).

In both figures, at GPS time 422100, as the single UWB range is added in, there is a significant drop in the DOP value. In the UWB & code DGPS plots, occasional spikes are seen that revert the DOP values back to as if only code DGPS measurements were

available. These are caused by a missing UWB measurement at that specific epoch where the DOP spike occurs.
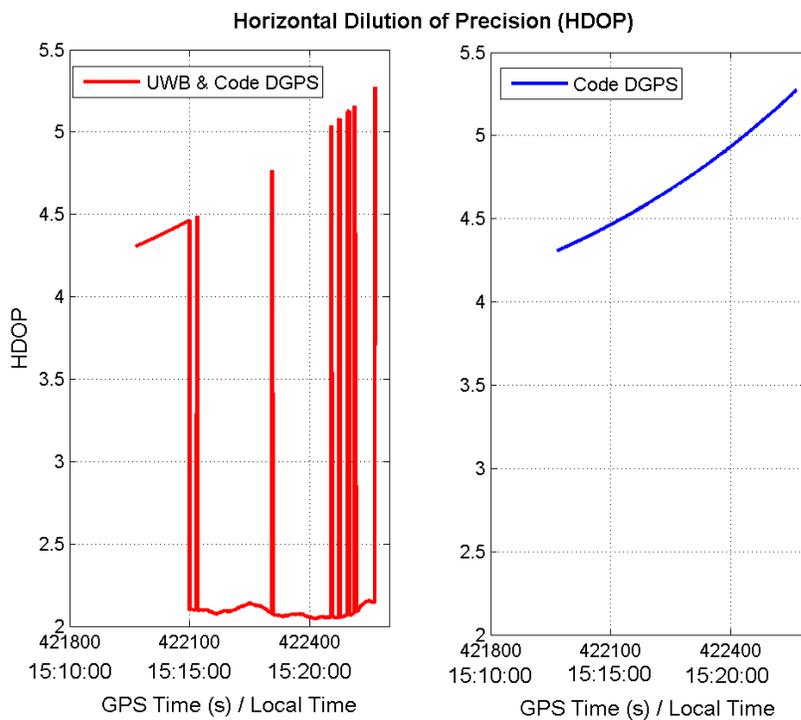
Figure 6.15: Horizontal DOP for single range UWB augmented to code DGPS, compared to code DGPS alone, for rover site #1

Vertical Dilution of Precision (VDOP)
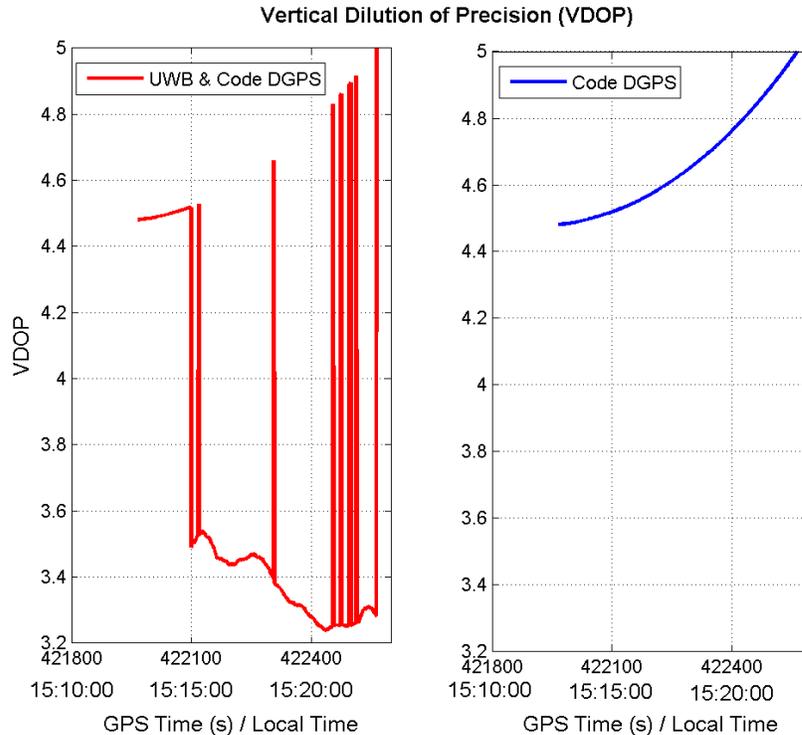
Figure 6.16: Vertical DOP for single range UWB augmented to code DGPS, compared to code DGPS alone, for rover site #1

6.2.2 Rover Site #2

At this rover site, UWB measurements are taken from the radio at "Point 1" in Table 6.2. For this test at rover site 2, only UWB measurements from "Point 1" are used. Single range UWB measurements are added into the code DGPS Kalman filter at GPS time 423300 and results are shown below.

6.2.2.1 Standard Deviation

Figures 6.17, 6.18 and 6.19, below, show the standard deviation values in the east, north and up direction for two different solutions:

- ♦ single range UWB augmented code DGPS (shown in red)
- ♦ code DGPS-only (shown in blue)

In all directions, a decrease in standard deviation is seen once the UWB measurement is added in; convergence is also faster. All final convergence values are sub-metre, which is consistent with results seen from rover site 1.
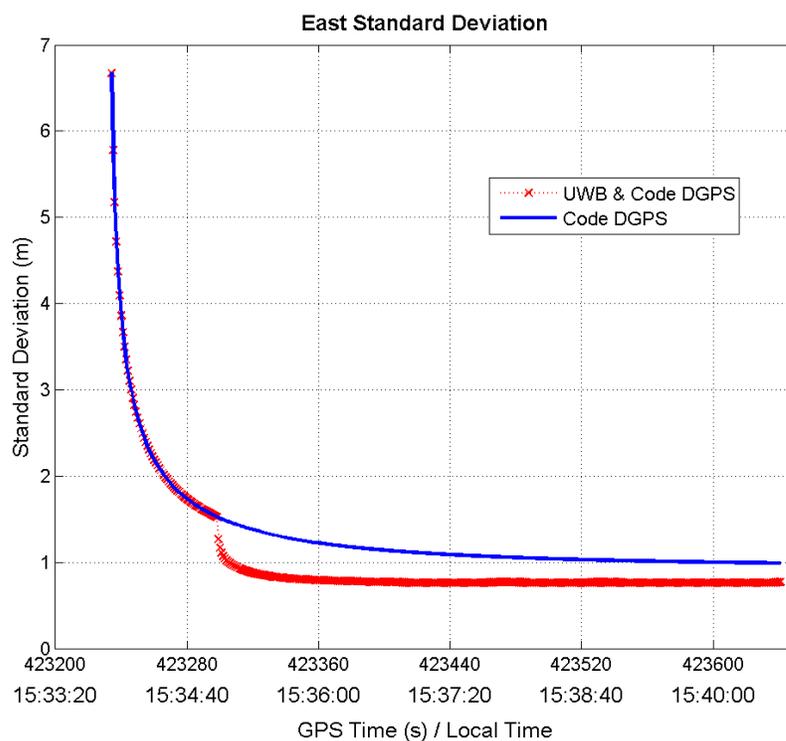
Figure 6.17: East position estimated standard deviation for single range UWB augmented to code DGPS, compared to code DGPS alone, for rover site #2
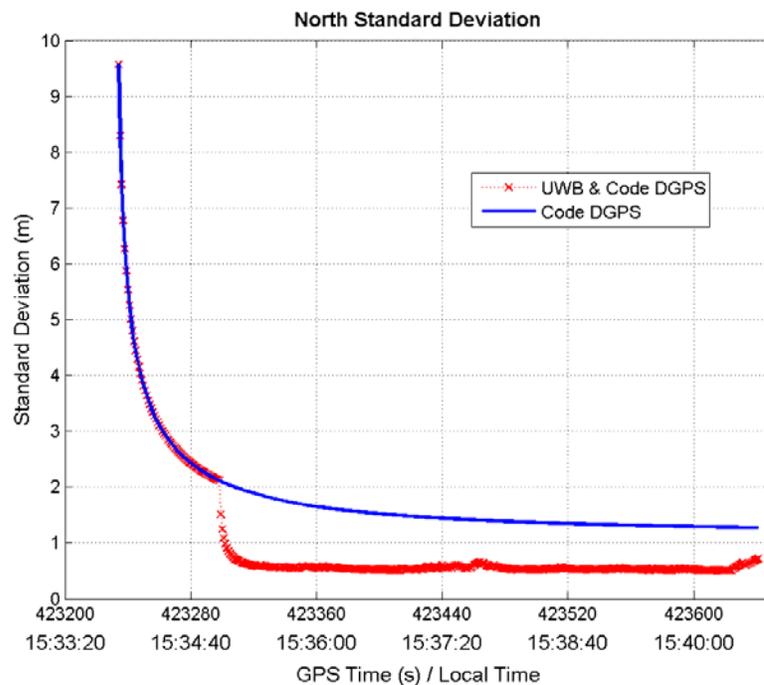
Figure 6.18: North standard position for single range UWB augmented to code DGPS, compared to code DGPS alone, for rover site #2
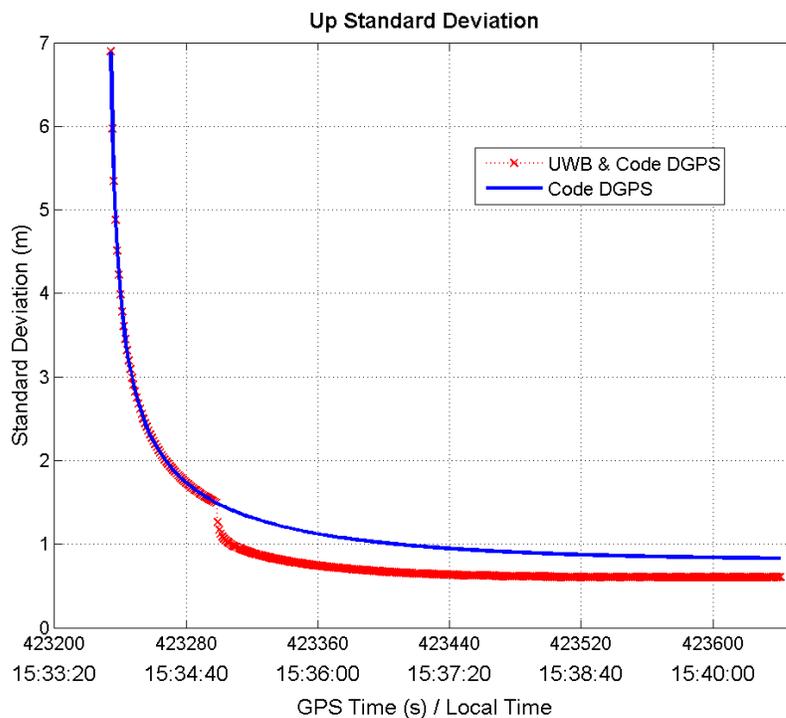
Figure 6.19: Up standard position for single range UWB augmented to code DGPS, compared to code DGPS alone, for rover site #2

6.2.2.2 Dilution of Precision

HDOP and VDOP for both solutions (code DGPS with and without single range UWB augmentation) are shown in Figures 6.20 and 6.21, below. The solution with the UWB range added is shown in red, while the code DGPS-only solution is shown in blue.

HDOP and VDOP values show a large drop once the UWB range is added into the filter. However, with periodic missing UWB ranges at some epochs, DOP values are seen to jump back up to the code DGPS-only solution values.
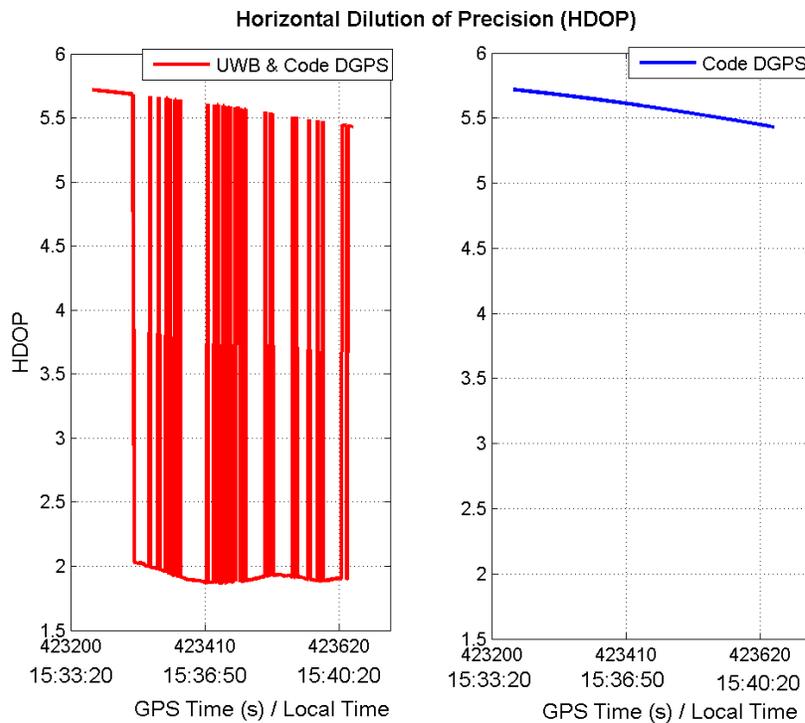
Figure 6.20: Horizontal DOP for single range UWB augmented to code DGPS, compared to code DGPS alone, for rover site #2
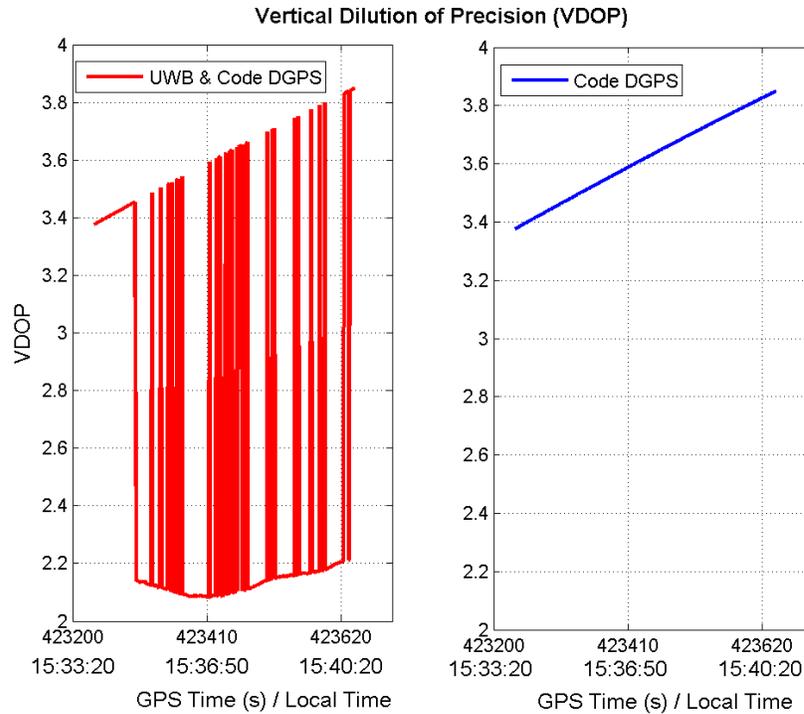
Figure 6.21: Vertical DOP for single range UWB augmented to code DGPS, compared to code DGPS alone, for rover site #2

6.2.2.3 Summary

In summary for this section:

♦ adding a single UWB measurement into the code DGPS filter results in a sub-metre level standard deviation solution even under poor signal conditions

♦ significant drops in DOP values are seen after the addition of a single UWB range measurement

6.3 MULTIPLE UWB RANGE AUGMENTATION TO CODE DGPS

GPS is used in a large number of places where its solution may not be accurate or reliable. Methods to better accuracy or reliability are constantly sought after and the integration of UWB ranges with GPS measurements provides just that. Because UWB signals have characteristics that enable them to accurately range in high multipath and indoor conditions, its augmentation to GPS is both beneficial and complementary.

6.3.1 OBJECTIVES

The goal of this section is to demonstrate that multiple range UWB can be used to augment code DGPS indoors and also outdoors in poor signal conditions while maintaining a position solution. The objectives of this research can be summarized as follows:

♦ show that an integrated multiple range UWB-code DGPS solution is more accurate and reliable than a code DGPS-only solution

♦ show that a position solution can be maintained seamlessly from outdoors to indoors

♦ show that a position solution can retain metre-level accuracy indoors, suitable for indoor pedestrian navigation

Three tests are conducted at the University of Calgary to reach these objectives. Two of these tests are conducted outdoors, with one test involving a static rover and the other test using a kinematic rover. The third and final study in this section deals with using multiple UWB ranges to augment/replace code DGPS as the rover unit enters into a building and suffers a complete GPS outage.

6.3.2 Test 1: Outdoor Multiple UWB Range & Code DGPS Static Test

In this experiment, two Trimble R8 receivers and four MSS UWB radios are used in a static test. Four UWB radios result in three UWB ranges. The test is performed outdoors at the University of Calgary. Figures 6.22 and 6.23, below, show a figure of the test area.

All solutions estimated in this outdoor multiple UWB range & code DGPS static test are from a 4-state square root filter with an elevation mask of 13 degrees and C/N_0 mask of 18.0 dB-Hz. The process noise is 0.05 m/s, 0.05 m/s, 0.05 m/s and 100.0 m/s for east, north, up and clock offset. The position and clock states are treated as random walk processes.
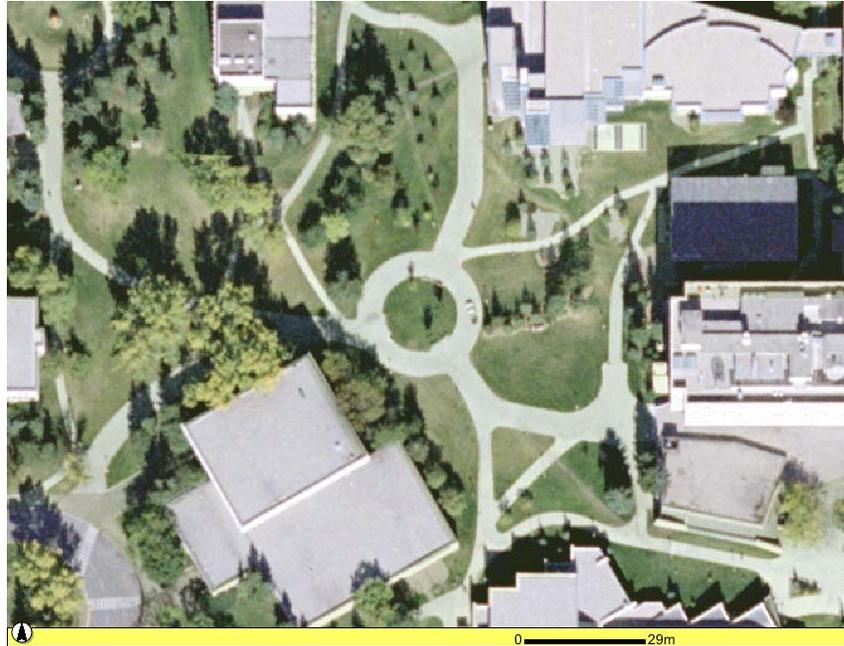
Figure 6.22: Aerial view of test area for static/kinematic testing (from Google Maps 2008)
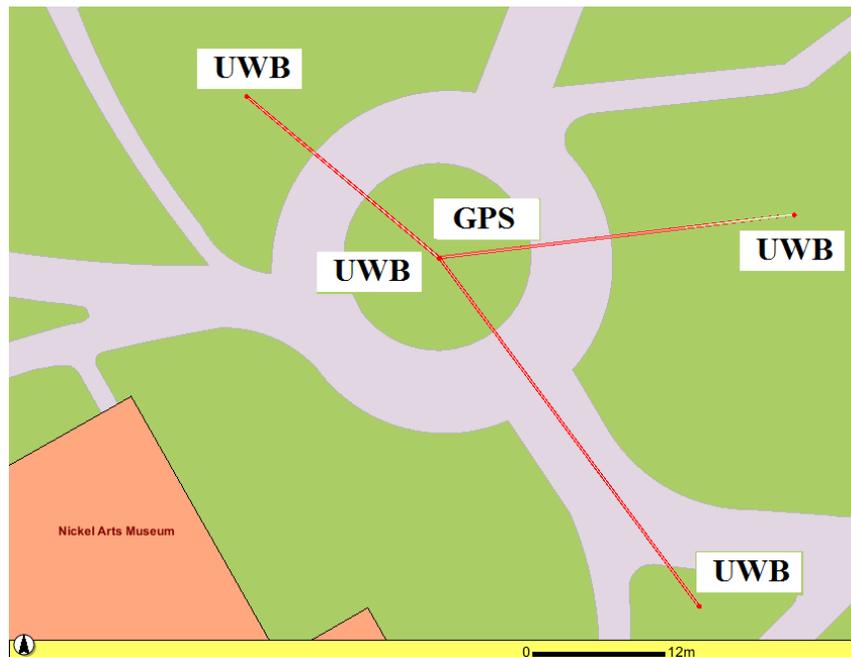
Figure 6.23: Digitized view of test area for static testing (from University of Calgary 2008)

For the static test, a single GPS base station is set up over a known coordinate point several hundred metres away. Three UWB beacons, also with known coordinates, are set up nearby the UWB-GPS rover unit.

After several minutes of data collection by the rover, the code DGPS-only solution is compared with the multiple range UWB augmented code DGPS solution, as shown in Figure 6.24.
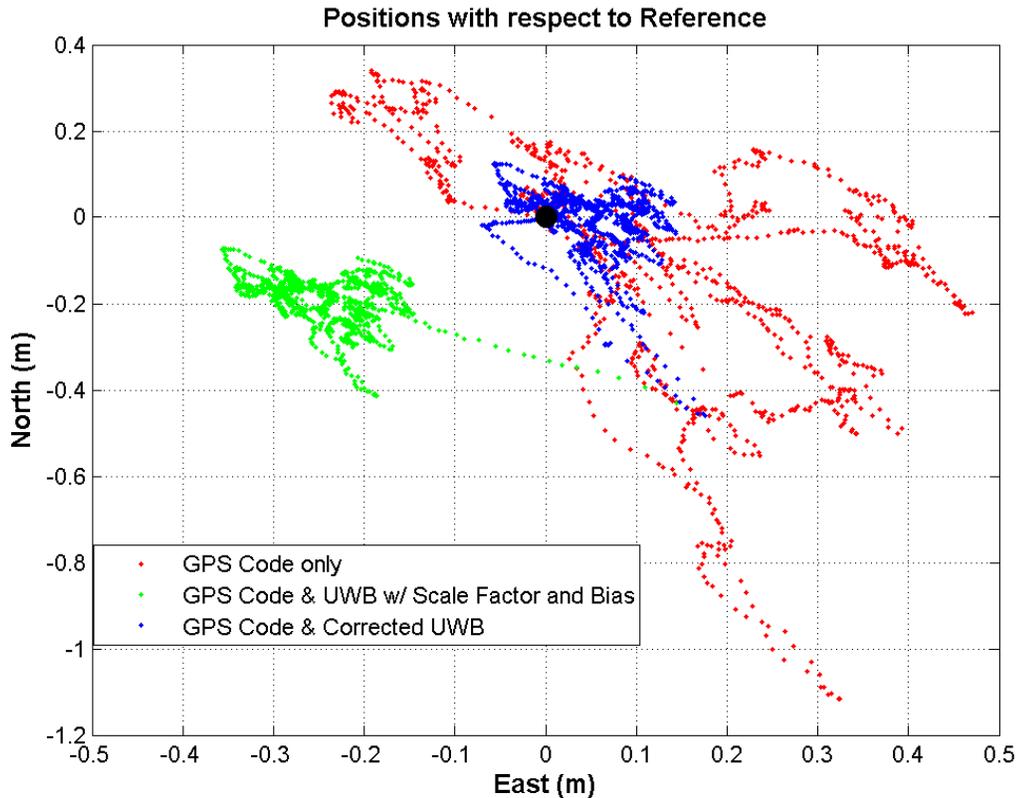
Figure 6.24: Position solutions for various processing schemes. The black dot is the reference truth point. [static]

In Figure 6.24, above, the black dot located at (0 m, 0 m) [Easting, Northing] is the truth position. The red-coloured solution is the code DGPS solution which shows deviations of over a metre compared to truth. However, once UWB ranges are combined with code DGPS measurements, it can be seen in that the variance of the solution decreases quite significantly. The green and blue solution in Figures 6.24 and 6.25 indicates the impact of the UWB radios' scale factor and bias on UWB measurements and thus, should be removed for accurate and reliable results.
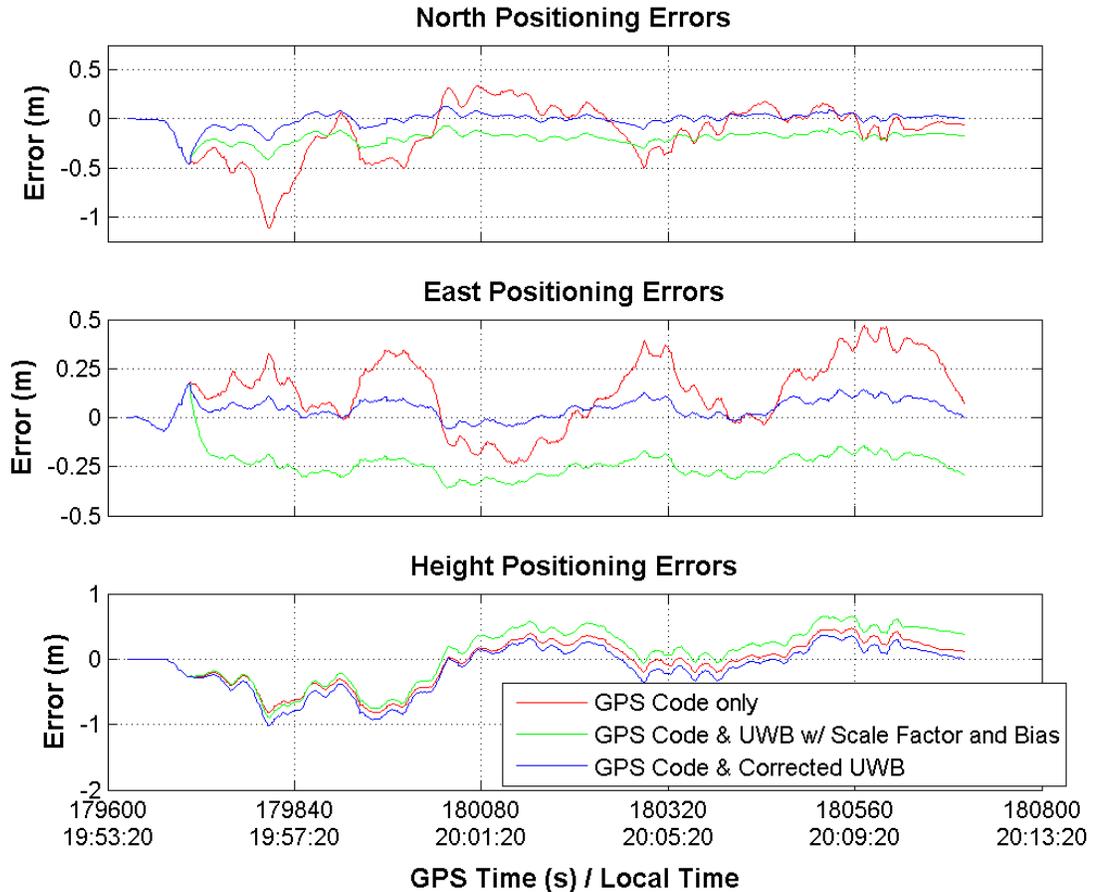
Figure 6.25: Positioning errors for various processing schemes [static]

In Figure 6.25, above, height positioning errors do not seem to be affected by the insertion of the three UWB range measurements with code DGPS measurements. This is because all of the UWB beacons are located at approximately the same height and thus, all distances are taken in the horizontal plane. Addition of horizontal range measurements should therefore not affect vertical or height positions significantly. Similar observations are made in the standard deviation of the positions seen in Figure 6.26, below.

Standard Deviation of Positions
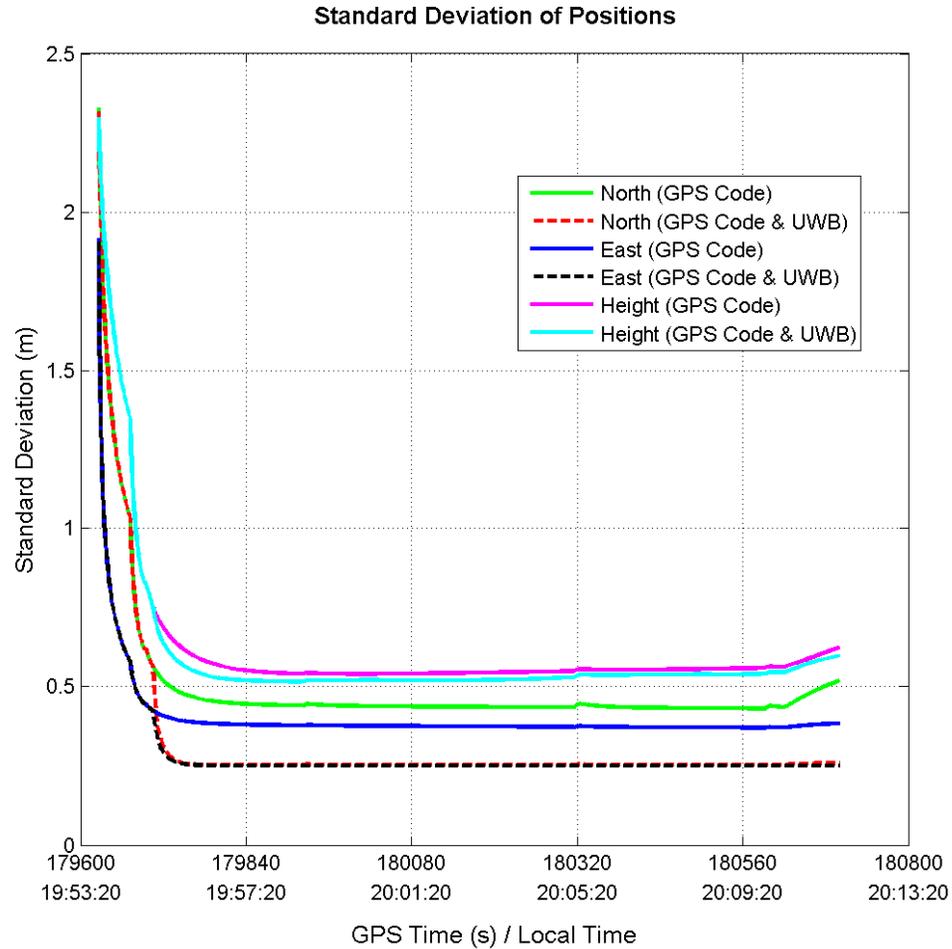
Figure 6.26: Standard deviation for position solutions [static]

6.3.3 Test 2: Outdoor Multiple UWB Range & Code DGPS Kinematic Test

The same GPS base station and three UWB stationary radios are used in the kinematic test. The difference between the static test and the kinematic test is that the rover is now walked along the outer edge of the concrete sidewalk loop, as seen in Figure 6.27. Please note that all UWB measurements shown and used herein have been calibrated for UWB scale factor and biases.

All solutions estimated in this outdoor multiple UWB range & code DGPS kinematic test are from a 4-state square root filter with an elevation mask of 13 degrees and C/N_0 mask of 18.0 dB-Hz. The process noise is 0.05 m/s, 0.05 m/s, 0.05 m/s and 100.0 m/s for east,

north, up and clock offset. The position and clock states are treated as random walk processes.

Figure 6.27: Test area for kinematic test

Figure 6.28 shows the rover's trajectory comparing three different solutions. The red and blue solutions in the figure show the difference between augmenting the code DGPS with and without UWB measurements. And to simulate hostile conditions, all but two satellites were taken out of the code DGPS solution and the solution with two satellites and three UWB ranges was computed. From the figure, the solution with two satellites and three UWB ranges still maintains metre level accuracy.
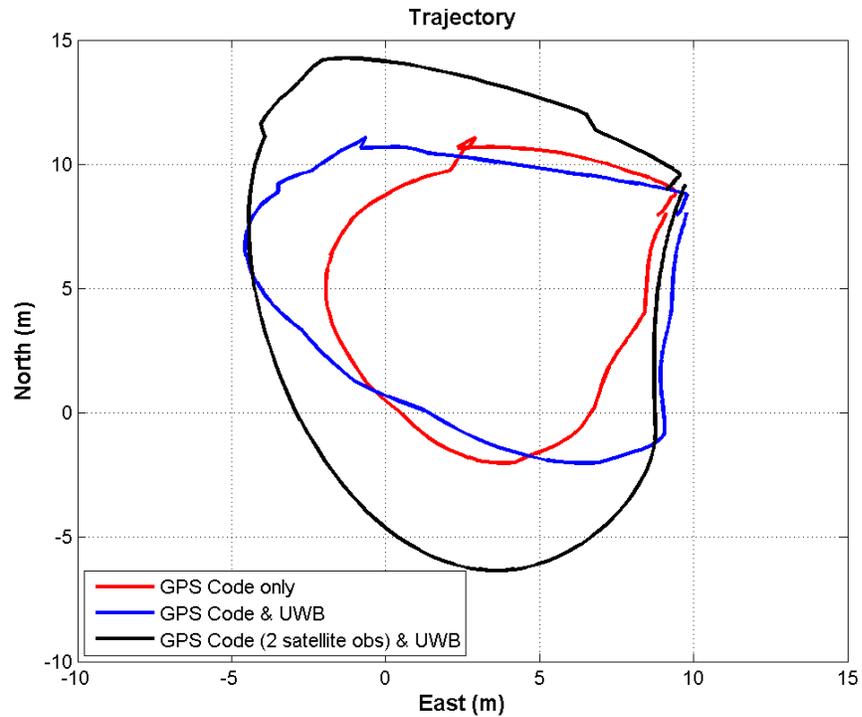
Figure 6.28: Trajectory for various positioning schemes [kinematic]

The HDOP solution in Figure 6.29, below, shows that the code DGPS (full constellation) with UWB ranges has the lowest DOP values. At GPS time 181580, the code DGPS HDOP solution spikes up to over 9, while the solutions with UWB ranges included do not observe such a dramatic increase. The reason for the sudden increase can be attributed to the fact that the rover unit was passing by several tall trees. Seeing that the other two solutions (both having UWB ranges) were able to weather this obstruction indicates that solutions with UWB ranges included, give a stronger geometric strength in the position solution.
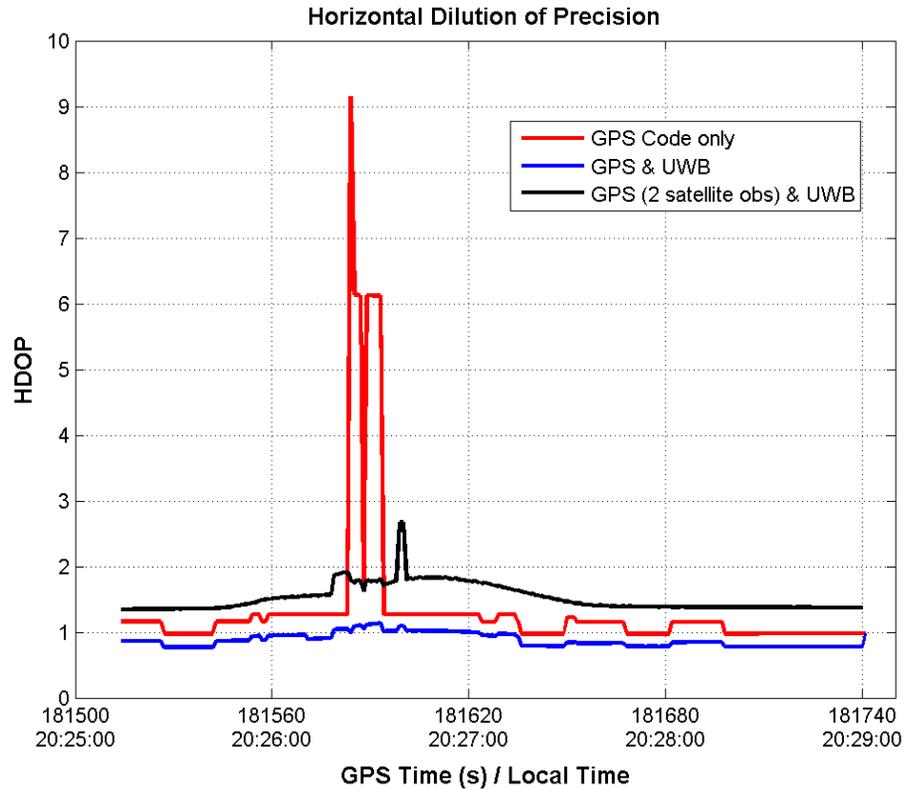
Figure 6.29: HDOP for various positioning schemes [kinematic]

6.3.4 Test 3: Outdoor-Indoor-Outdoor Multiple UWB Range & Code DGPS Kinematic Test

For this outdoor-indoor-outdoor test procedure, two Trimble R8 receivers, four MSS UWB radios and one total station are used. Four UWB radios produce three ranges.

Testing is done at the Information and Communications Technologies (ICT) building at the University of Calgary, as seen in Figure 6.30 and 6.31, below. Three of the UWB radios are set up in fixed and surveyed positions inside the building. The fourth UWB radio and one of the Trimble R8 receivers act as the rover. The second Trimble R8 receiver is used as a DGPS base station several hundreds of metres away from the data collection site.

Figure 6.30: Aerial view of the ICT building (from Google Maps 2008)
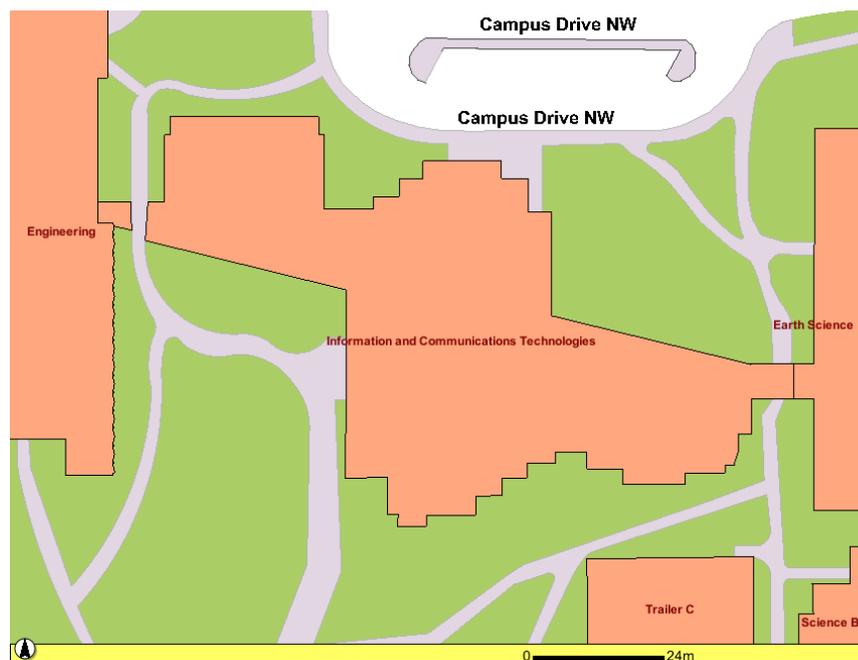
Figure 6.31: Digitized view of the ICT building (from University of Calgary 2008)

Prior to testing, the trial trajectory outside and inside the building is surveyed using a total station so that Code GPS and UWB positions have a reference to compare to. Additionally, the positions of the stationary UWB points, where three of the UWB radios

are placed, are also surveyed so that their absolute positions are known. This is necessary because the absolute position of the rover can only be determined if the absolute positions on the stationary UWB points are known. Otherwise, UWB trilateration only results in relative positioning. The location of the UWB points is selected strategically to ensure low DOP values for the rover unit.

Once the code DGPS base station is set up and three of the UWB radios are placed on the surveyed points, the test begins. The rover unit is placed outside the building in an area with relatively clear signal conditions for the GPS receiver. Once the rover has initialized, it is slowly brought towards the building, stopping at several outdoor waypoints that have been surveyed. The rover is then brought into the building and stopped on the first waypoint on the trajectory path. During the indoor segment of this test, all GPS signals are lost immediately after entering the building. Luckily though, the UWB radio on the rover still continues to receive LOS and NLOS range measurements from the stationary UWB radios located in the building. Each waypoint is occupied for several minutes, before proceeding back outdoors into clearer skies where the test concludes. In Figure 6.32, below, the blue dots indicate the locations where the rover unit is stopped along the trajectory path.

Figure 6.32: Blue dots indicate positions that have been surveyed. The rover unit will stop on the blue dots and travel along the trajectory (from University of Calgary 2008)

The GPS solution while outside uses a 4-state square root filter to estimate its positions and clocks. An elevation mask of 5 degrees and C/N_0 mask of 0 dB-Hz is used to try to capture as many satellite signals as possible in a very hostile environment. The indoor UWB solution uses the same 4-state square root filter, but the clock term is fixed once the rover suffers from a GPS outage. The same process noise is used for both solutions and it is 0.8 m/s, 0.8 m/s, 0.8 m/s and 100.0 m/s for east, north, up and clock offset (for GPS only). The states are treated as random walk processes.

Looking at the number of observations in Figure 6.33, below, a Kalman filter is able to maintain a position throughout the test. During outdoor data collection, the only measurements observed are ones from GPS. No UWB ranges are measured during this time. On the other hand, during indoor data collection, only UWB ranges are able to be observed, while the rover suffers from a complete GPS outage.

Figure 6.33: Number of observations for the outdoor-indoor test

Figure 6.34, below, shows the rover trajectory while inside the building. Again, once the rover enters the building, all GPS measurements are lost and only three UWB ranges are used to maintain the solution. Sub-metre level accuracy can be observed at all truth points and is sufficient for indoor pedestrian applications.
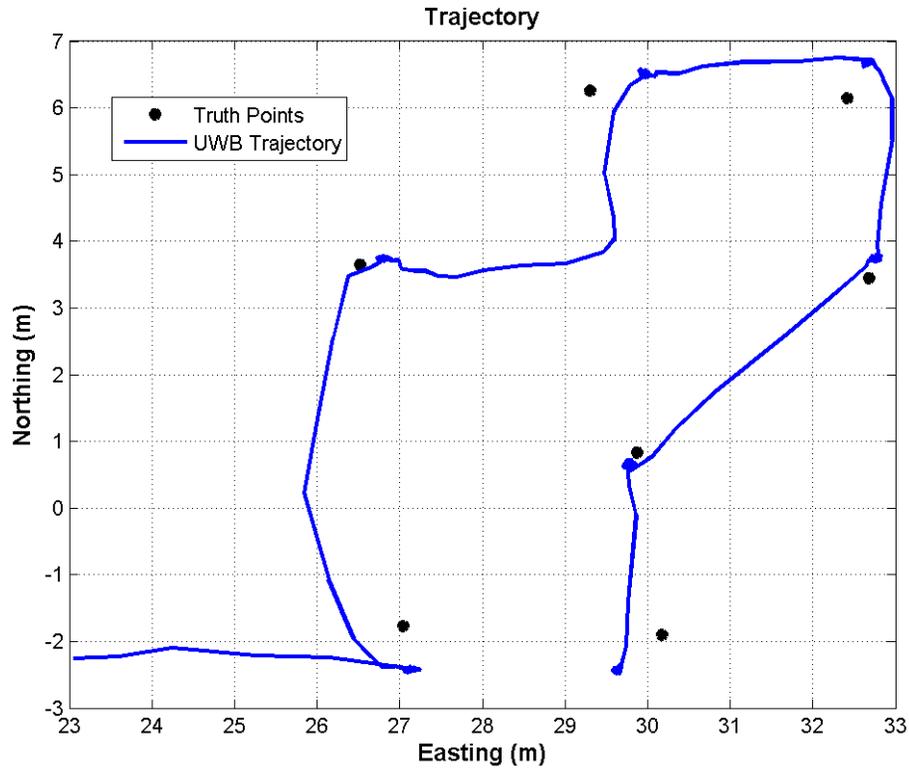
Figure 6.34: Indoor UWB trajectory versus truth points

In Figure 6.35, the standard deviation of the solution shows that the standard deviation is quite poor just as the rover is entering and leaving the building. However, once the rover unit enters the building and begins to receive UWB ranges, the standard deviation drops down to metre-level again.
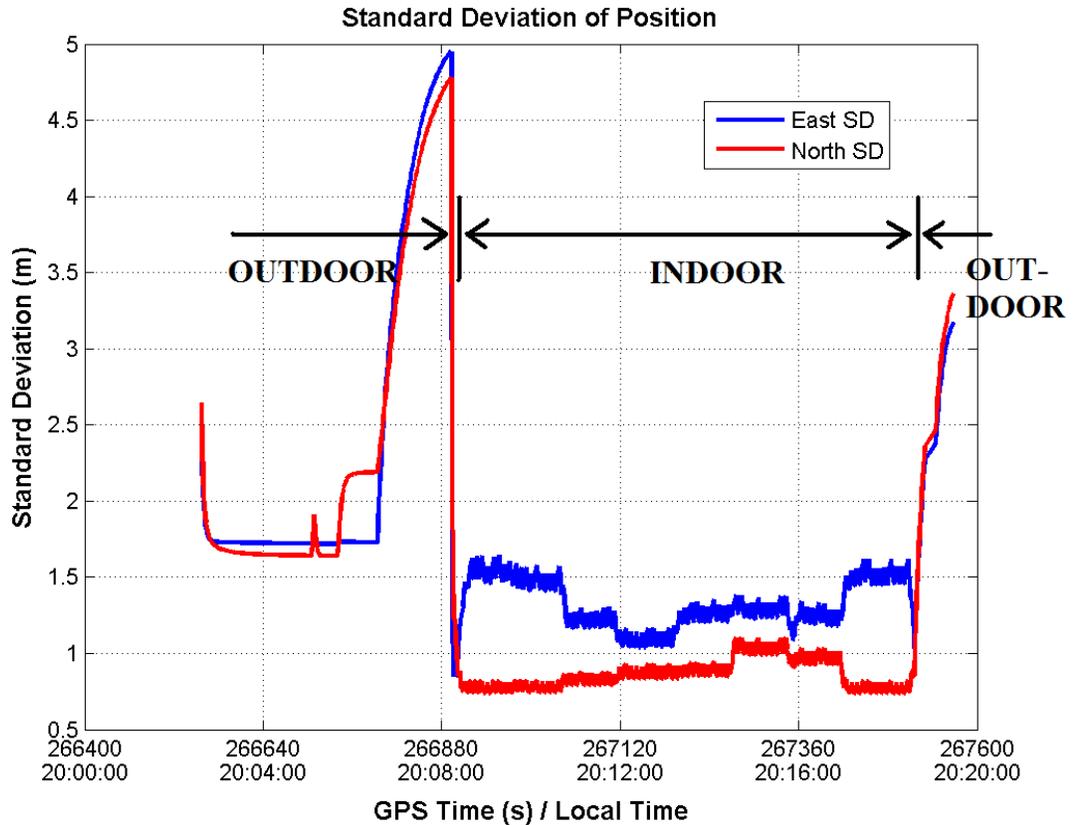
Figure 6.35: Standard deviation of positions for outdoor-indoor test

Code DGPS measurements alone will have major difficulties estimating a solution while indoors. However, with the addition of several UWB ranges, the position solution continues to be estimated even with an insufficient number of GPS measurements. The accuracy of the indoor position solution is highly correlated to the accuracy of the UWB ranges. Indoor multipath, attenuation and fading do not affect the indoor solution significantly.

6.3.5 Summary

UWB measurements were combined with code DGPS measurements in a static and kinematic test. In the static test, multiple range UWB augmented code DGPS solution reported more accurate and precise results compared to the code DGPS-only solution. Standard deviation values for Northing and Easting decreased and converged more quickly once UWB measurements were added into the solution. For the kinematic test, a

simulation of "indoor" or hostile signal conditions was created by removing all but two GPS satellites in the solution. UWB measurements integrated with code DGPS (two satellite constellation) reported metre-level deviations from the UWB-code DGPS (full constellation) and code DGPS-only solutions. HDOP values showed that UWB-code DGPS (full constellation) had the lowest DOP values and was resistant to sudden DOP increases observed by the code DGPS-only solution.

The final test in this chapter studied whether or not a solution was able to be maintained between outdoor to indoor navigation. Several points outdoors and indoors were surveyed by a total station so that their absolute positions would be known and could be used to compare the UWB-GPS rover trajectory. While outdoors, only GPS measurements and no UWB ranges were observed. However, once the rover traveled indoors, only UWB measurements were made and GPS suffered from a complete outage. The solution whilst indoors reported accuracies in the sub-metre level. A position solution was maintained as the rover traveled outdoors, to indoors, then back outdoors.

In all tests where UWB was used to augment GPS, metre-level or better accuracies were observed and thus, sufficient for most pedestrian navigation applications. However, this level of accuracy is inadequate for numerous other applications requiring high-accuracy and high-precision. The next chapter deals with the addition of GPS carrier-phase measurements in search of even more accurate position solutions.

CHAPTER 7: ULTRA WIDEBAND AND THE GPS RTK FLOAT SOLUTION

In the previous chapter, UWB measurements were used to augment code DGPS measurements to provide metre to sub-metre level accuracy. This degree of accuracy is sufficient for applications such as pedestrian or vehicle navigation, however, this is often not accurate enough for a host of other applications. Hence, the need to combine UWB measurements with more accurate and precise GPS measurements will be the topic of this chapter.

This chapter is divided into two sections. The first part describes single range UWB augmentation to a GPS RTK float filter and the results are shown Section 7.1. The second section of the chapter deals with the integration of multiple UWB ranges with the GPS RTK float filter. Several varying signal conditions are created and tested with this integration. Details can be found in Section 7.2. The proposed augmentation of UWB ranges to GPS measurements has the potential to provide a user with the ability to survey or navigate in hostile signal environments.

7.1 SINGLE RANGE UWB AUGMENTATION TO THE GPS RTK FLOAT FILTER

Two tests are conducted to study the GPS RTK float solution augmented with single UWB range. The first UWB-augmented GPS test is performed on the rooftop of the engineering building at the University of Calgary, while the second test is conducted in a suburban neighbourhood in Calgary, Canada.

7.1.1 Single UWB Range Augmentation to GPS RTK Float: Test #1

Two Trimble R8 GNSS receivers and two TD UWB radios are used. The GNSS receivers and the UWB radios are mounted on the co-axial antenna mount previously described in Section 4.5.5.

The estimated solution uses a 4-state Kalman filter with process noise in east, north, up and clock offset as 0.05 m/s, 0.05 m/s, 0.05 m/s and 100.0 m/s. The states are treated as random walk processes.

The float solution from GPS alone is compared to the solution from UWB augmented GPS and is shown in Figures 7.1 and 7.2, below.
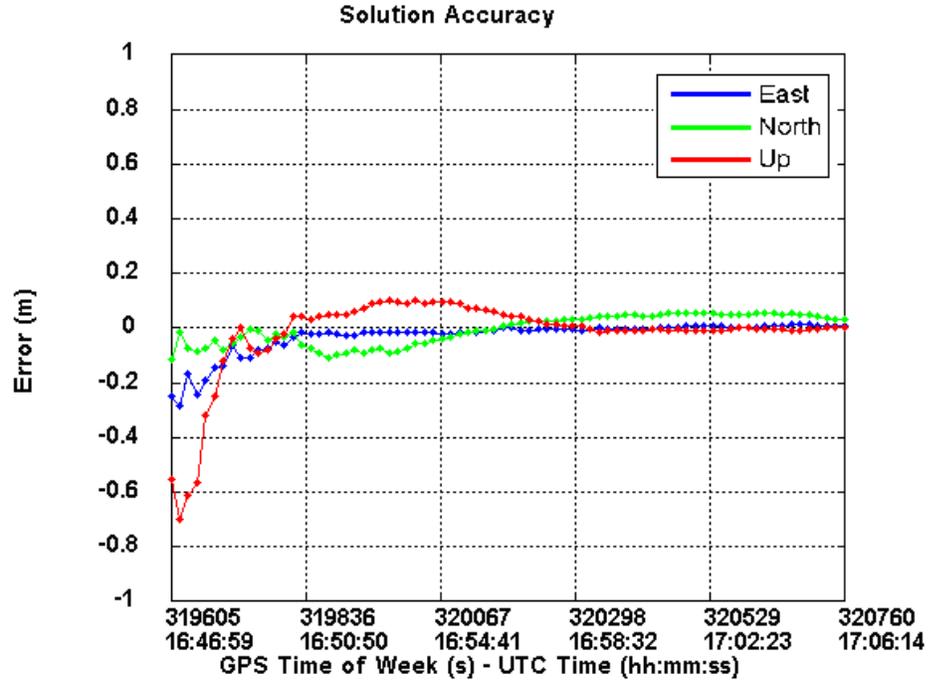
Figure 7.1: Position Errors for GPS-alone solution
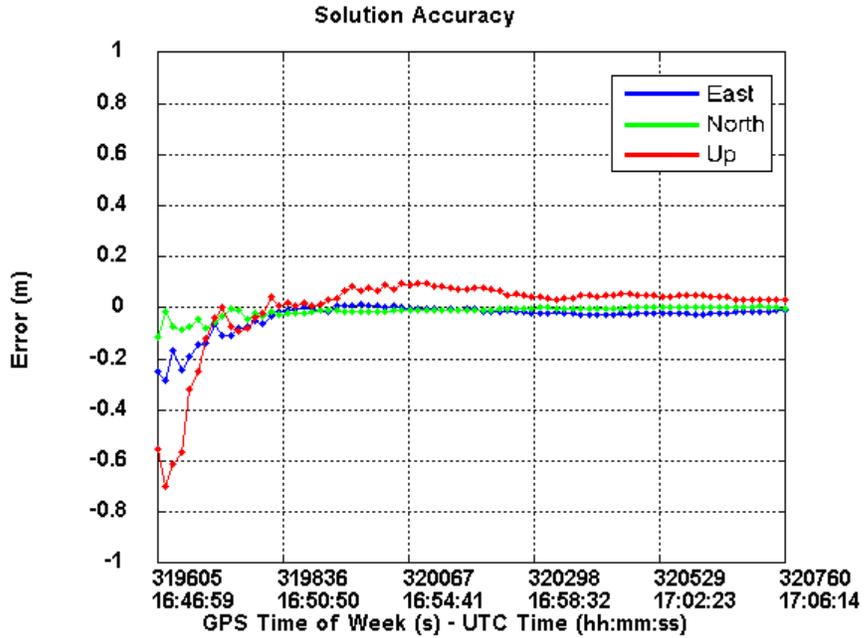
Figure 7.2: Position Errors for UWB-GPS solution

Table 7.1: Position RMS error for GPS-alone and UWB-GPS solutions

	North (m)	East (m)	Up (m)
GPS	0.0679	**0.0543**	0.154
GPS & UWB	0.0686	**0.0261**	0.156

From Table 7.1, above, there is noticeable improvement in the East solution position error. This is primarily due to the orientation of the pillars used. The pillars have East-West orientation and shared approximately the same height and latitude.

If the estimated standard deviation of the position solutions is compared, there is visible drop in the longitude uncertainty when UWB ranges are added into the GPS measurements. This can be clearly seen in Figures 7.3 and 7.4, below.

137
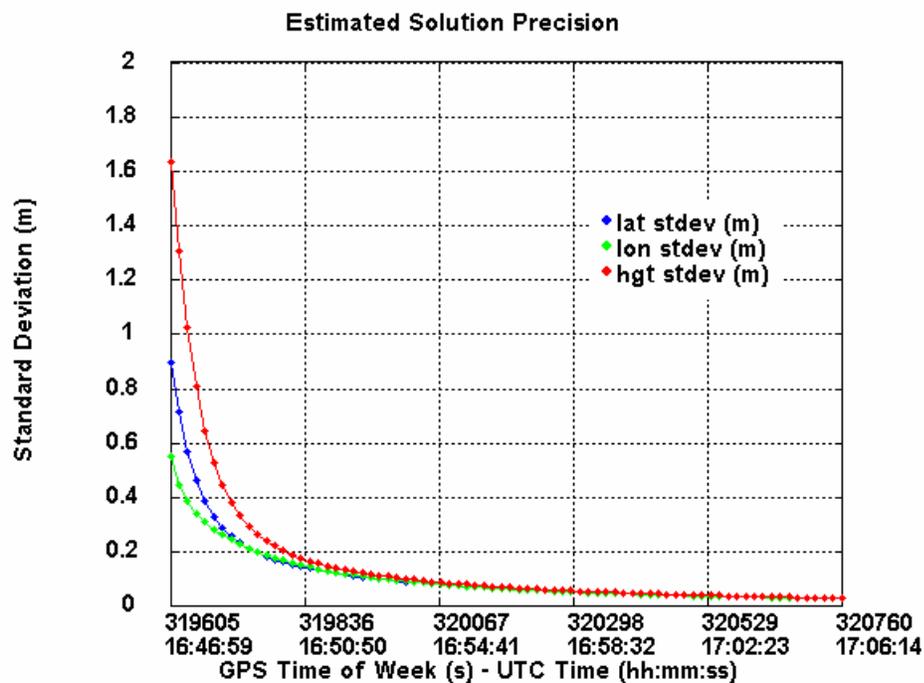
Figure 7.3: Standard deviation for GPS-alone solution
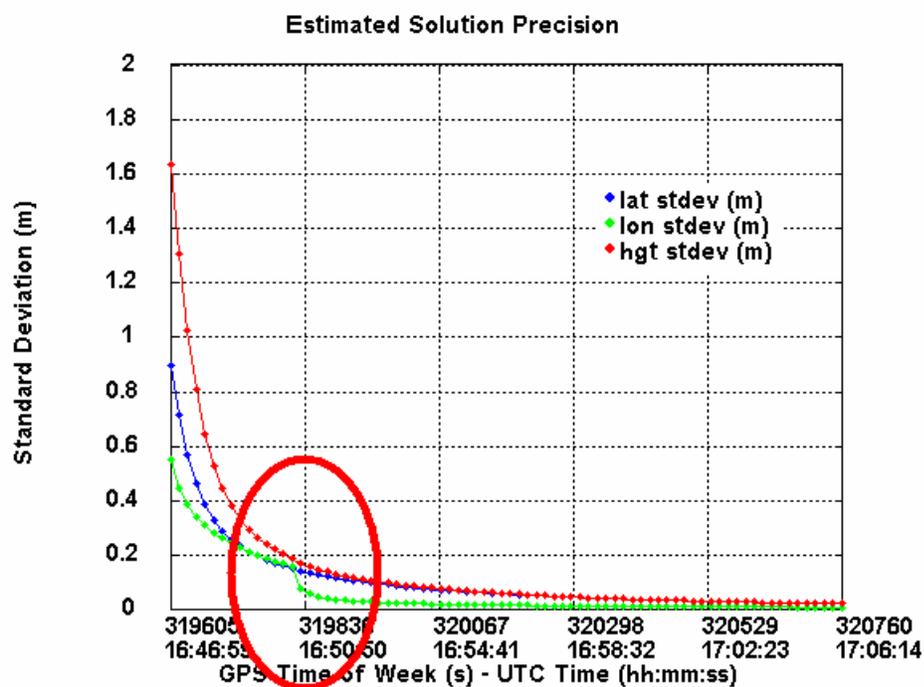
Figure 7.4: Standard deviation for UWB-GPS solution. Red circle represents the time when UWB is introduced into the GPS measurements.

7.1.2 Single UWB Range Augmentation to GPS RTK Float: Test #2

The second single range UWB-GPS augmentation test is conducted in Brentwood, a suburban community of Calgary, Canada. The location is selected because the community has relatively dense tree cover. Again, two Trimble R8 GNSS receivers and two TD UWB radios are used. One of the systems is positioned on a tripod as seen in Figure 7.5, below, while the other mount is placed on a rover pole.

Figure 7.5: UWB-GPS mounted on a tripod

The tripod is set up in a location where the GPS receiver has clear signal reception and it remains there for the duration of the test. The rover pole, on the other hand, is set up in initially good signal conditions, but is brought to points under a large tree and near the north-east side of a house where signal conditions are degraded by signal masking, multipath and attenuation. At each test point the rover pole is held stationary for approximately three minutes.

UWB ranges vary from 13 to 17 metres and the number of satellites used in the solution range from 7 to 11, as seen in Figures 7.6 and 7.7, respectively.
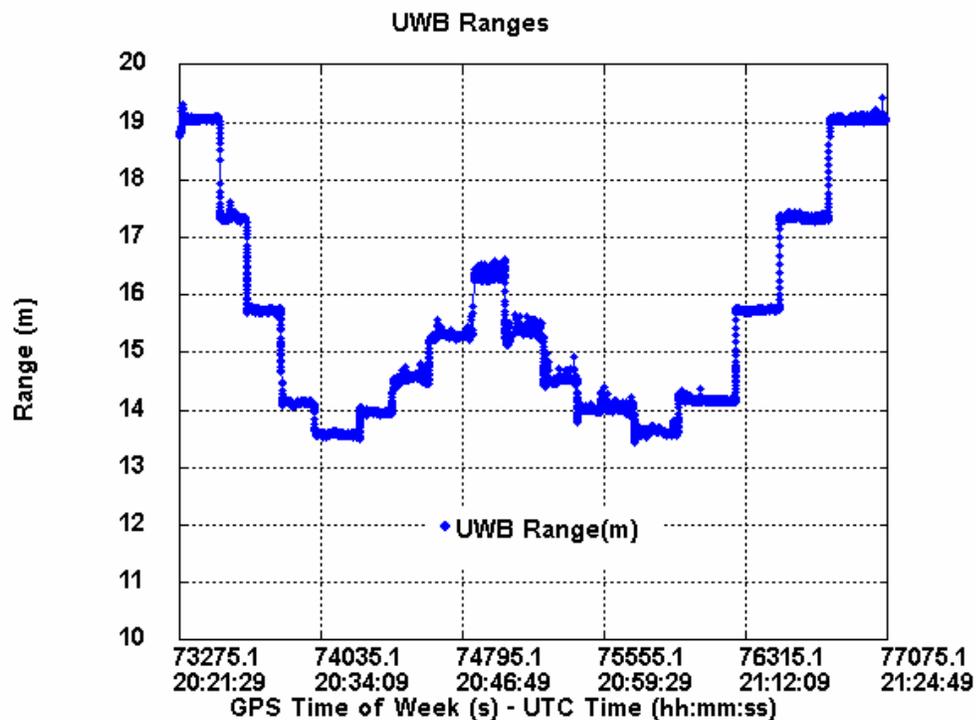
Figure 7.6: Observed UWB range as a function of time
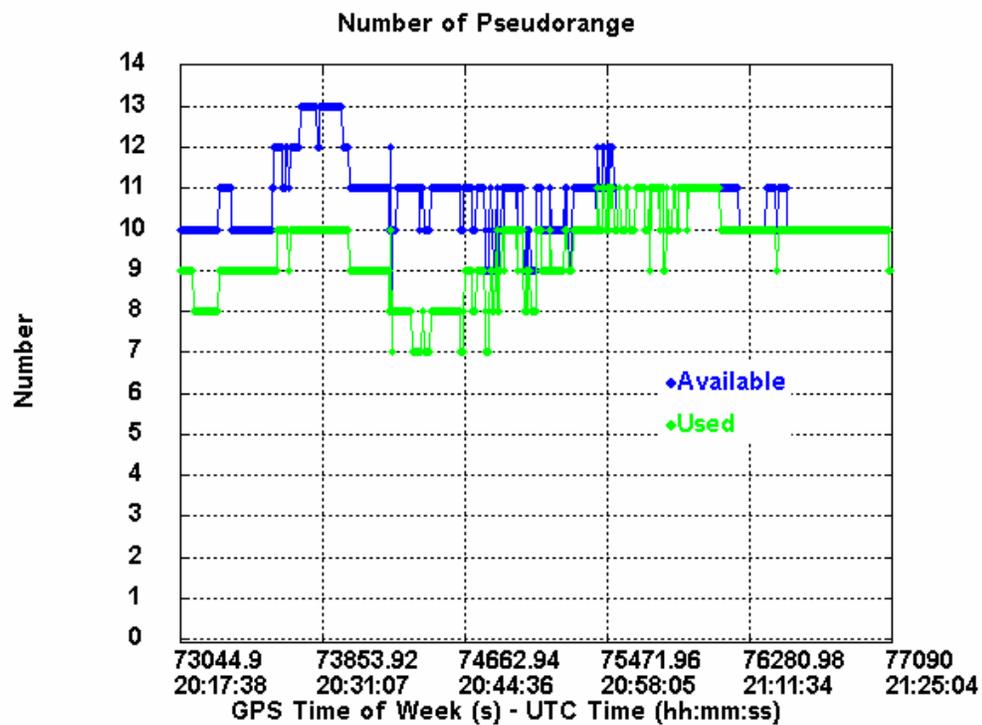
Figure 7.7: Number of satellites available (pseudorange and phase measurements are used)

Float position solutions, their estimated standard deviations and dilution of precision values are compared between the GPS-only case (Figure 7.8) and the GPS-UWB case (Figure 7.9).

Although not initially intuitive, the solution from the UWB augmented GPS is better than GPS alone. From Figures 7.8 and 7.9, above, clear physical steps can be observed in the position solution in the UWB-GPS solution. On the contrary, physical steps taken during data collection can hardly be made out in the GPS-only solution. Furthermore, the GPS-only position solution clearly drifts even when the rover is stationary. This is not observed with UWB augmentation.
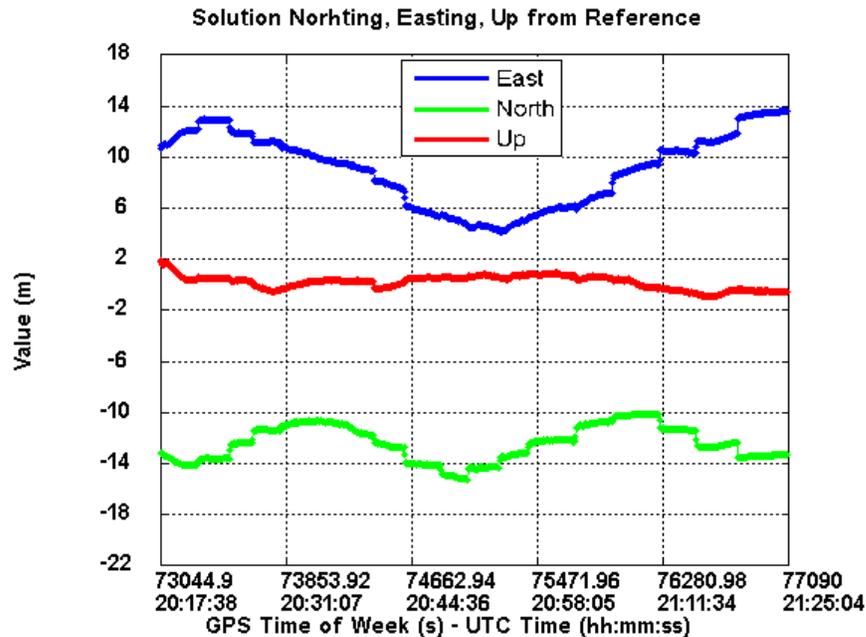
Figure 7.8: Float position solution for GPS-alone
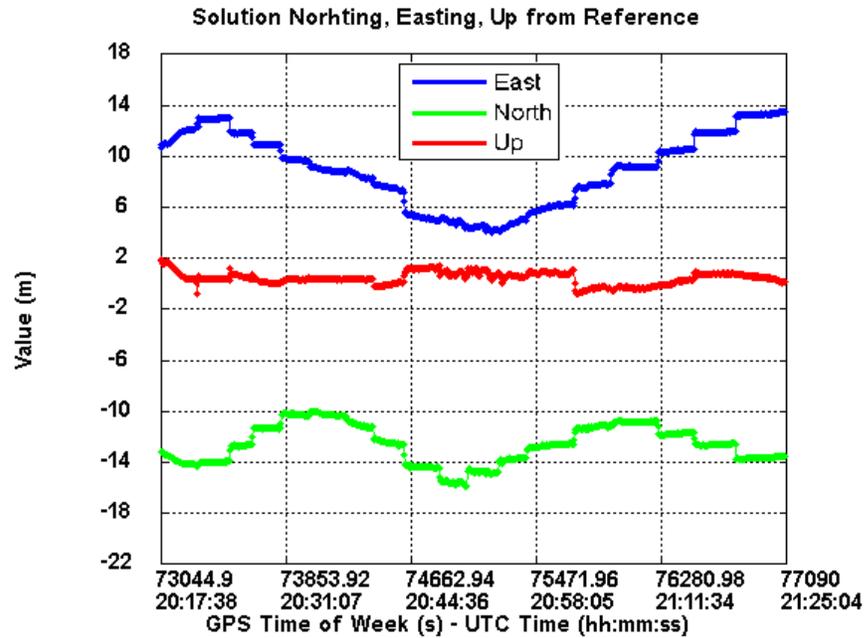
Figure 7.9: Float position solution with UWB augmentation

The estimated standard deviation of the position solution, shown below in Figures 7.10 and 7.11, also shows improvement in the UWB-GPS integrated solution. Faster convergence time is observed, as well as overall smaller standard deviation values in latitude, longitude and height.
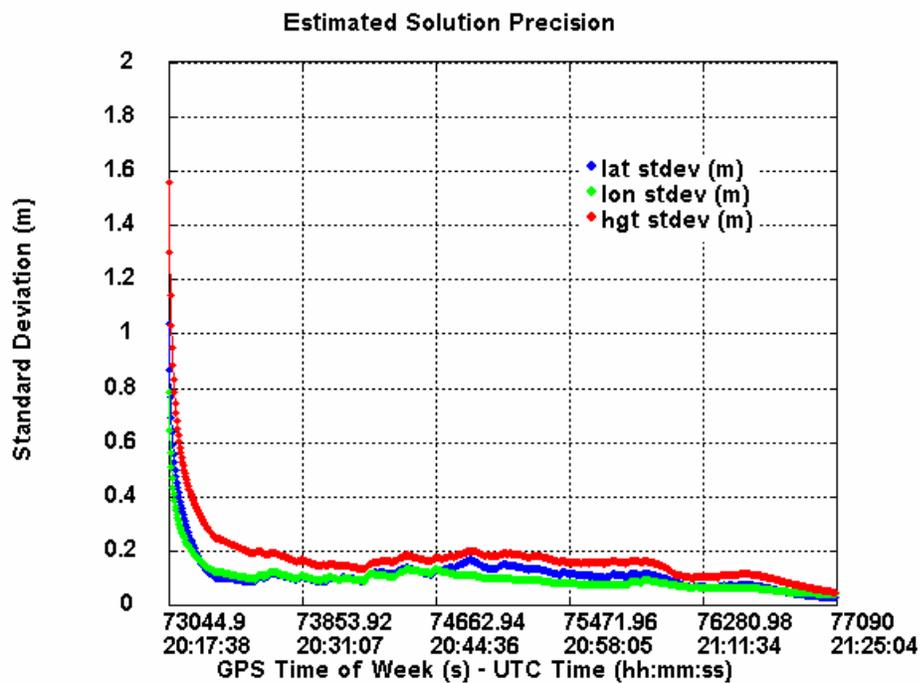
Figure 7.10: Standard deviation for the GPS-only solution
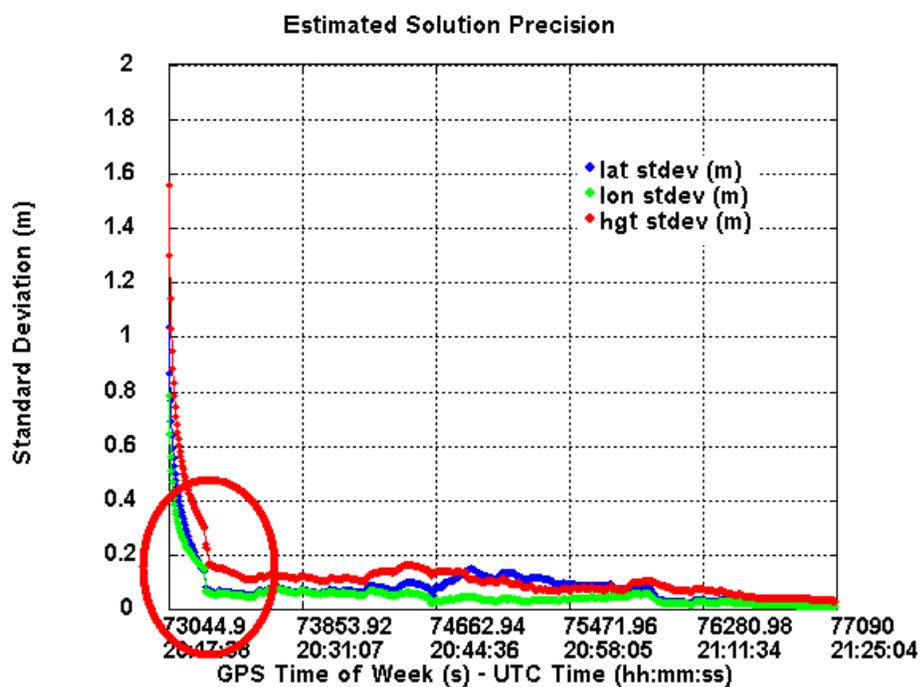
Figure 7.11: Standard deviation for the UWB-GPS solution. Red circle represents the time when UWB is introduced into the Kalman filter.

With the addition of a UWB source, the DOP is expected to decrease and this is observed in Figures 7.12 and 7.13. With many satellites, the addition of UWB sources may not be overly advantageous. However, when the number of satellites drops due to signal masking or attenuation, introduction of extra RF sources will become crucial in order to maintain a low DOP value.

	♦HDOP	♦PDOP	♦GDOP
Min	0.957177	1.42622	1.60412
Max	2.47542	3.92383	4.78663
Mean	1.24671	1.91571	2.21195
RMS	1.30477	1.99533	2.31766
σ	0.385137	0.558351	0.692412
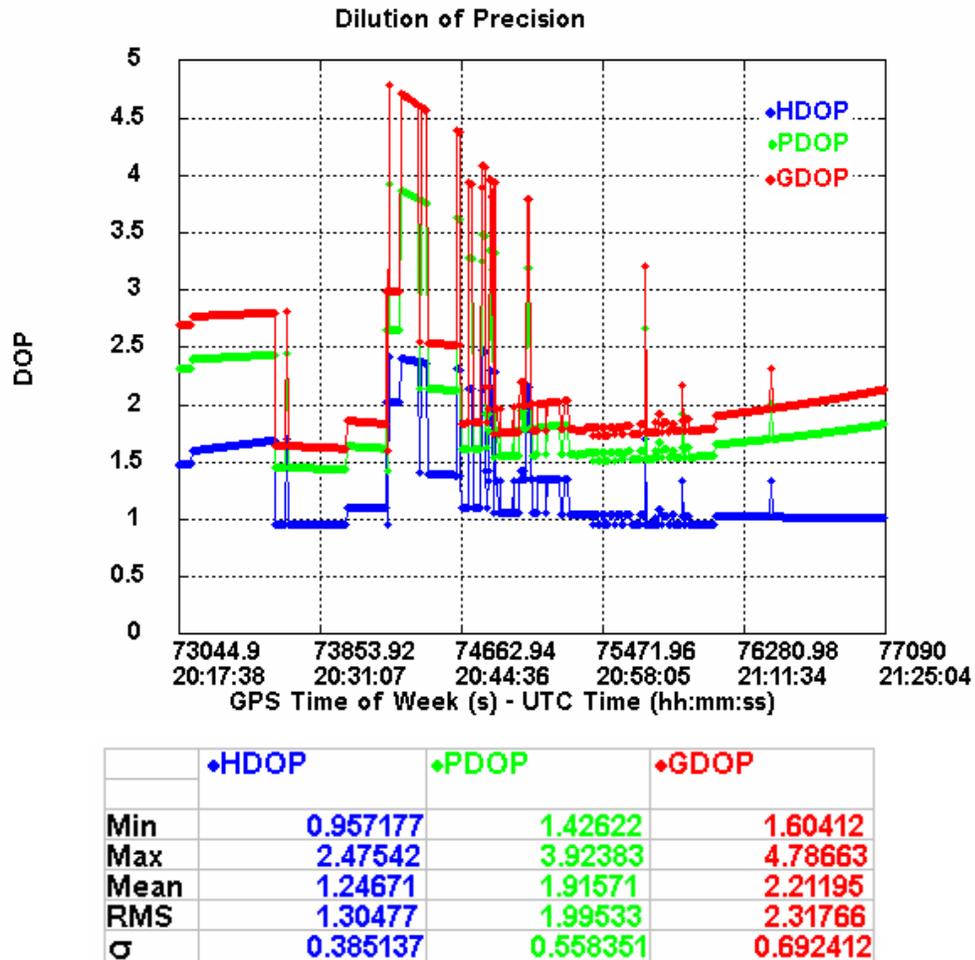
Figure 7.12: Dilution of Precision for GPS-alone solution
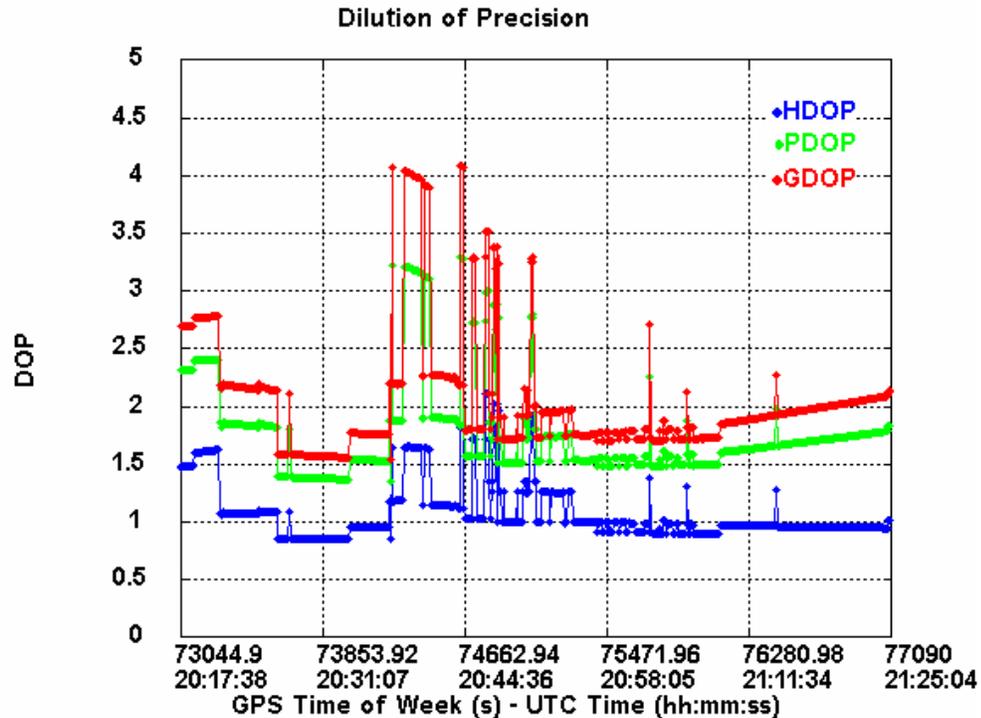
Figure 7.13: Dilution of Precision for UWB-GPS solution

UWB is a complementary system to GPS under poor signal conditions because of its apparent immunity to multipath. And since a UWB system's power is spread over such a large bandwidth, selective frequency fading is minimized. These two characteristics are largely the reason why a range can still be measured, even in hostile environments, such as around buildings or foliage, where RTK GPS may fail.

7.2 MULTIPLE RANGE AUGMENTATION OF A GPS RTK FLOAT SOLUTION

It is evident that adding a single range UWB into the GPS RTK float Kalman filter gives notable improvement in accuracy, precision and geometric strength of the constellation (ie. DOP), but what kind of results would be attained if multiple UWB ranges are added

to the filter? Would the user be able to travel into extreme hostile signal environments and still be able to accurately navigate? The final section of this chapter explores this topic.

7.2.1 Objective

The objective of this investigation is to show improvements in positioning and navigation with multiple range UWB augmentation to GPS under several test scenarios representing varying signal conditions. The metrics used to determine if positioning and navigation have improved are accuracy, precision and DOP.

7.2.2 Procedure

For this test, two Trimble R8 GNSS receivers and four MSS UWB radios are used. The test area is the same vicinity as where outdoor multiple UWB range augmentation to code DGPS was conducted. The test area is described in Sections 6.3.2 and 6.3.3. To re-iterate, testing is conducted outdoors on the University of Calgary campus. One Trimble R8 GNSS receiver is placed over a known point and this is the base station for RTK purposes. Three UWB radios are placed along the outside edge of the test area and are stationary throughout this test. They act as range request responders to the rover unit, which consists of an UWB radio and GPS receiver mounted together on a co-axial mount, described in Section 4.5.5. Please refer to Figure 7.14, below, for a picture of the test area.

Figure 7.14: Test area for multiple UWB range augmentation to GPS RTK

In Section 6.3.3, when multiple UWB ranges were added in with code DGPS measurements, the rover unit walked along the outer circle of the sidewalk loop in Figure 7.14, above. In this study, to differentiate the investigation, the rover is walked along the inner circle of the sidewalk loop, instead of the outer circle. For more pictures of the test area, please refer to Figures 6.22 and 6.23 in the previous chapter.

For all solutions computed in the GPS float augmented with UWB tests, a 4-state square root filter is used to estimate the states. The elevation mask is set to 13 degrees, while the C/N_0 mask is 18.0 dB-Hz. The process noise for the east, north, up, and clock states are 0.1 m/s, 0.1 m/s, 0.05 m/s and 100.0 m/s, respectively. The states are treated as random walk processes.

Four different signal conditions are used to reach the objective. They are summarized in the following table:

Table 7.2: Test scenarios for multiple range UWB augmentation to GPS RTK

Signal condition	# of satellites	# UWB ranges added	Scenario
Very good	7	3	Open field
	7	0	
Good	4	3	Forest or medium foliage
	4	0	
Bad	4	3	Beside a building
	4	0	
Very bad	2	3	In a canyon or deep valley

In Table 7.2, above, the 7 satellites with 3 UWB ranges solution, with "very good" signal conditions, is used as the reference solution since this produces the most accurate and reliable results. Please refer to Figure 7.15, below, for the sky plot of "very good" signal conditions.
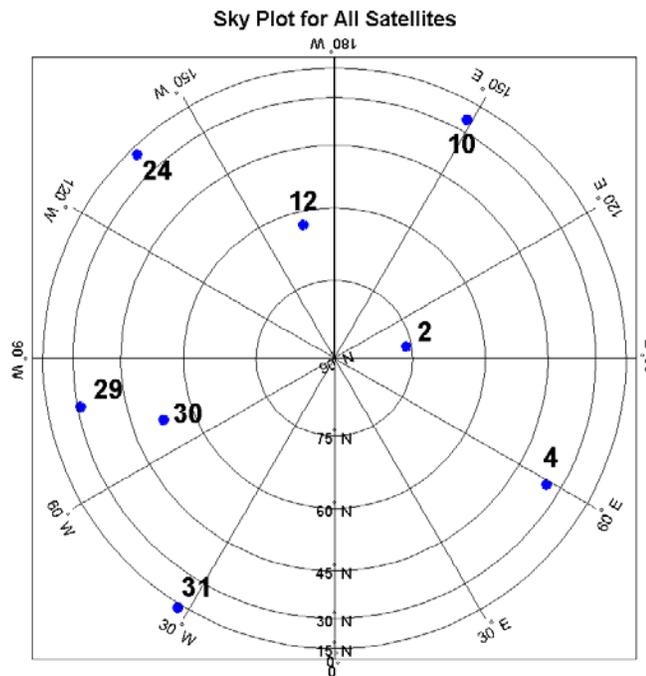
Figure 7.15: Sky plot for the "very good" scenario

"Good" and "bad" signal conditions are simulated by masking out 3 satellites. The difference between these two signal conditions is that in "good" signal conditions, the remaining satellites are evenly spread out through the sky as seen in Figure 7.16, below, while in "bad" signal conditions (Figure 7.17, below), the satellites are all on one side of the sky. The "good" signal conditions set-up is representative of a receiver suffering from attenuation, such as in a forest or foliage. "Bad" signal conditions correspond to signal masking caused by standing beside a building (ignoring multipath effects), where half of the sky is masked out.
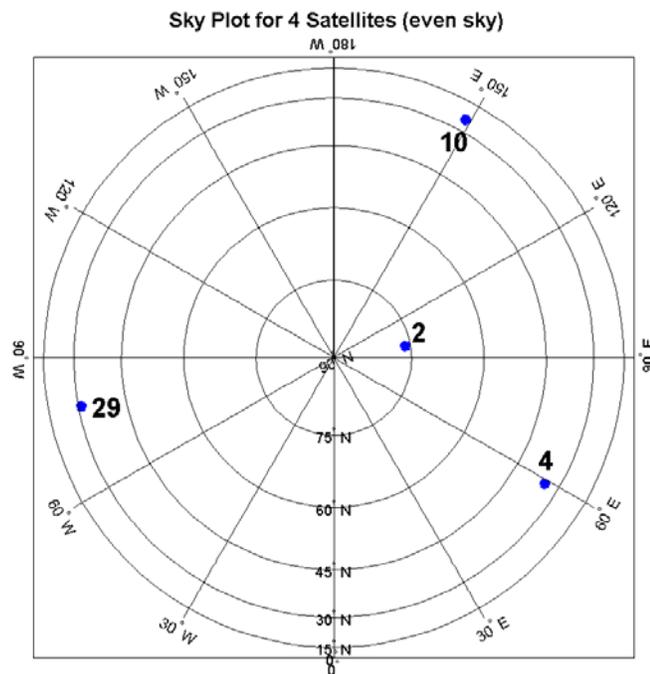
Figure 7.16: Sky plot for the "good" scenario
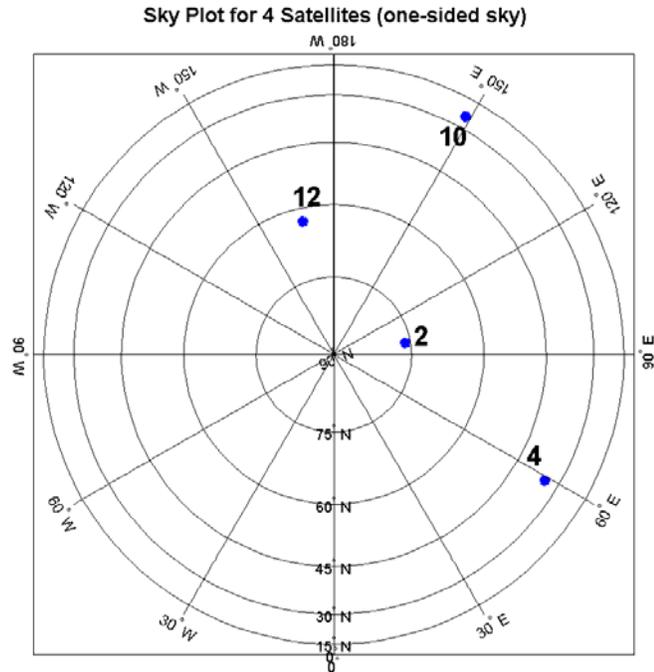
Figure 7.17: Sky plot for the "bad" scenario

Finally, the worst-case scenario studied is when only 2 satellites remain. This is the most hostile condition studied in this investigation and represents a user trying to position in a canyon or deep valley, where typically most of the satellites are masked. The sky plot of the "very bad" scenario is shown in Figure 7.18, below.
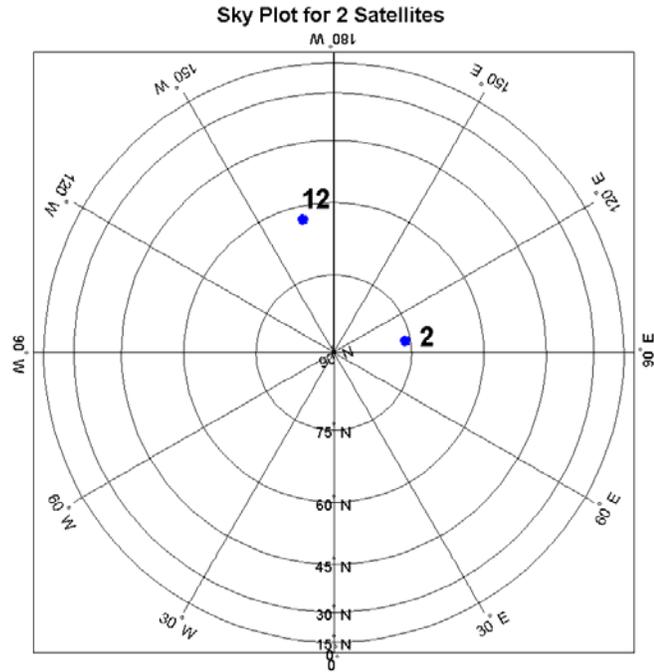
Figure 7.18: Sky plot for the "very bad" scenario

7.2.3 Results

7.2.3.1 "Very good" Scenario

The "very good" case has 7 satellites. No satellites are masked for this case. Figure 7.19, below, shows the total number of observations available for this scenario. Throughout the test, 3 UWB ranges are available, giving a total of 10 available observations.
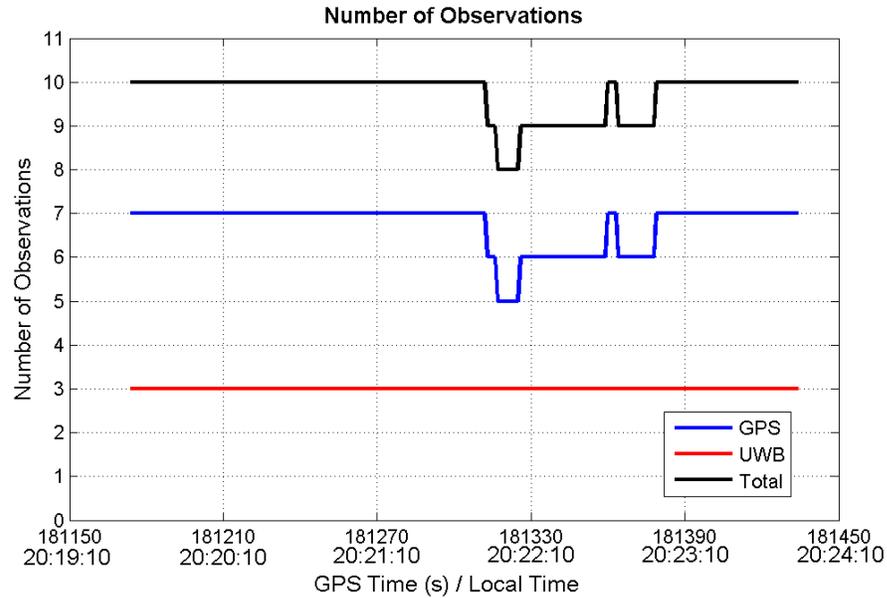
Figure 7.19: Total number of observation for the "very good" scenario. UWB observations are shown in red, GPS in blue and the combined observations in black.

The HDOP values for RTK float with and without 3 UWB ranges added in are shown in Figure 7.20, below. Even though the RTK float filter with 7 satellites reports an excellent HDOP value of around 1.2, this value decreases even more when 3 UWB range measurements are added in.
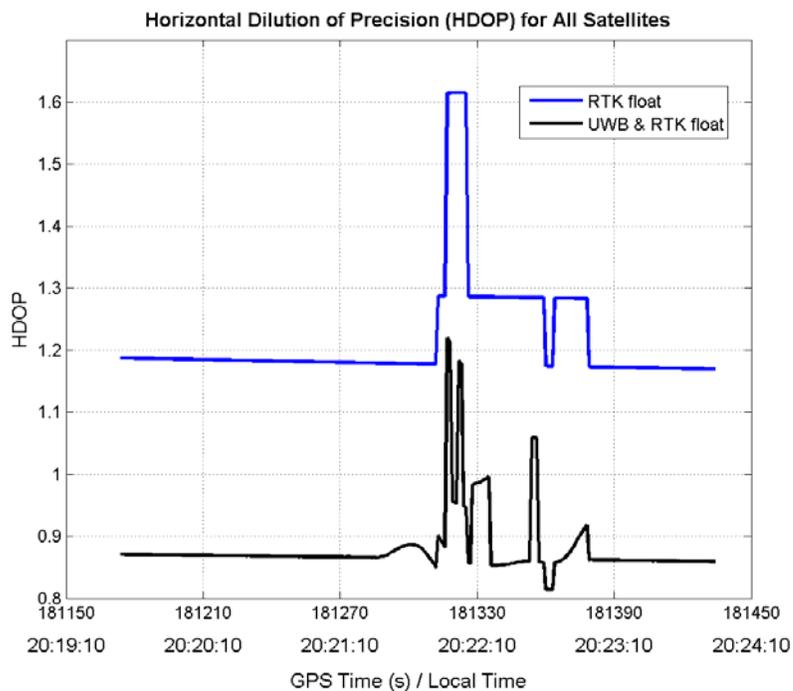
Figure 7.20: HDOP for the "very good" scenario
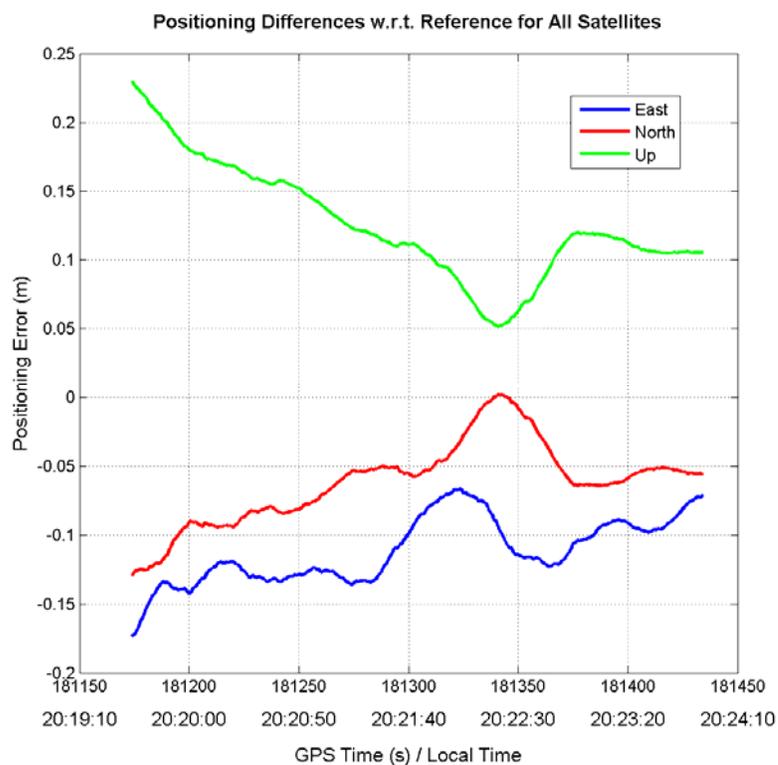
Figure 7.21: Positioning differences between all satellites solution with reference. The reference solution is chosen to be the all satellites solution augmented with 3 UWB ranges.

The accuracy of both solutions is fairly close. Figure 7.21, above, shows the positioning differences of RTK float with the reference solution for all satellites. The solutions tend to be off by a little more than a decimetre. Figure 7.22, below shows the trajectory of the rover unit.
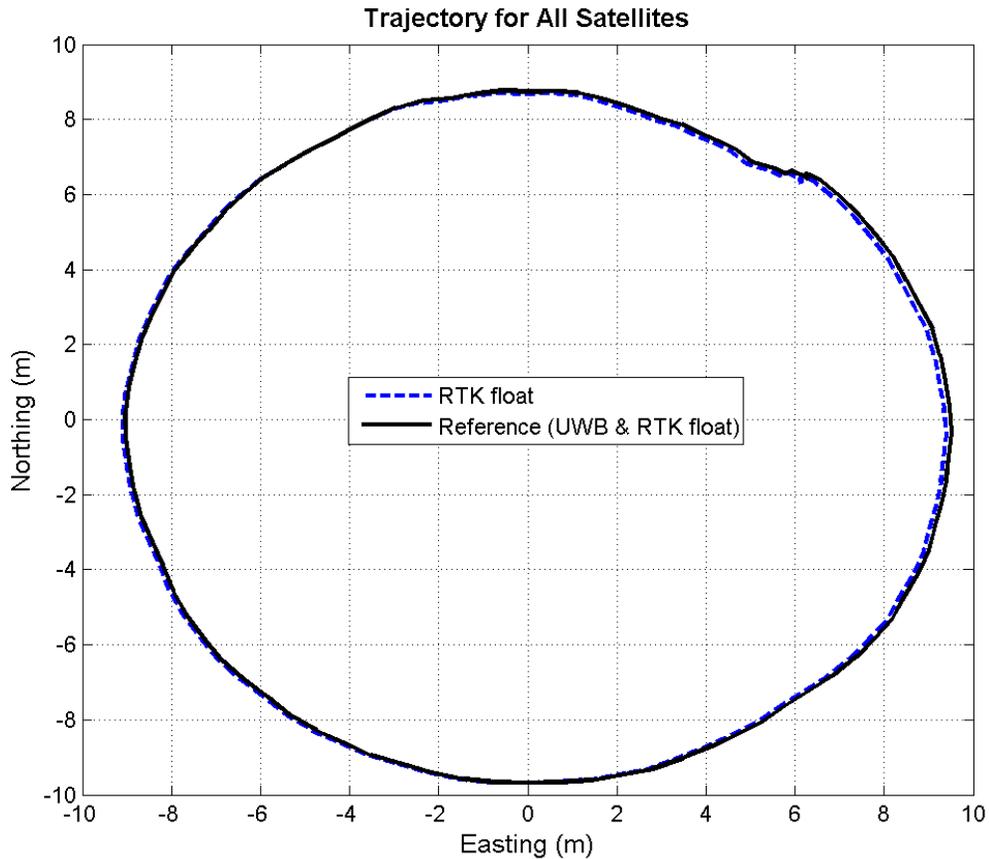
Figure 7.22: Trajectory for the "very good" scenario

The standard deviation values for East, North and Up directions are shown in Figure 7.23, below, for the 7 satellite solution with and without UWB augmentation. Again, despite the 7 satellite solution showing relatively low standard deviations, these values drop to a lower convergence value once the UWB measurements are added in. This shows that the solution with UWB range measurements gives a more precise solution.
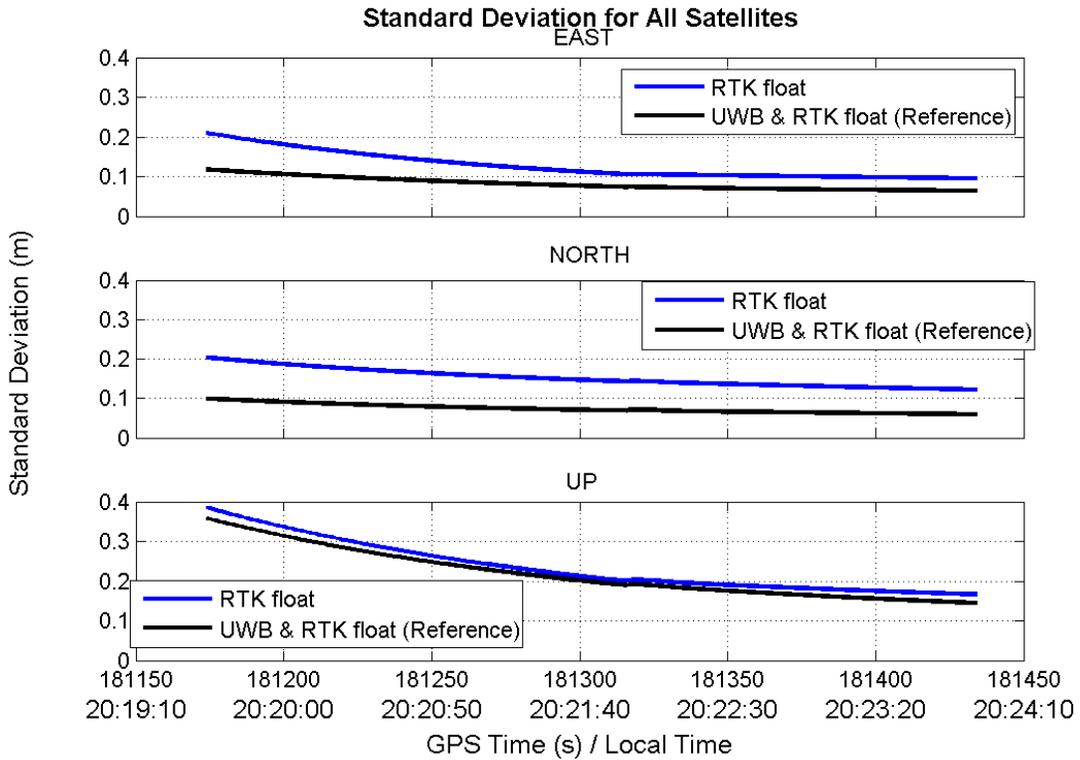
Figure 7.23: Standard deviation values for the "very good" scenario

The 3 UWB range augmented 7 satellite solution is the most accurate and precise solution and will be used as a reference solution herein.

7.2.3.2 "Good" Scenario

The "good" case consists of 4 satellites that are evenly spaced out in the sky. To create this scenario, 3 satellites are masked. For the sky plot of this scenario, please refer back to Figure 7.16, above.

The HDOP for this setup is shown in the figure below. HDOP values are still low for the RTK float filter with only 4 satellites, however, at GPS time 181320, one satellite drops out for several seconds. This can be seen in the sudden disappearance and subsequent spike in HDOP values. With 3 UWB range measurements added in, a smaller HDOP spike is seen but an accurate and reliable solution still continues to be estimated.
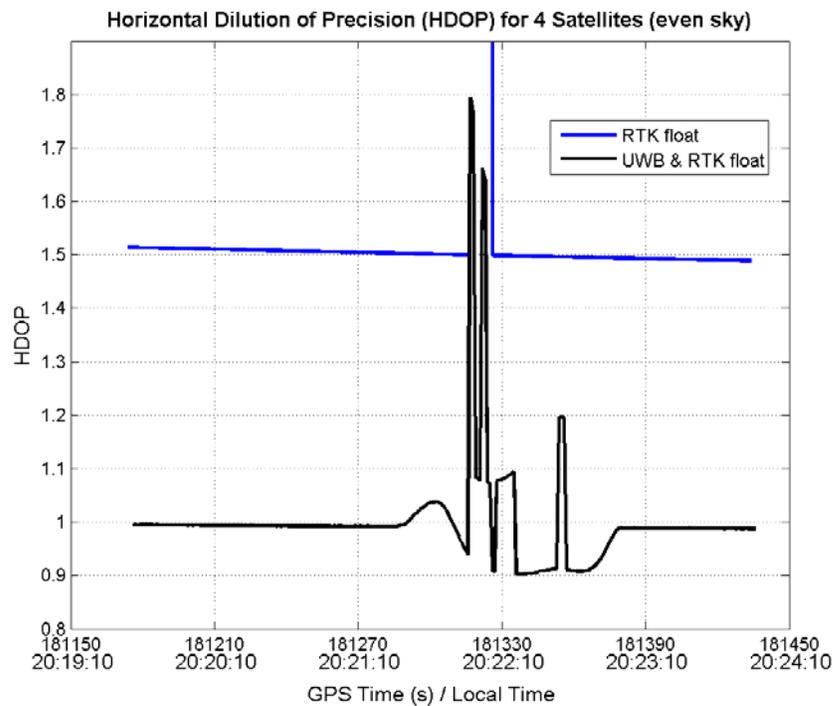
Figure 7.24: HDOP for the "good" scenario
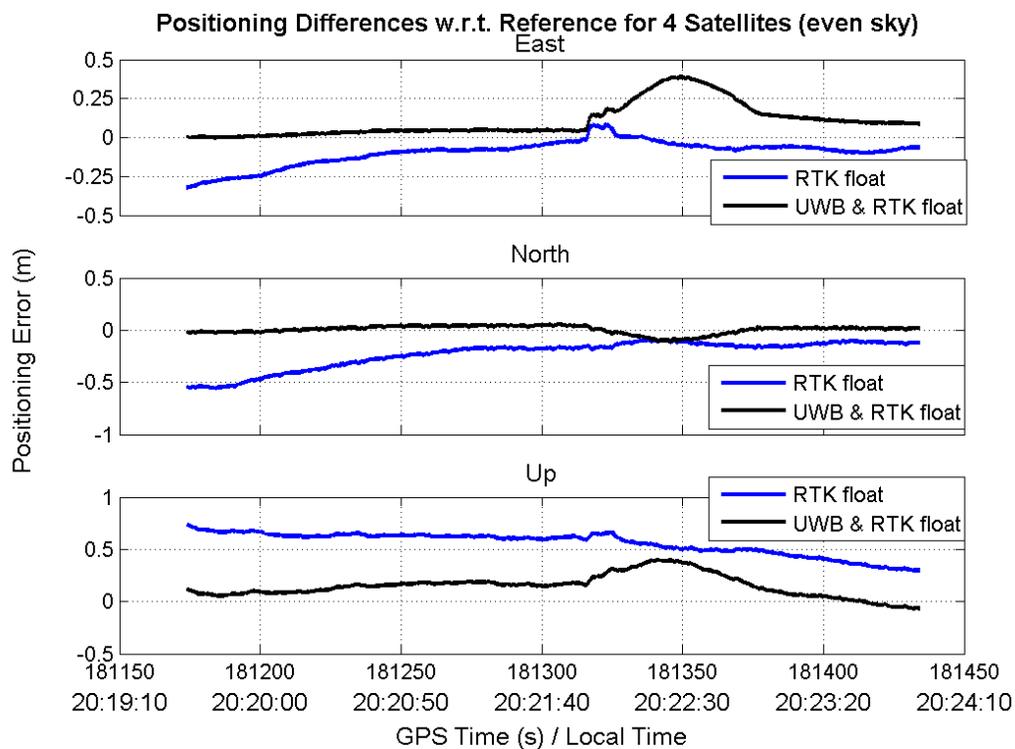
Figure 7.25: Positioning differences between the reference solution and RTK float with and without UWB augmentation for the "good" signal case

Figure 7.25, above, shows two things. First, the RTK float solution differenced with the reference for 4 evenly spread-out satellites is shown in blue, while the RTK float solution with 3 UWB ranges differenced with reference is in black. Please note that the reference solution has been chosen to be the 7 satellite RTK float solution augmented with 3 UWB range measurements. For the majority of the time, the black solution is close the reference solution. Differences between the reference and the black solution are in the several decimetre-level range, while it is slightly greater for the blue solution. The path of the rover for both solutions plus the reference solution is shown in Figure 7.26, below. The trajectory between the three solutions is seen to be very close.
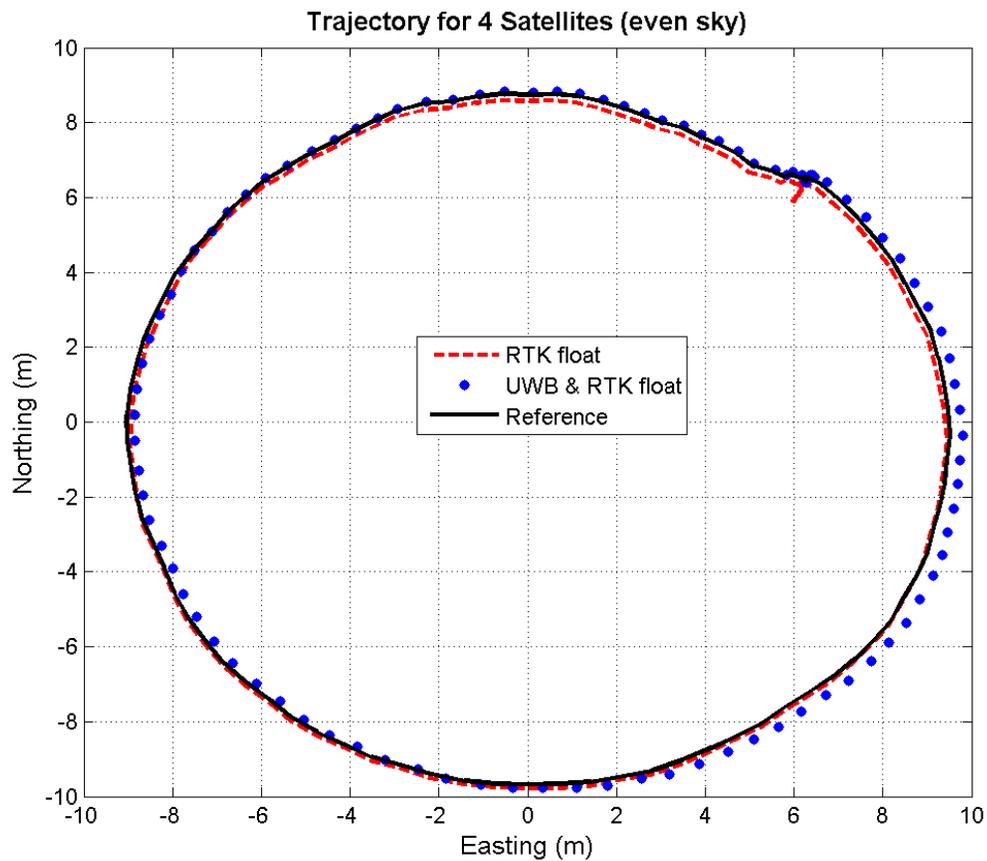
Figure 7.26: Trajectory for the "good" scenario

A notable drop in standard deviation values are seen in the solution with 3 UWB range measurements added in. Standard deviation plots for East, North and Up directions are

shown in Figure 7.27, below. Another important observation is that East and North errors drop much more with the augmentation of the UWB ranges, compared to the Up standard deviation. The logical explanation for this is because adding in new information (ie. UWB ranges) in the horizontal plane will not affect the vertical solution as greatly as in the horizontal domain. All 4 UWB radio stations are located at approximately the same height.
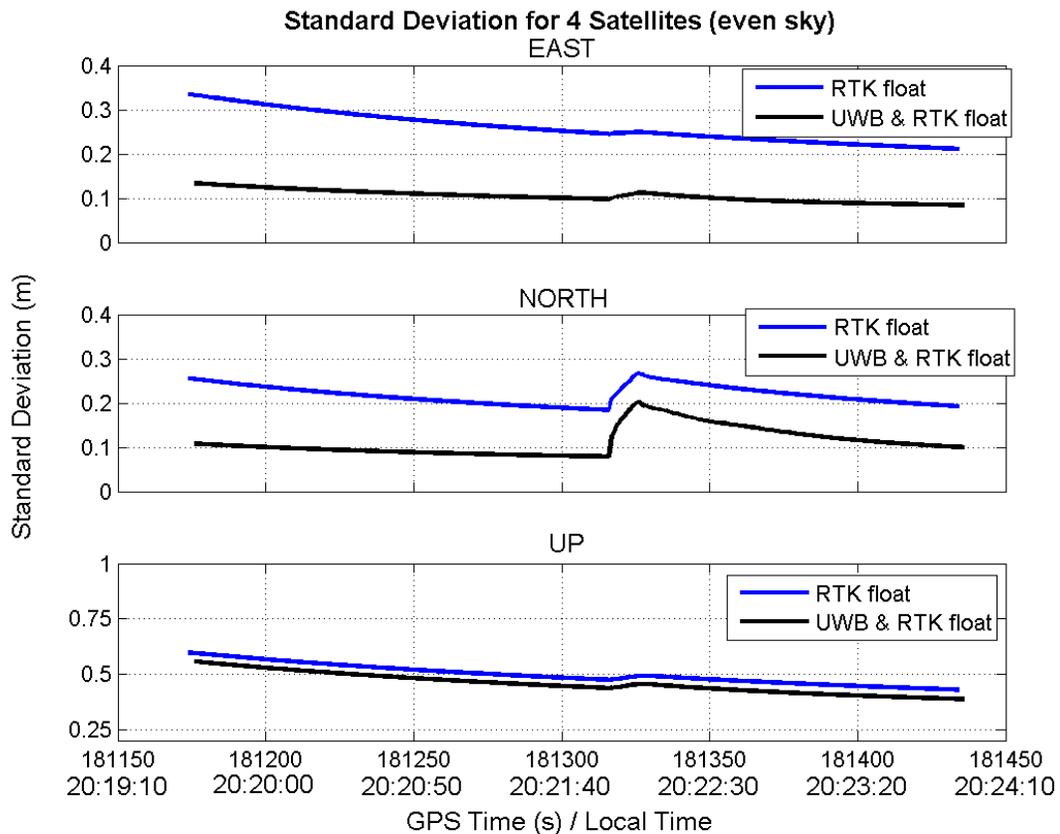
Figure 7.27: Standard deviation for the "good" scenario

7.2.3.3 "Bad" Scenario

The "bad" case also consists of 4 satellites. However, instead of having the 4 remaining satellites evenly spread out across the sky, the satellites in this scenario are all in one corner of the sky as previously seen from the sky plot in Figure 7.17 from Section 7.2.3.2.

Because all the satellites are located in one part of the sky, naturally, the DOP values should be high. This is observed in Figure 7.28, below. HDOP values for the solution with only 4 satellites are between 6 and 7, which are considered poor. On the other hand, HDOP values for the 3 UWB range augmented to 4 satellites solution still maintains HDOP values close to 1, which is considered excellent.
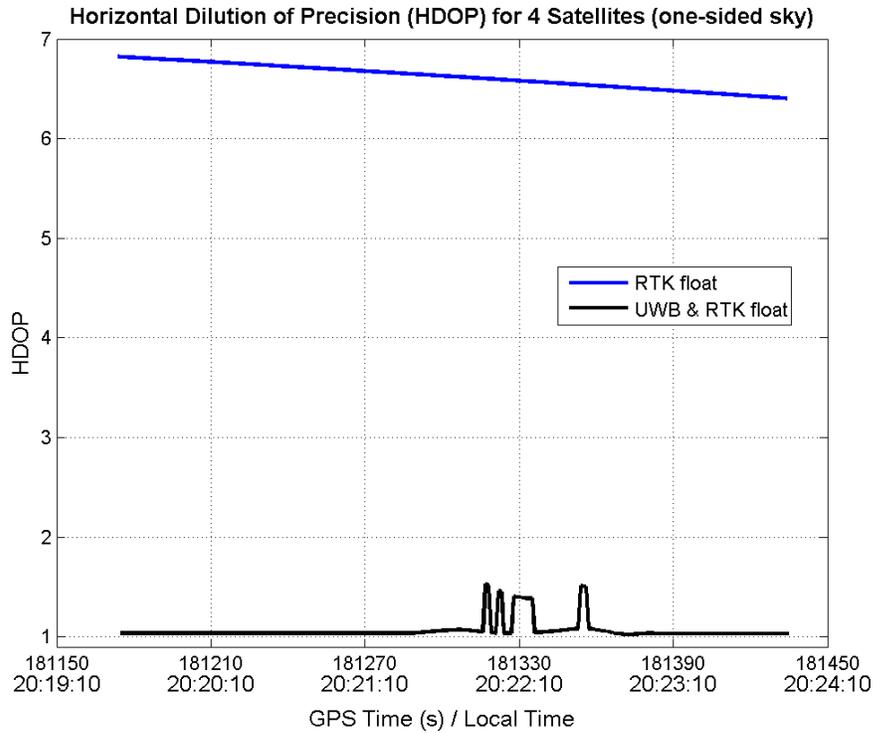
Figure 7.28: HDOP for the "bad" scenario
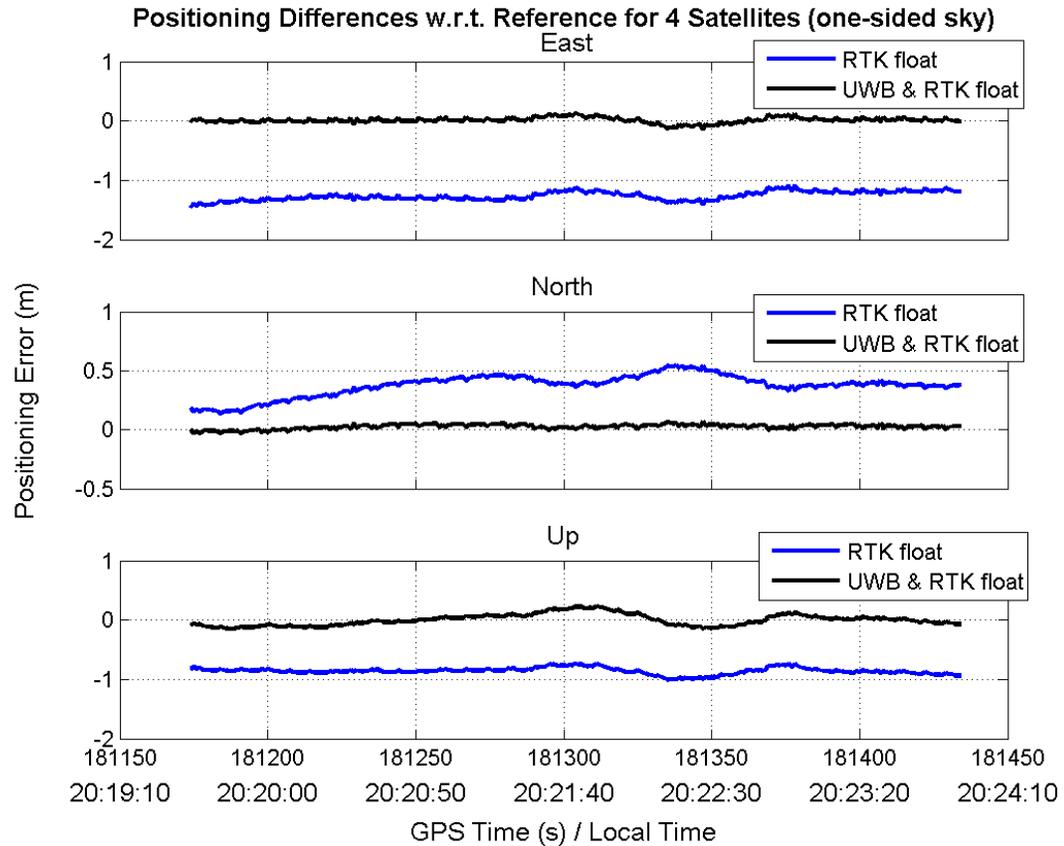
Figure 7.29: Positioning differences between the reference solution and RTK float with and without UWB augmentation for the "bad" signal case

Positioning errors for RTK float with and without UWB augmentation for 4 satellites in one corner of the sky is shown in Figure 7.29, above. The solution with UWB augmentation shows remarkable accuracy with respect to the reference solution. The solution is within a decimetre of the reference solution. The RTK float solution without UWB augmentation shows metre-level accuracy even though the solution is quite precise. This implies a biased solution as seen in the rover's trajectory in Figure 7.30, below. This is due to poor satellite/receiver geometry.
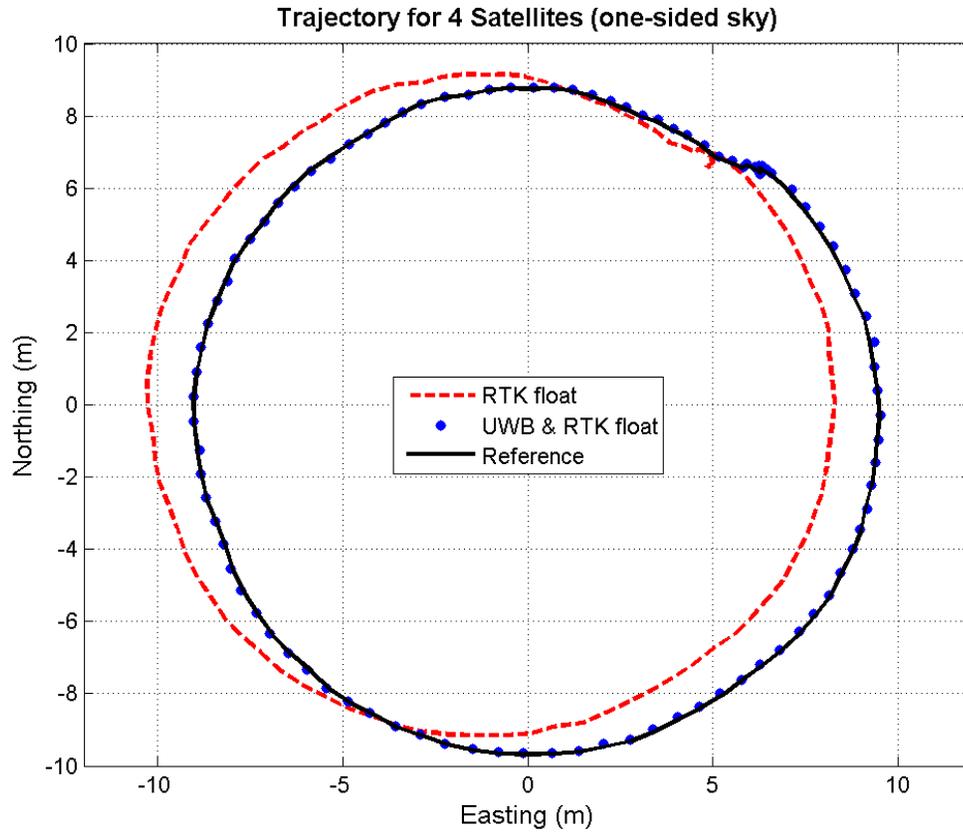
Figure 7.30: Trajectory for the "bad" scenario

A significant drop in standard deviation values is seen in all directions once the UWB measurements are augmented to GPS. This is clearly seen in Figure 7.31, below.

Standard Deviation for 4 Satellites (one-sided sky)
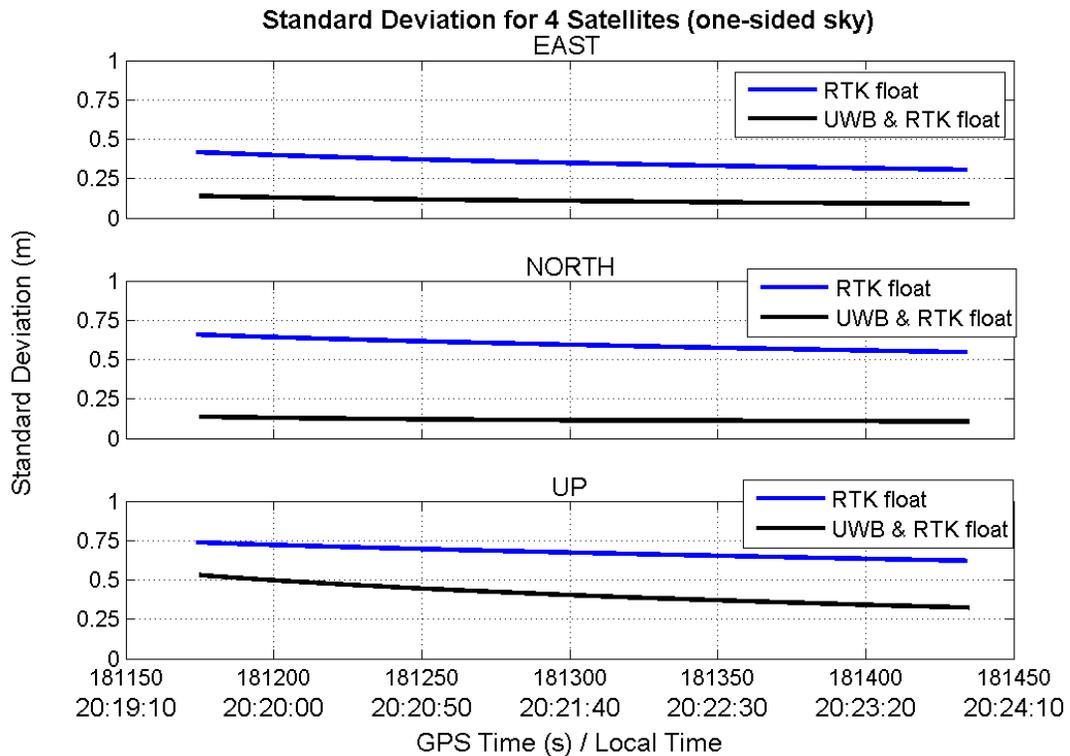
Figure 7.31: Standard deviations for the "bad" scenario

7.2.3.4 "Very bad" Scenario

The worst scenario consists of only 2 satellites overtop of the receiver. Unlike the previous three scenarios, this scenario will compare its solution with the reference solution since a solution cannot be estimated by the square-root filter using only 2 satellites alone. So, in order for a solution to be possible, the 2 satellite measurements are augmented with 3 UWB ranges.

HDOP values for the "very bad" scenario are seen in Figure 7.32, below, and values are generally low. However, HDOP values seem to be more susceptible to sudden spikes, caused by walking beside a tree or other temporary obstructions. For the most part, values are not too much greater than the reference solution, which has 7 satellites and 3 UWB ranges.
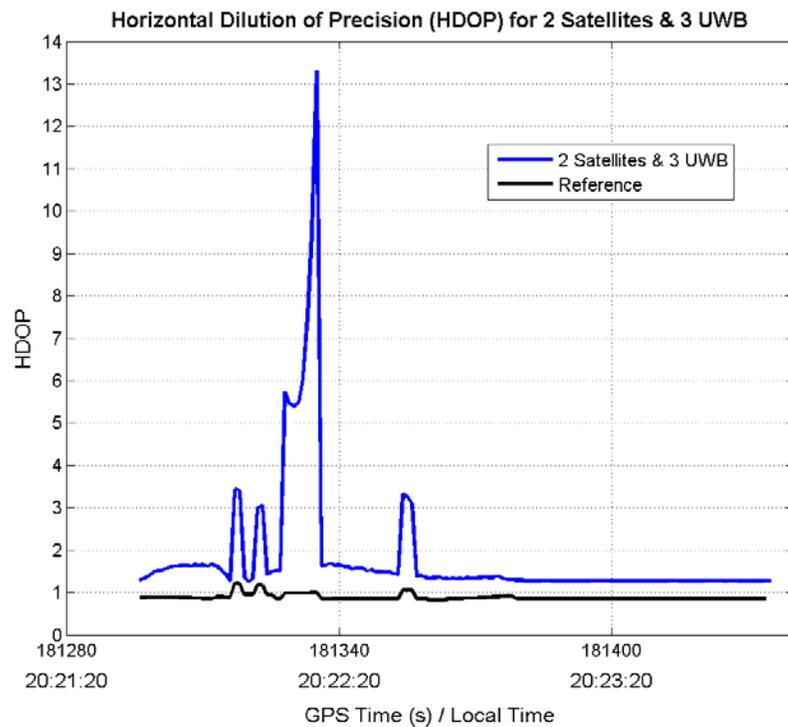
Figure 7.32: HDOP for the "very bad" scenario
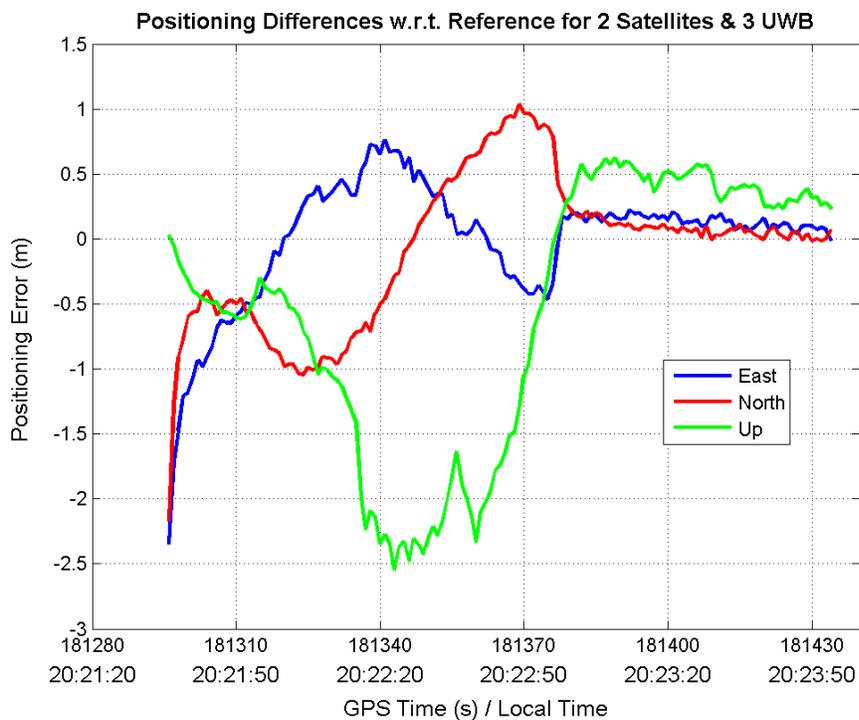
Figure 7.33: Positioning differences between reference and the 2 Satellites & 3 UWB solution.

This represents the "very bad" case.

The high HDOP values seen in Figure 7.32, above, can also be observed in the positioning difference between this solution and the reference in Figure 7.33, above. Near the end of the time series, HDOP values are seen to drop significantly and this is also reflected in the positioning differences. Overall, the RTK float solution with 2 satellites and 3 UWB ranges shows consistency with the reference solution. In Figure 7.34, below, differences between the two solutions are generally metre-level. Please note that the first part of the solution could not be estimated by the filter.
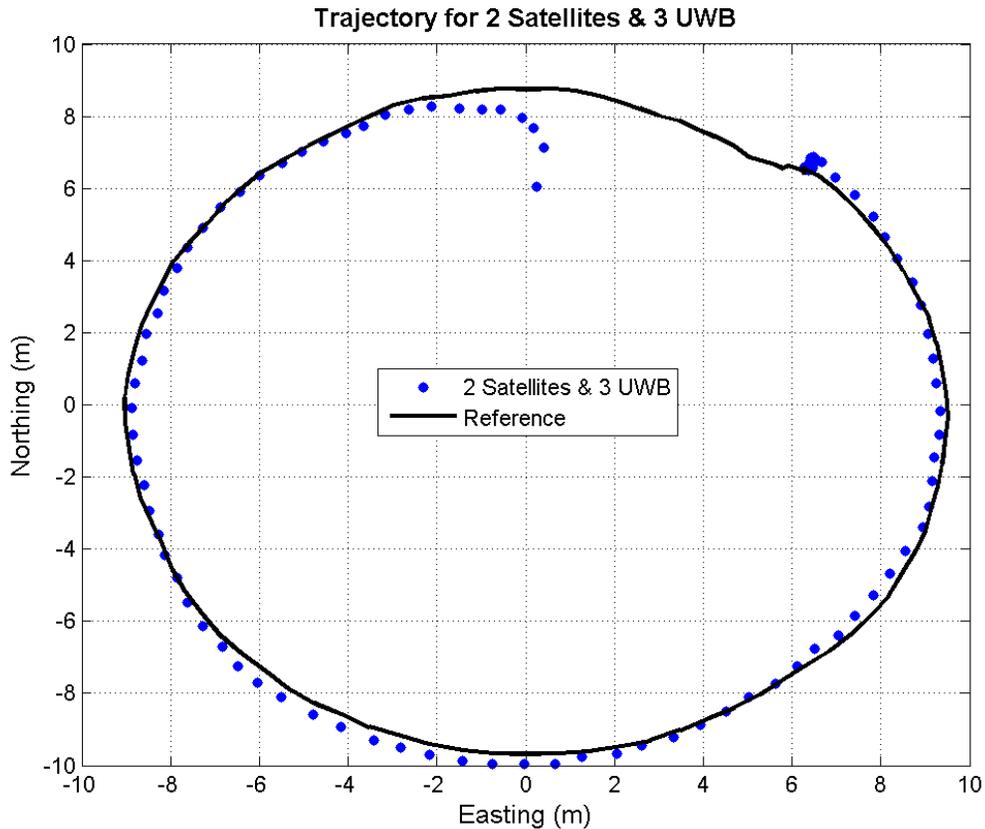
Figure 7.34: Trajectory for the "very bad" scenario

Standard deviation values for the East and North directions are still below 1 m for the "very bad" case. Sub-metre level precision in 2 directions for such a setup is acceptable. However, the Up direction shows metre-level precision, which is due to poor vertical geometry of the satellite/UWB radios. The black solution in Figure 7.35, below, is the reference solution.
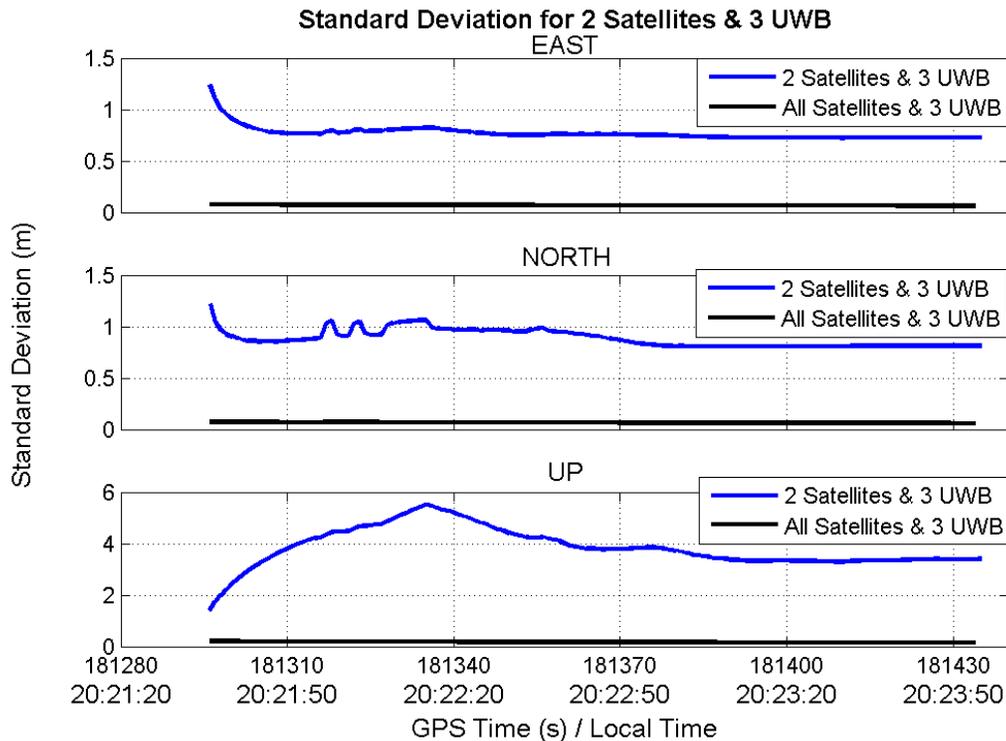
Figure 7.35: Standard deviation for the "very bad" scenario

7.2.4 Summary

Table 7.3, below, shows the average positioning differences with respect to the reference solution for all cases. The reference solution is the 7 satellite & 3 UWB scenario. Remarkably small position differences can be seen in the "very bad" case, especially in the east and north directions. However, the "very bad" solution is not very precise, as seen by its standard deviation values.

The solutions augmented with UWB observations generally had differences within a decimetre to the reference and solution accuracy does not seem to be correlated with how many satellites are in the sky. In other words, solution accuracy is not dependent on scenario or signal condition when UWB is augmented, as the "very bad" and "bad" cases are just as accurate (if not more accurate) than the "good" scenario. Finally, when looking at the standard deviation values in the following table, it is important to remember that the standard deviation plots in Figures 7.23, 7.27, 7.31 and 7.35, are

standard deviations of the position solutions alone, while the standard deviation values found in Table 7.3, below, are the standard deviation values for the differences between each scenario's solution with the reference.

Table 7.3: Average positioning differences between different solutions and the reference. The standard deviation of the difference with reference and the solution is also included.

Signal condition	# satellites + # UWB	Average Positioning Differences w.r.t Reference		
		East (m) + std	North (m) + std	Up (m) + std
Very good	7 + 3	0	0	0
	7 + 0	-0.112 ± 0.024	-0.062 ± 0.030	0.126 ± 0.041
Good	4 + 3	0.1046 ± 0.107	0.005 ± 0.039	0.149 ± 0.108
	4 + 0	-0.097 ± 0.081	-0.229 ± 0.134	0.558 ± 0.109
Bad	4 + 3	0.011 ± 0.047	0.0248 ± 0.020	0 ± 0.098
	4 + 0	-1.264 ± 0.075	0.374 ± 0.093	-0.860 ± 0.056
Very bad	2 + 3	-0.002 ± 0.479	-0.088 ± 0.580	-0.542 ± 1.016

7.3 CONCLUDING REMARKS

In the study of multiple range UWB augmentation to a GPS RTK float solution, several varying test scenarios were created. These scenarios varied from benign signal conditions to very hostile signal environments. Multiple range UWB augmentation was seen to be most beneficial to GPS RTK float solutions that were poor. However, improvement, although not as extreme, was also seen when UWB measurements were integrated with a good GPS RTK float solution. The degree of improvement with augmenting UWB measurements into the square-root filter depends on how good or bad the RTK float solution is. Nonetheless, in all scenarios tested, the addition of UWB range measurements provided more accurate, precise and reliable results compared to a solution without integrated UWB measurements.

CHAPTER 8: CONCLUSION

UWB being used as a method to range and position has only recently emerged in literature within the past few years. Combining UWB measurements to GPS is an even more novel approach. Sensor integration via tightly-coupled integration is common for GPS with other sensors like Inertial Navigation System (INS), but UWB-GPS integration using this integration scheme has not previously been reported prior to the publication of this thesis.

In the beginning of this research work, several objectives were stated and they are repeated here for reference.

1) UWB range accuracy and signal effects are assessed in multipath conditions
2) UWB positioning is compared to code DGPS positioning in benign and hostile environments
3) UWB augmented code DGPS positioning in clear sky, hostile and indoor conditions is demonstrated and compared to DGPS alone.
4) UWB augmented carrier-phase GPS in clear and hostile signal environments

For the first objective, assessing the accuracy and precision of UWB systems alone prior to augmentation to GPS is needed because UWB technology used for positioning is recent and its characteristics are not fully understood. UWB range characteristics for two sets of UWB radios from two different manufacturers were studied in Chapter 5. Both TD and MSS UWB radios were tested indoors and outdoors. It was shown that while TD UWB radios produce lower mean errors and more precise measurements than MSS UWB radios, they are more sensitive to attenuation effects and are not as well-suited for the indoor environment as their MSS counterparts are. Both sets of radios suffer from scale factor and bias errors. Hence, from this chapter, it was found that a correction for these errors is needed in post-processing, prior to further data analysis or integration with GPS measurements in the following chapters.

The second objective compares UWB-only positioning to code DGPS-only positioning and this was done in Chapter 6. UWB-only positioning resulted in sub-metre level accuracies with centimetre-level precision, while code DGPS-only positioning gave metre-level accuracies and precision in hostile signal conditions. This test showed that UWB-only positioning performed better than code DGPS-only positioning in those signal conditions. So, the next step was to see if improvement was seen by augmenting a single UWB range to code DGPS in the same hostile signal environments, leading to the third objective.

Single UWB augmentation to code DGPS demonstrated that standard deviation levels were dropped to below 1 m and DOP values decreased to 2; both results unattainable with code DGPS alone in those signal conditions. Similar results were obtained when augmenting multiple UWB ranges to code DGPS measurements. In addition to this, when the number of satellites is dropped to 2 for the multiple UWB range augmentation case, the UWB-code DGPS combination maintained metre-level accuracy. In a subsequent test, indoor positioning resulted in complete GPS outage. Only 3 UWB ranges remained for the indoor segment of the test. These UWB ranges continued to produce sub-metre level accuracy with respect to indoor reference points while GPS was absent. Such accuracy is sufficient for numerous applications, including indoor pedestrian navigation. Seamless navigation from outdoors to indoors and back to outdoors seamlessly was also demonstrated when the UWB-GPS rover unit was walked from outside to inside the ICT building. This chapter is significant because it shows that UWB is able to both augment and replace GPS in very poor signal areas. However, only sub-metre to metre-level accuracy was attained, primarily due to the fact that only code DGPS was used.

For increased accuracy, carrier phase measurements were used in Chapter 7 to reach the fourth objective. A GPS RTK float solution was augmented first with a single UWB range, followed by multiple UWB ranges. Single UWB range augmentation to a RTK float solution showed decreases in both standard deviation and DOP values. Faster convergence time to the solution was also observed. For the RTK float solution

augmented with multiple UWB ranges, several test scenarios were set up replicating varying signal environments. These scenarios ranged from excellent, to extremely poor signal conditions. UWB augmentation demonstrated improvement in all cases. However, most improvement was seen when signal conditions were poor. The worst case tested was with 2 satellites and 3 UWB ranges. Another important conclusion from this chapter was that with UWB ranges augmented, solution accuracy did not change significantly when GPS signal conditions got increasingly worse. So, accurate position solutions were still obtained in the worst of scenarios with the help of UWB ranges.

A summary of these 4 objectives is to prove the effectiveness of using UWB to augment and/or replace GPS in varying signal conditions. Improvements in accuracy, precision and reliability were seen in all cases when UWB was augmented to GPS in all signal conditions tested.

8.1 FUTURE WORK

All research objectives set out in this thesis have been met; however, there are still years of work to do in order to exploit the full benefits of UWB technology. Future work into this subject includes integration of UWB range measurements with a fixed ambiguity carrier phase GPS solution in hostile signal conditions. Further testing in different hostile environments is also needed to fully understand the effects attenuation and fading on UWB signals. Finally, methods to estimate and correct for the scale factor and bias errors "on-the-fly" (OTF) for real-time applications needs to be investigated.

<u>REFERENCES</u>

Barrett, T.W. (2000) "History of Ultrawideband (UWB) Radar and Communications: Pioneers and Innovators," *Proc. Progress in Electromagnetics Symposium (PIERS) 2000*, Cambridge, MA

Barrett, T.W. (2001) "History of Ultrawideband Communications and Radar: Part 1, UWB Communications," *Microwave Journal*, pp.22-56

Bond, E.J., X. Li, S.C. Hagness, and B.D. van Veen (2003) *Microwave Imaging via Space-Time Beamforming for Early Detection of Breast Cancer*, IEEE Transactions on Antennas and Propagation, vol. 51, no. 8, pp. 1690-1705

Buehrer, R.M., W.A. Davis, A. Safaai-Jazi, and D. Sweeney (2004) *Ultra-Wideband Propagation Measurements and Modeling*, DARPA NETEX Program Final Report

F.C.C. (2008) *Part 15 – Radio Frequency Devices*, Federal Communications Commission, Title 47 – Communications, Part 15 – Radio Frequency Devices, Section 15.507 – 15.521, http://www.access.gpo.gov/nara/cfr/waisidx_07/47cfr15_07.html, last accessed September 22, 2008

F.C.C. (2002) "First Report and Order," *Revision of Part 15 of the Commission's Rule Regarding Ultra-Wideband Transmission Systems*, FCC 02-48, Federal Communications Commission, Washington D.C. http://hraunfoss.fcc.gov/edocs_public/attachmatch/FCC-02-48A1.pdf, last accessed October 6, 2008

Fontana, R.J. (2006) *Ultra Wideband (UWB) Frequently Asked Questions (FAQ)*, Multispectral Solutions Inc. http://www.multispectral.com/, last accessed on October 8, 2008

Gao, Y. (2004) *Geodetic Positioning*, ENGO 423 Course Notes, Department of Geomatics Engineering, University of Calgary, Canada

Google Maps (2008) *Shouldice Park*, Google Inc., Mountain View, CA http://maps.google.com/, last accessed October 5, 2008

Grewel, M.S., A.P. Andrews (2001) "Implementation Methods" [Chapter 6] in *Kalman Filtering: Theory and Practice Using MATLAB*, Second Edition, Wiley InterScience Publication, John Wiley & Sons Inc., Hoboken, NJ, pp. 202-269

IEEE 802-15.4a (2007) "Part 15.4: Wireless Medium Access Control (MAC) and Physical Layer (PHY) Specifications for Low-Rate Wireless Personal Area Networks (WPANs) - Amendment 1: Add Alternate PHYs", *IEEE Standard for Information Technology*, IEEE, New York, NY http://standards.ieee.org/getieee802/download/802.15.4a-2007.pdf, last accessed October 4, 2008

Lachapelle, G. (2006) *Navstar GPS Theory and Applications*, ENGO 625 Course Notes, Department of Geomatics Engineering, University of Calgary, Canada

Leick, A. (2004) "Least Squares Adjustment" [Chapter 4] in *GPS: Satellite Surveying*, Third Edition, Wiley & Sons Inc., Hoboken, NJ, pp. 92-170

Marsh G. (2005) *UWB – Europe is Concerned too*, Avionics Magazine, Access Intelligence LLC. http://www.aviationtoday.com/av/categories/commercial/995.html, last accessed October 30, 2006

Muquibel, A.H., A. Safaai-Jazi, "A new formulation for characterization of materials based on measured insertion transfer function", *IEEE Transactions on Microwave Theory and Techniques*, vol. 51, no. 8, pp. 1946-1951

Nekoogar, F. (2006) *Ultra-Wideband Communications: Fundamentals and Applications*, Prentice Hall, Indianapolis IN, pp. 131-137

Opshaug, G.R., P. Enge (2002) "Integrated GPS and UWB Navigation System: Motivates the Necessity of Non-Interference", published in 2002 IEEE Conference on Ultra wideband Systems and Technologies, pp. 123-127

Pace, S., G.P. Frost, I. Lachow, D.R. Frelinger, D. Fossum, D. Wassem, and M. M. Pinto (1995) "GPS HISTORY, CHRONOLOGY, AND BUDGETS" [Appendix B] in *The Global Positioning System*, RAND Research, Santa Monica, CA, pp. 237 – 243

Palojärvi, P. (2003) "Integrated Electronic and Optoelectronic Circuits and Devices for Pulsed Time-Of-Flight Laser Rangefinding," Dissertation, University of Oulu, Finland, http://herkules.oulu.fi/isbn9514269667, last accessed October 8, 2008

Raquet, J. (2006) *Advanced GNSS Receiver Technology*, ENGO 699.45 Course Notes, Department of Geomatics Engineering, University of Calgary, Canada

Reed, J.H. (2005) *An Introduction to Ultra Wideband Communication Systems*, Prentice Hall, Upper Saddle River NJ, pp. 1-66, 73-82, 253-258 & 509-524

Ross, G.F. (1973) "Transmission and Reception System for Generating and Receiving Base-Band Duration Pulse Signals without Distortion for Short Base-Band Pulse Communication Systems," U.S. Patent 3,728,632 issued April 17, 1973

Ruotsalainen, T. (1999) "Integrated Receiver Channel Circuits and Structures for a Pulsed Time-Of-Flight Laser Radar" Dissertation, University of Oulu, Finland, http://herkules.oulu.fi/isbn9514252160, last accessed October 7, 2008

Ruotsalainen, T., P. Palojärvi, and J. Kostamovaara (2001) "A Wide Dynamic Range Receiver Channel for a Pulsed Time-of-Flight Laser Radar," IEEE Journal of Solid-State Circuits, vol. 36, No. 8, August 2001, pp. 1228-1238

Saberinia, E. and A.H. Tewfik (2002) *Multicarrier UWB*, IEEE P802.15 Wireless Personal Area Networks, P802.15-02/03147r1-TG3a

Scholtz, R.A. (1993) "Multiple Access with Time-Hopping Impulse Modulation," *IEEE MILCOM*, vol. 2, pp. 447-450

Siwiac, K. (2002) *SG3a Application Summary*, IEEE P802.15 Working Group for Wireless Personal Area Networks Publications, doc: IEEE 802.15-02/149r0 http://grouper.ieee.org/groups/802/15/pub/2002/Mar02/02149r0P802-15_SG3a-Application-Summary.doc, last accessed October 6, 2008

Skone, S. (2007) *Atmospheric Effects on Satellite Navigation Systems*, ENGO 633 Course Notes, Department of Geomatics Engineering, University of Calgary, Canada

Staderini, E.M. (2002) "UWB radars in medicine," *IEEE Aerospace and Electronic Systems Magazine*, vol. 17, no. 1, pp. 13-18

Time Domain (2008) *Time Domain PulsON 210*, www.timedomain.com, last accessed August 15, 2008

University of Calgary (2008) *University of Calgary Campus Maps*, University of Calgary, Calgary, Canada http://www.ucalgary.ca/map/index.html, last accessed September 14, 2008

Yang, L. and G.B. Giannakis (2004) "Ultra-Wideband Communications – An Idea Whose Time Has Come," IEEE Signal Processing Magazine, vol. 21, No. 6, November 2004